2013

Networked Differential GPS Methods

Simon P. Barr
University of Rhode Island, sbarr@ele.uri.edu

NETWORKED DIFFERENTIAL GPS METHODS

BY

SIMON P. BARR

A THESIS SUBMITTED IN PARTIAL FULFILLMENT OF THE

REQUIREMENTS FOR THE DEGREE OF

MASTER OF SCIENCE

IN

ELECTRICAL ENGINEERING

UNIVERSITY OF RHODE ISLAND

2013

MASTER OF SCIENCE THESIS

OF

SIMON P. BARR

APPROVED:

Thesis Committee:

Major Professor Dr. Peter F. Swaszek

Dr. Richard J. Hartnett

Dr. Manbir S. Sodhi

Dr. Nasser H. Zawia

DEAN OF THE GRADUATE SCHOOL

UNIVERSITY OF RHODE ISLAND

2013

ABSTRACT

Historically, maritime organizations seeking accurate shipboard positioning have relied upon some form of differential GNSS, such as DGPS, WAAS, or EGNOS, to improve the accuracy and integrity of the GPS. Ground-based augmentation systems, such as DGPS, broadcast corrections to the GPS signal from geographically distributed terrestrial reference stations—often called beacons. Specifically, pseudorange corrections to the GPS L1 C/A signal are computed at each reference site, then broadcast in the nearby geographic area using a medium frequency (approximately 300 kHz) communications link. The user then adds these corrections onto their measured pseudoranges before implementing a position solution algorithm. Within the United States, the U.S. Coast Guard operates 86 DGPS reference beacons. Similar DGPS systems are operated in Europe and elsewhere around the globe.

While current DGPS receiver algorithms typically use one set of pseudorange corrections from one DGPS reference site (often the one with the "strongest" signal), many user locations can successfully receive two or more different DGPS broadcasts. This suggests two obvious questions: "If available, how does one select the corrections to use from multiple sets of corrections?" and "Is it advantageous to combine corrections in some way?" A number of factors might influence the effectiveness of any particular station's corrections. Some of these refer to the effectiveness of the communications link itself, including concerns about interference from other beacons (skywave interference from far-away beacons on similar frequencies, a notable problem in Europe) and self-interference (skywave fading). Other factors refer to the accuracies of pseudorange corrections: for example, ionospheric storm-enhanced plasma density (SED) events can cause the corrections to have large spatial variation, making them poor choices even for users close to a beacon.

Earlier work in the area of DGPS beacon selection has identified several options, including choosing the beacon closest to the user or the beacon with the least skywave interference. There have also been suggestions on how to combine corrections when multiple beacons are available. The most common among these is a weighted sum of the

corrections, where the weights are typically inversely proportional to the distance from the user to the individual beacon.

This thesis re-examines the concept of multi-beacon DGPS by evaluating methods of combining beacon corrections based on spatial relativity. Recent research determines that DGPS accuracy performance is biased: the mean scatter of DGPS-corrected positions does not fall on the true receiver position. This finding was re-established this using networked DGPS methods both by processing GPS L1 C/A observables from dozens of CORS (Continuously Operating Reference Station) sites around the U.S.A. and via simulation using a Spirent GSS8000 GPS simulator. Specifically, we found that (a) the position solution computed using DGPS beacon corrections is typically biased in a direction away from the beacon and (b) the magnitude of the bias depends upon the distance from the beacon. This bias grows with a slope of approximately one-third of a meter per 100 km of user-to-beacon distance. We also found that networking DGPS corrections decreases the errors of bias magnitude and scatter radius inherent in single-beacon solutions.

This thesis compares the performance of several multi-beacon algorithms assessed using both GPS simulator and real-world data. These algorithms include simple averaging, a weighted sum based on inverse-range to each beacon, a weighted sum based on inverse-range-squared to each beacon, and spatial linear interpolation correction. Spatial linear interpolation factors in distances and angles to the known locations of the DGPS transmitters.

As part of this research effort, we developed a DGPS receiver using a software-defined radio platform. Ettus Research's USRP was chosen as the SDR device to collect and digitize GPS and DGPS radio signals. For the real-world tests, we applied networked DGPS pseudorange corrections to post-processed CORS data. The results of these tests confirm the spatial behavior of the simulator trials with respect to bias magnitude and scatter radius. A complete description of this system is included in the thesis.

ACKNOWLEDGMENTS

I would like to highlight the numerous contributions to this research by my advisor, Dr. Peter Swaszek. His in-depth knowledge of GPS, Differential GPS and signal processing methods have proved invaluable to me throughout the course of this work.

I would like to thank the other members of my committee, Dr. Richard Hartnett from the U.S. Coast Guard Academy; Dr. Manbir Sodhi from the Department of Mechanical, Industrial, and Systems Engineering; and Dr. Robert Tyce from the Department of Ocean Engineering for taking time from their busy schedules in order to further my education.

I would also like to thank the faculty of the U.S. Coast Guard Academy, whose scholarly and material support have greatly assisted in the completion of this thesis. Dr. Richard Hartnett was both a source of motivation and information—whose wealth of knowledge in the area of Coast Guard radionavigation systems is unparalleled. Commander Joe Staier and Commander Rob Oatman subsidized both my time and material resource requirements with good humor and sacrificed nearly 4000 pounds of peanut M&M's. Lieutenant Steve Myers expedited the purchase of specific equipment necessary for my research and Lieutenant Matt Kempe forfeited numerous servers, hard drives, and untold hours keeping my research bandwidth requirements satiated. Senior Chief Electronics Technician Ken McKinley provided technical expertise to set up and improve the infrastructure used to conduct this research.

Many thanks are deserved by those who—for no reason other than curiosity—persistently took the time to assist my research efforts. Tim Toolan was of great help in providing access to URI facilities and expertise with Linux, Jim Daly provided a number of material resources necessary to modify my equipment, and Andrew Cavanaugh helped lug test equipment all over the WPI campus.

Finally, I would like to thank Meredith Leach Sanders and Melyssa Lennox, who were able to make each day on campus much more interesting while simultaneously keeping the ECBE Department running. Turn to!

TABLE OF CONTENTS

Page

Page

LIST OF TABLES

LIST OF FIGURES

Figure **Page**

CHAPTER 1

Introduction

1.1 Overview of the Global Positioning System

The United States Air Force owns and operates the Navigation Signal Timing and Ranging Global Positioning System (NAVSTAR GPS), which is a space-based radio-navigation system that provides positioning, navigation, and timing information to users around the world. Reaching initial operational capability in 1993, it has quickly become ubiquitous in the military and civilian sectors and used in a variety of applications [1]. GPS consists of a space segment with a constellation of 24+ satellite vehicles (SVs) and a ground segment comprised of integrity monitoring and control stations. A minimum of 24 SVs travel in several different orbits about the globe, staggered in time such that four are visible from any point on Earth at any time of day. The satellites broadcast two levels of service, Precise Precisioning Service (PPS) for military users and Standard Positioning Service (SPS) for civilian users.

The Air Force fields several versions of SVs, called Blocks, which will broadcast, when modernized, several civil signals as part of the SPS: C/A, L1C, L2C, and L5 [2]. Of interest in this thesis is the L1-band coarse acquisition (C/A) signal broadcast as part of the Standard Positioning Service (SPS) at 1575.42 MHz because it is the most prevalent signal in use by the civilian sector.

Each SV broadcasts a unique pseudorandom noise (PRN) sequence known as C/A code at the L1 frequency. The unique PRN sequences allow the user's GPS receiver to separate the satellite signals and decode the information contained within. Each PRN sequence, also known as a "Gold code," is 1023 bits (termed *chips*) in length and designed to be mathematically near-orthogonal to one other [3]. In other words, no two different codes will have a high correlation to each other. This property allows GPS receivers to search for and synchronize to each satellite easily. Once a receiver has locked onto a satellite's PRN sequence, it reads the transmitted navigation message, which contains clock corrections, ephemeris, and almanac information [1]. These are

used by the receiver to adjust when and where it expects the satellite constellation to be and aides the calculation of the user's position.

Because L1 C/A signals are transmitted at a high chipping rate (1023 $\mathrm{Mbit \cdot s^{-1}}$), a high frequency (1575.42 MHz), and must travel from mid-Earth orbit to the ground, the signal is subject to a variety of electromagnetic interference types. The most common sources of intereference are: clock errors, atmospheric delays, and multipath. When GPS was made available to the public, an additional error called Selective Availability (SA) was introduced in order to intentionally degrade the accuracy of non-U.S. military positioning. The U.S. Coast Guard (USCG) fielded a ground-based augmentation system (GBAS) intended to improve GPS-based user positions by correcting the errors introduced by SA and the atmosphere [4]. Selective Availability was discontinued in May 2000 and DGPS-corrected positions experienced a coincidental improvement in accuracy. The current SPS specifies an accuracy of better than 8 meters 2DRMS (2 $\times$ distance root-mean-squared) [2].

There are several satellite-based positioning systems and a number of corresponding differential correction systems for each system. Major Global Navigation Satellite Systems (GNSSs) in operation and in production include: U.S.A.'s NAVSTAR GPS, Russia's GLONASS, the European Union's GALILEO, China's Compass–Beidou, Japan's QZSS, and India's IRNSS. Differential GNSS (DGNSS) is a GNSS augmentation system that can be either satellite-based (SBAS) or ground-based (GBAS), where corrections are broadcast by SBAS satellites over a regional area and GBAS beacons over a local area. DGNSSs based on NAVSTAR GPS include the U.S. Coast Guard's Differential GPS (DGPS) system and the Federal Aviation Administration's Wide-Area Augmentation System (WAAS). The E.U. fields an SBAS DGNSS called the European Geostationary Navigation Overlay Service (EGNOS) which provides integrity and correction information for multiple GNSS constellations.

1.2 Overview of U.S. Coast Guard Differential GPS

The U.S. Coast Guard is a user, developer, and supplier of a variety of maritime radio-navigation systems, including Differential Global Positioning System (DGPS). In brief, DGPS provides correction information to the user so as to improve the accuracy of GPS measurements. Pseudorange corrections for the GPS L1 coarse acquisition (C/A) signals are computed for each satellite at a reference site, and then broadcast in the nearby geographic area at each beacon's assigned radio frequency (between 285 kHz and 325 kHz, with 500 Hz width) using minimum-shift keying (MSK) modulation at $100\,\mathrm{bit{\cdot}s^{-1}}$ or $200\,\mathrm{bit{\cdot}s^{-1}}$. Messages are encoded with the RTCM SC-104 standard [4, 5]. Fig. 1.1 is a diagram of typical DGPS operation in the United States.

For user safety, these DGPS corrections must be both reliably transmitted and accurate. In recent years, expansion to a greater number of beacons in the Nationwide DGPS (NDGPS) network has increased DGPS coverage, with the intent of reaching a stated goal of 99% coverage of the continental United States. Now, in most areas of the United States and its surrounding maritime waterways, at least two overlapping beacons are "visible" to littoral DGPS users—in many areas, three or more beacons are visible. A map detailing the number of beacons covering the continental United States is shown in Fig. 1.2. In typical implementations, DGPS receivers apply the corrections from the "strongest" beacon—the beacon with the highest signal-to-noise ratio (SNR) received at the user's location.

The availability of additional information from multiple beacons raises the possibility of combining (also termed "networking" in this thesis) the corrections to increase both system robustness and the accuracy of the resulting position solutions. This thesis proposes and evaluates various methods for networking DGPS corrections with comparison against the current method.

The DGPS radio-navigation system maintained by the U.S. Coast Guard is critical to the U.S. economy and national security, assuring reliable and accurate positioning capability. Eighty-six DGPS stations throughout the country broadcast signals containing correction information about GPS satellites [6]. Broadcast of a parallel Coast Guard elec-

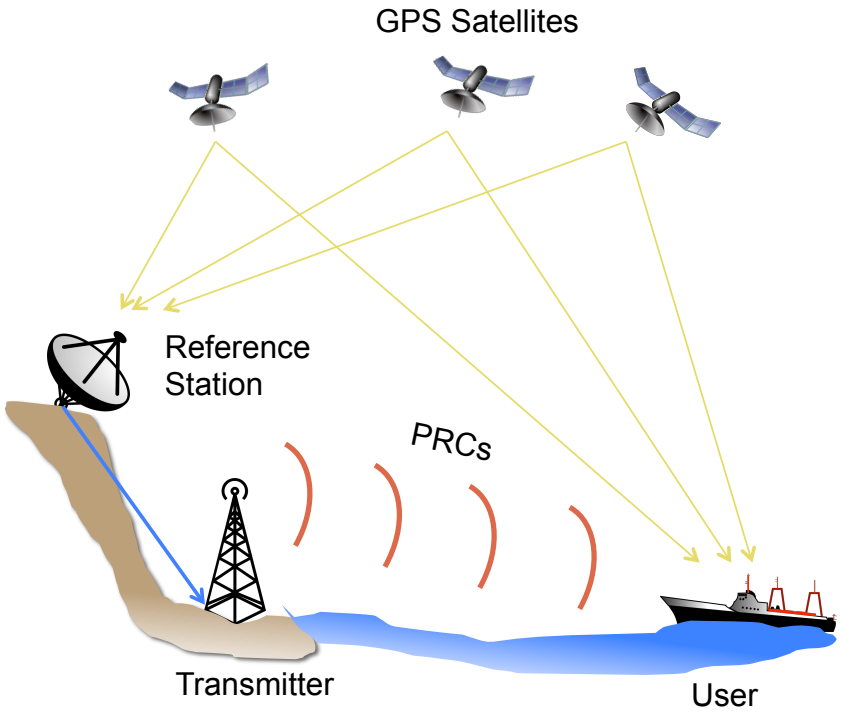

Figure 1.1: Typical DGPS implementation. The reference station receives and calculates pseudoranges to visible GPS satellites, then determines the error in each satellite's pseudorange by comparison to the reference site's surveyed position. The error corrections (pseudorange corrections, or PRCs) are then broadcast from the transmitter to the user, who adds the PRCs to his own calculated pseudoranges.

tronic navigation signal, LORAN-C, was terminated in 2010, leaving the North American continent with only GPS-based navigation systems [7]. Because a loss of the positioning accuracy provided by DGPS is hazardous to navigation, ensuring robustness and accuracy of the signal is important to both the Coast Guard and the user base.

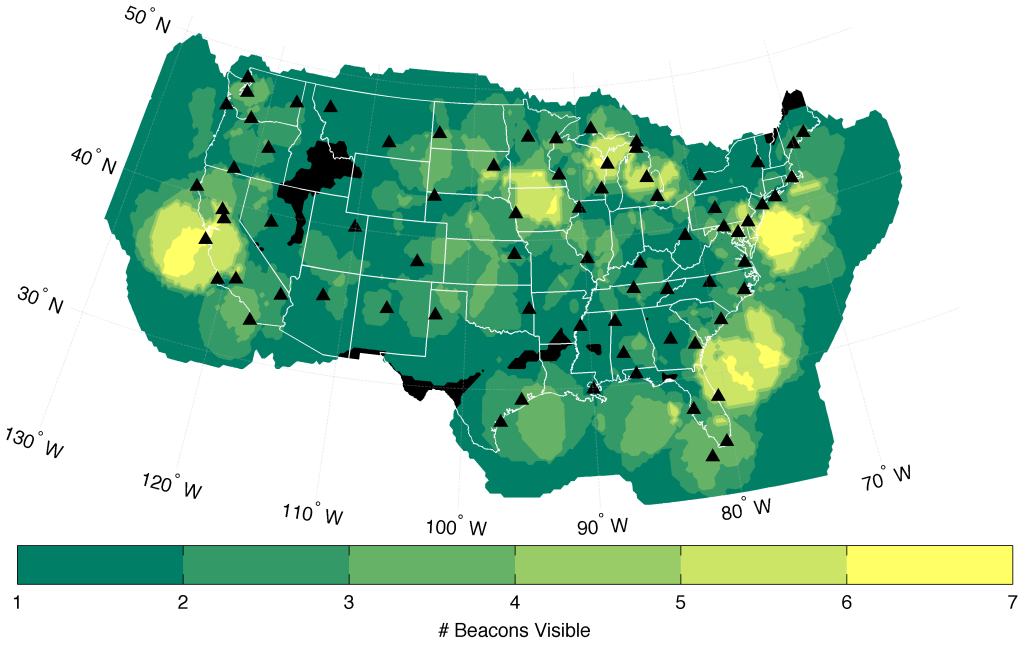

Figure 1.2: Coverage map of the continental U.S.A. displaying number of DGPS beacons available (assuming signal strength greater than $37.5\,\mathrm{dB{\cdot}\mu V{\cdot}m^{-1}}$). Note the typical presence of three or more beacons along the three coasts, Mississippi River, and Great Lakes areas. Coverage area signal strengths were calculated using Millington's model [8].

1.3 Impetus for current work

Networking DGPS broadcasts has the potential to improve both position accuracy and system robustness over the current DGPS solution method. Previous work indicates that positions corrected with a DGPS beacon display a bias away from the beacon used, which increases in magnitude and variation as the user travels farther from the beacon [9]. This research shows that a user's mean position and 95% scatter radius (the radius from the mean bias containing 95% of the user's positions[1]) are nearly linearly proportional to the user's distance from the beacon, representative of spatial decorrelation for DGPS-corrected GPS positions [9]. Figs. 1.3(a) and 1.3(b) show the bias and scatter

[1]Note: this is not the same as another common accuracy measure, R95, which is the radius from true position containing 95% of the user's positions

radius decorrelation, respectively. Currently, a modern DGPS receiver collects and adds the pseudorange corrections from a single beacon to its calculated GPS satellite pseudoranges. Typically, the beacon with the highest signal-to-noise ratio is selected as the beacon to use, which may or may not be the beacon closest to the user [10]. Some DGPS receivers offer the user options as to the beacon selection algorithm, with typical choices including "highest SNR", "closest beacon", and "manual selection". Typical SNR is calculated from the ratio of beacon signal strength and expressed in decibels relative to atmospheric noise level.

While single-beacon solutions currently meet U.S. Coast Guard positioning specifications (ten meters 2DRMS everywhere, and three meters 2DRMS in critical waterways [4]), why not take advantage of all the available correction information? Knowing there is an inherent bias in the user's position because all users employ a single-beacon correction method necessitates evaluation of a better positioning algorithm [9, 11, 12]. Ionospheric SED events have been shown to cause disruptions to wide areas of DGPS service [13, 14], again raising the question: if it's possible that the user's primary beacon is compromised, why not use the information from a wider area of beacon coverage? Because a user's receiver can potentially collect information from two or more DGPS beacons, it is very likely that the use of information from multiple beacons can improve the DGPS user's position accuracy. Users become more confident that their navigation systems are operating properly if they know that the receivers are applying correction information from more than just one beacon. That confidence comes from the systems potentially mitigating sources of error (such as thermal noise, SED effects, and latency error) while simultaneously increasing position accuracy.

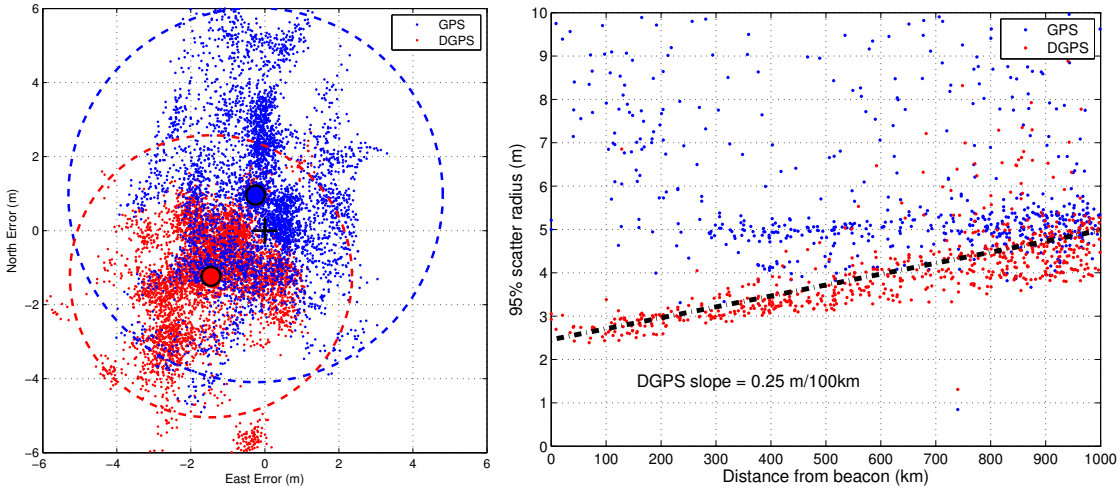

(a) (b)

Figure 1.3: (a) Typical DGPS-corrected GPS position plot for a user, showing a characteristic bias away from the beacon in use. (b) Comparison of DGPS and GPS position 95% scatter radii vs. distance from Saginaw Bay DGPS station (applied to CORS data), showing spatial decorrelation in the form of an increase in 95% scatter radius as the users distance to the beacon increases. Both plots reprinted with permission from [11].

1.4 Discussion of related work

Certain aspects of networked DGPS have been previously examined by a number of authors: discussion of enhanced beacon availability in Europe; existing and novel methods of beacon selection; sources of beacon errors; and several methods of networking DGPS. Below is a brief discussion of those research efforts pertinent to the topic of networking multi-beacon DGPS.

Grant considers various methods for choosing amongst multiple Differential Global Navigation Satellite System (DGNSS) beacons [10]. He considers two obvious methods: choose the nearest beacon by distance to user or the strongest beacon measured by SNR using atmospheric noise only. He also proposes including two other noise sources in the strongest beacon category: a comparison of self to skywave and signals from other beacons. In addition to existing integrity measures, Grant proposes adding time-to-alarm, recognizing that weak stations have latency in data between time-of-arrival, subsequent calculation of DGPS corrections, and broadcast time to user. Grant's work

introduces new sources of error and emphasizes the strategy for selecting appropriate beacons to maximize algorithm productivity.

The research of Last *et al.* into Europe's DGNSS examines the value of DGNSS PRC interpolation and whether this would cause problems for the user [15]. The clock bias question arises from the difference between user and GPS satellite time, which is usually resolved by calculating this difference during locking to the frequency and phase difference. With DGNSS, there is another latency introduced by the time-to-calculation of the reference station, which is typically not of concern since all the latencies introduced by a single station are the same. During their test, the authors assessed the quantity of multi-beacon coverage areas in the United Kingdom, where three beacons was common and seven beacons was the maximum—interestingly, the maximum on the European mainland was 23! Testing consisted of using four DGNSS receivers to record transmissions and an Ashtech receiver locally-placed for actual values, which were recorded for 24 hours. They discovered that the effect of merging different clock biases was minimized due to the averaging and weighting process when combining the PRCs, and therefore was negligible. The combination method weighted the inverse of the user-beacon ranges, resulting in an improvement in correlation between calculated PRC and actual PRC (termed Regional Area Augmentation System, RAAS). Also compared were the solutions computed using single-beacon (23 km away) and RAAS (219, 358, and 419 km away) methods. They find that the single-beacon position solutions are better, but only slightly, suggesting that RAAS solutions might be useful. Their work also suggests that further work should explore a combination of two beacons, and that a RAAS could extend the boundaries of the current DGNSS system.

List of References

[1] *Navstar GPS Space Segment/Navigation User Segment Interfaces*, Global Positioning Systems Directorate Specification IS-GPS-200, Rev. F, Sept. 2011.

[2] *Global Positioning System Standard Positioning Service Performance Standard*, Global Positioning Systems Directorate Specification GPS SPS PS, Sept. 2008.

[3] K. Borre, D. M. Akos, N. Bertelsen, P. Rinder, and S. H. Jensen, *A Software-Defined GPS and Galileo Receiver: a Single-Frequency Approach.* Boston, MA: Birkhäuser, 2007.

[4] *Differential Global Positioning System Broadcast Standard*, United States Coast Guard Manual COMDTINST M16 577.1, Apr. 1993.

[5] *RTCM Recommended Standards for Differential Navstar GPS Service*, Radio Technical Commission for Maritime Services (RTCM) Special Committee No. 104 Standard 2.1, Jan. 1994.

[6] United States Coast Guard Navigation Center. "NDGPS general information." [Accessed: 10 Jan. 2013]. Jan. 2013. [Online]. Available: http://www.navcen.uscg.gov/?pageName=dgpsMain

[7] "Record of Decision (ROD) on the U.S. Coast Guard Long Range Aids to Navigation (Loran-C) Program," *Federal Register*, vol. 75, no. 4, pp. 997–998, Jan. 2010.

[8] G. Millington, "Ground-wave propagation over an inhomogeneous smooth earth," in *Proc. IEE—Part III: Radio and Commun. Eng.*, vol. 96, Jan. 1949, pp. 53–64, doi:10.1049/pi-3.1949.0013.

[9] G. W. Johnson, C. Oates, M. Wiggins, P. F. Swaszek, A. T. Page, R. J. Hartnett, and A. B. Cleveland, "USCG NDGPS accuracy and spatial decorrelation assessment," in *Proc. 2012 Global Navigation Satellite Syst. Inst. Navigation (ION GNSS 2012)*, San Diego, CA, Sept. 2012, pp. 3665–3674.

[10] A. J. Grant, "Availability, continuity, and selection of maritime DGNSS radiobeacons," Ph.D. dissertation, Sch. Informatics, Univ. Wales, Bangor, United Kingdom, 2002.

[11] G. W. Johnson, P. F. Swaszek, and R. J. Hartnett, "Performance assessment of the recent NDGPS recap—initial simulation results," in *Proc. 2012 Int. Tech. Meeting Inst. Navigation (ION ITM 2012)*, Newport Beach, CA, Jan. 2012, pp. 1369–1376.

[12] L. Sjöberg, G. Hedling, and A. Tiwari, "A wide area solution that takes advantage of the existing radio broadcast and national geodetic network infrastructure," in *IEEE Position Location Navigation Symp. (IEEE PLANS 1996)*, Atlanta, GA, Apr. 1996, pp. 596–603, doi:10.1109/PLANS.1996.509133.

[13] S. Skone and A. Coster, "Performance evaluation of DGPS versus SBAS/WADGPS for marine users," in *Proc. 20th Int. Tech. Meeting Satellite Division Inst. Navigation (ION GNSS 2007)*, Fort Worth, TX, Sept. 2007, pp. 1904–1913.

[14] S. Skone, R. Yousuf, and A. Coster, "Combating the perfect storm: improving marine Differential GPS accuracy with a wide-area network," *GPS World*, pp. 31–38, Oct. 2004.

[15] D. Last, A. Grant, A. Williams, and N. Ward, "Enhanced accuracy by regional operation of Europe's new radiobeacon differential system," in *Proc. 15th Int. Tech. Meeting Satellite Division Inst. Navigation (ION GPS 2002)*, Portland, OR, Sept. 2002, pp. 2723–2732.

CHAPTER 2

Networked DGPS Methods

2.1 Background

We considered various methods of networking DGPS, both previously proposed and novel, for inclusion into this research. The main criterion for evaluation was the ready availability of information to a typical user: namely, could a considered algorithm be easily employed on existing equipment? Candidate algorithms should be mathematically simple to perform and dependent only on the data broadcast through the existing DGPS. These two requirements ensure that the algorithm is capable of deployment on low-cost hardware and does not require any further changes to infrastructure for the user and or the DGPS provider. In the case of this research, only DGPS within the United States is considered. While Mueller's minimum-variance algorithm showed promising performance, it was excluded from this research because station-specific beacon characterization data are not available [1].

2.2 Pseudorange calculation and correction

DGPS-corrected pseudoranges are calculated by the simple subtraction of the correction to the calculated pseudoranges.

$$\mathring{\rho}_s = \mathrm{c}\,(\delta_{\mathrm{tr}} - \delta_{\mathrm{rcv}}) \tag{2.1}$$

$$\hat{\rho}_s = \rho_s - \mathrm{c}\,(\delta_{\mathrm{tr}} - \delta_{\mathrm{rcv}}) \tag{2.2}$$

$$= \rho_s - \mathring{\rho}_s \tag{2.3}$$

where $\mathring{\rho}_s$ is introduced as the PRC for satellite s, ρ_s denotes the true range to satellite; $\hat{\rho}_s$ denotes the calculated pseudorange; c denotes the speed of light ($2.997\,924\,58 \cdot 10^8\,\mathrm{m{\cdot}s^{-1}}$); and $\delta_{\mathrm{tr}} - \delta_{\mathrm{rcv}}$ denotes the difference between the transmitted and received times (s) introduced by the combination of a number of errors. The sources and description of these errors are discussed further in Chapter 4.

2.3 Networking algorithms

Two categories of combining DGPS beacon PRCs are considered: (1) to weight the PRCs using some criteria and (2) to recalculate the PRC based on a beacon grouping's spatial orientation to the user. The first category includes three algorithms, each using different criteria to weight each available satellite's PRC, where the PRC is weighted as such:

$$\mathring{\rho}_s = \sum_{b=1}^{B} a_b \mathring{\rho}_{b,s} \tag{2.4}$$

where s denotes the target satellite, a_b is the weight a applied to beacon b, and B is the total number of beacons available.

2.3.1 Simple averaging

The first DGPS networking algorithm considered is an average of the available beacons. In particular, the pseudorange corrections are weighted equally and a single PRC is applied to the satellite at that time. This weighting is described as:

$$a_b = \frac{1}{B} \tag{2.5}$$

where B, again, is the available number of beacons. This algorithm is proposed with the assumption that a region of tightly-spaced beacons will broadcast relatively similar pseudorange corrections and this method might serve as a simple way to remove small perturbations between the beacons' PRCs.

2.3.2 Inverse-range

The second DGPS networking algorithm considered is based on weighting the PRCs by the inverse of the range from the user to the beacon. This method of combining multiple beacons was first proposed by Last *et al.* in [2], with the intent of minimizing the effect of beacons distant from the user's position. The user's position may, in this case, be established *a priori* via a raw GPS fix, since the distances in question are typically expressed in kilometers, such that the error in a rough GPS fix is negligible in

comparison. The weights for the inverse-range method are calculated as:

$$a_b = \frac{1}{r_b}\left(\sum_{k=1}^{B}\frac{1}{r_b}\right)^{-1} \tag{2.6}$$

where r_b is the range from the user to beacon b, and the second term normalizes the weights.

2.3.3 Inverse-range-squared

The third DGPS networking algorithm considered is based on weighting the PRCs by the inverse of the range-squared from the user to the beacon. We propose this new method in order to further reduce the effects of long-distance beacons on the user's position. Particularly, since it is known that a user in close proximity to a beacon (less than about 50 km) will have a small bias length and scatter radius when applying a single DGPS beacon's corrections that particular beacon's weight should, therefore, dominate within both range-based algorithms [3]. As with the inverse-range method, the user's position is established *a priori* with a GPS fix. The weights for the inverse-range-squared algorithm are calculated as:

$$a_b = \frac{1}{r_b^2}\left(\sum_{k=1}^{B}\frac{1}{r_b^2}\right)^{-1} \tag{2.7}$$

where the variables are represented in the same manner as the inverse-range method.

2.3.4 Spatial linear interpolation (SLI)

The fourth and final DGPS networking algorithm considered is based on fitting a hyperplane to the known locations and distances of the beacons relative to the user's location. In the case of three beacons, this method describes linear interpolation between three points and the user's general location. We propose this new method because it takes into account the spatial geometry and orientation of the beacon grouping (i.e.: ranges and azimuths to the beacons) relative to the user, which, as described previously, are a factor in DGPS-user position bias. Because the precise locations of all the U.S. DGPS beacons are known, this information may be stored so the user may apply received PRCs to a grid representing the local area. The beacons' positions are transferred onto

the grid as the x, y coordinates and the PRCs assume the z values. The three points that are created form the basis of an SLI hyperplane, which is evaluated at the user's assumed location (which, again, may be provided through a rough GPS fix). The SLI algorithm is described by:

$$\mathring{\rho}_s = ax + by + c\Big|_{\boldsymbol{p}_\mathrm{R}} \tag{2.8}$$

$$\boldsymbol{p}_b = \begin{bmatrix} D_\mathrm{N} \\ D_\mathrm{E} \\ \mathring{\rho}_{b,s} \end{bmatrix} \tag{2.9}$$

where x and y denote the grid coordinates, akin to longitude and latitude, a, b, and c describe the coefficients of the equation of the plane (note: this a is unrelated to the weighting coefficient, a_i) through the three beacon-PRC points ($\boldsymbol{p}_b$), $\boldsymbol{p}_\mathrm{R}$ is the position vector of the rover (the user)—by convention here, the point (0, 0), and D_N and D_E are the great circle distances North and East of the user. The plane equation coefficients, a, b, and c are given by:

$$\Delta = x_1(y_2 - y_3) - x_2(y_1 - y_3) + x_3(y_1 - y_2) \tag{2.10}$$

$$a = (-\Delta)^{-1}\big((z_1 - z_2)(x_1 - x_3) - (z_1 - z_3)(x_1 - x_2)\big) \tag{2.11}$$

$$b = (+\Delta)^{-1}\big((z_1 - z_2)(y_1 - y_3) - (z_1 - z_3)(y_1 - y_2)\big) \tag{2.12}$$

$$c = z_1 - ax_1 - by_1 \tag{2.13}$$

Spatial linear interpolation computational methods

Because the area of interest is linearized in x, y and z, the pseudorange correction may be calculated directly with either vector or linear algebra. Selection of an appropriate computation method is dependent on the requirements of the user and may depend on computing capabilities.

Vector method

This method calculates the user's PRC by manipulating the position-PRC vectors at each beacon described in (2.9):

$$\boldsymbol{n} = (\boldsymbol{p}_1 - \boldsymbol{p}_3) \times (\boldsymbol{p}_2 - \boldsymbol{p}_3) \tag{2.14}$$

$$p_0 = -\boldsymbol{p}_3^\top (\boldsymbol{p}_1 \times \boldsymbol{p}_2) \tag{2.15}$$

$$\mathring{\rho}_s = -\frac{p_0}{\boldsymbol{n}_z} \tag{2.16}$$

where $\boldsymbol{n}$ is the vector normal to the plane, $(\times)$ is the cross product of two vectors, p_0 is the pseudorange correction at a point on the plane at $(0, 0)$, $\boldsymbol{p}_1$ through $\boldsymbol{p}_3$ represent the 3-dimensional position-PRC vectors of the beacons, relative to the user position at $(0, 0)$, and $\boldsymbol{n}_z$ represents the z component of the normal vector.

Linear algebra method

This method calculates the user's PRC by rearranging the plane equation such that it satisfies a set of simultaneous linear equations, then solved at the user's location:

$$\underbrace{\begin{bmatrix} z_1 \\ z_2 \\ z_3 \end{bmatrix}}_{\boldsymbol{z}} = \begin{bmatrix} ax_1 + by_1 + c \\ ax_2 + by_2 + c \\ ax_3 + by_3 + c \end{bmatrix} = \underbrace{\begin{bmatrix} x_1 + y_1 + 1 \\ x_2 + y_2 + 1 \\ x_3 + y_3 + 1 \end{bmatrix}}_{\boldsymbol{A}} \underbrace{\begin{bmatrix} a \\ b \\ c \end{bmatrix}}_{\boldsymbol{c}} \tag{2.17}$$

$$\boldsymbol{c} = \boldsymbol{A}^{-1}\boldsymbol{z} \tag{2.18}$$

$$\mathring{\rho}_s = \boldsymbol{x}^\top \boldsymbol{z}\Big|_{\boldsymbol{x}^\top = [0,0,1]} \tag{2.19}$$

where $\boldsymbol{A}$ is non-singular and represents the beacon x, y position matrix, $\boldsymbol{c}$ represents the vector containing the coefficients of the plane equation $[a, b, c]^\top$, $\boldsymbol{z}$ represents the vector containing the pseudorange correction values, and $\boldsymbol{x}$ represents the user's position-PRC vector at the origin.

Weighting coefficients

So as to conform to the convention of (2.4), the coefficients of the SLI algorithm may be obtained by rearranging the algebraic forms of the equation of the plane, (2.11) to (2.13), such that the PRC weighting coefficients, a_i, correspond to their respective beacon PRCs, z_i:

$$a_1 = \Delta^{-1}\big((y_2 - y_3) - (x_2 - x_3) + (x_2 y_3 - x_3 y_2)\big) \tag{2.20}$$

$$a_2 = \Delta^{-1}\big((y_1 - y_3) + (x_1 - x_3) - (x_1 y_3 - x_3 y_1)\big) \tag{2.21}$$

$$a_3 = \Delta^{-1}\big((y_1 - y_2) - (x_1 - x_2) + (x_1 y_2 - x_2 y_1)\big) \tag{2.22}$$

List of References

[1] T. Mueller, "Minimum variance network DGPS algorithm," in *IEEE Position Location Navigation Symp. (IEEE PLANS 1994)*, Las Vegas, NV, Apr. 1994, pp. 418–425, doi:10.1109/PLANS.1994.303344.

[2] D. Last, A. Grant, A. Williams, and N. Ward, "Enhanced accuracy by regional operation of Europe's new radiobeacon differential system," in *Proc. 15th Int. Tech. Meeting Satellite Division Inst. Navigation (ION GPS 2002)*, Portland, OR, Sept. 2002, pp. 2723–2732.

[3] G. W. Johnson, P. F. Swaszek, and R. J. Hartnett, "Performance assessment of the recent NDGPS recap—initial simulation results," in *Proc. 2012 Int. Tech. Meeting Inst. Navigation (ION ITM 2012)*, Newport Beach, CA, Jan. 2012, pp. 1369–1376.

CHAPTER 3

Simulating Networked DGPS

3.1 Applicable software

We performed the simulator testing on a Spirent GSS8000 GNSS simulator, which was governed by the SimGEN software package. Data were logged in SimGEN and post-processed in the MATLAB environment, using L3NAV Systems' GPS toolbox. We replace the word "user" with a new term "rover" when discussing a simulated vehicle's position, so as to clearly differentiate between the simulator vehicle and the real-life equipment user.

3.2 Simulator testing overview

We tested the effectiveness of the various networked DGPS algorithms was performed on a Spirent GSS8000 simulator. This GNSS simulator provided a reliable and verbose output log of the settings and states of the variables-of-interest, such as distinct satellite ranges, pseudoranges, ionospheric and tropospheric offsets. Because southeastern New England contains good multi-beacon coverage (sufficient quantity and spatial variety of DGPS beacons) and a balanced mix of land and water that forms the entrance to New York harbor, we chose this area for the testing region. We configured the simulator to best compare the networking algorithms against each other; in this vein, the simulator was set to produce only ionospheric and tropospheric delays. Ionospheric effects were generated using the Klobuchar model; tropospheric effects were generated using the NATO STANAG 4294 model. The surface refractivity index was set to the recommended value of 324.8 [1]. Error modeling with thermal and spurious noise sources is outside the scope of this thesis and is part of future work. Receiver-GPS clock bias was turned off, and the rover maintained a static position for the duration of each test. All simulations used the World Geodetic System 1984 geodetic reference ellipsoid (WGS84) and rover reference positions of 0 m altitude for the sake of simplicity.

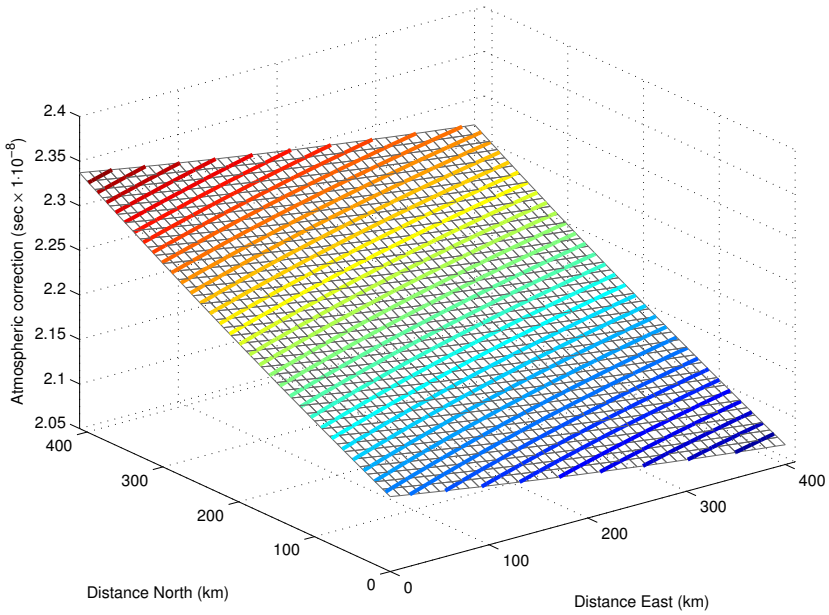

Figure 3.1: Total atmospheric correction (ionospheric + tropospheric error terms) for SV 22 observed across 400 km by 400 km area over New England during GNSS simulation. This is referenced in this thesis as the "actual PRC" plot.

First, the simulator was used to produce a representation of the atmospheric offsets at a single time, across the New England region. The New England area tested was a grid originating with its southwest point at 40.0°N, 74.5°W (approximately Joint Base McGuire-Dix-Lakehurst, located in northeast New Jersey) and advancing approximately 400 km north and east. The area chosen encompassed the DGPS beacons of interest, with the intent of determining the appearance and behavior of the atmospheric corrections over a geographic area. Data points were collected every 10 km north and east from the origin for the same time. This representation provides a baseline for comparing the suitability of each networking algorithm. Fig. 3.1 shows the grid and contours of the simulation for a single satellite; of particular note is the near-planar behavior over the region of interest.

The second simulator test plotted the position solutions calculated by the networking algorithms over a 24-hour period and specific DGPS beacon groups. Two beacon groups were selected to be "visible" to the rover on the basis of their spatial geometries. Group

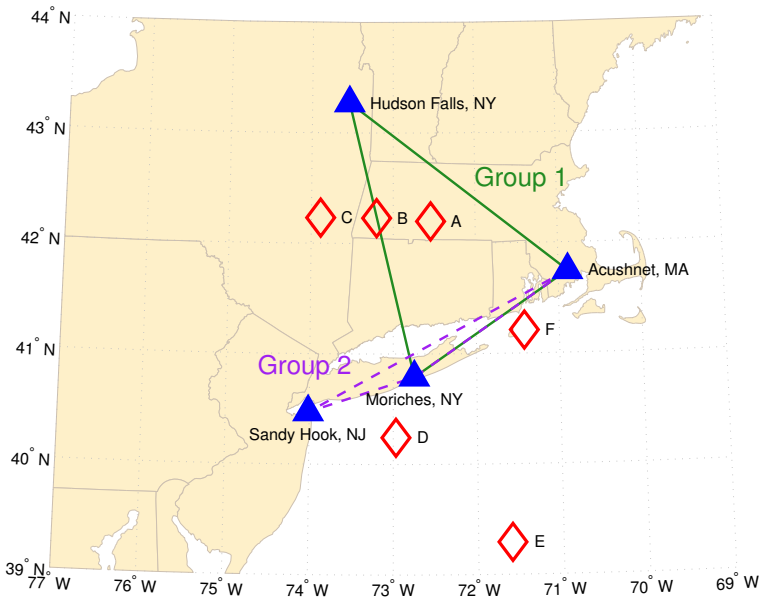

Figure 3.2: Map of simulator testing locations (red diamonds) and DGPS beacons (blue triangles), with beacon groups labeled. Lambert projection.

1 was intended to represent the region's actual atmospheric effects most accurately, and was comprised of a widely-spaced beacon group including Acushnet, MA; Hudson Falls, NY; and Moriches, NY. The Group 1 beacon geometry could be considered as "optimal" to a user because it is well-spaced geographically. Group 2 was intended to be a "realistic" set of beacons that might be typically visible to a marine user, comprised of a nearly-linear beacon group including Acushnet, MA; Moriches, NY; and Sandy Hook, NJ. Rover positions were labeled "A" through "F", and were chosen to place the rover and beacons in unique and interesting configurations, such as: "optimal"—rover in the center of the beacon triangle, rover between two beacons, and rover outside the beacon triangle. Fig. 3.2 indicates the beacon positions, beacon group outlines, and rover static positions used during testing.

In addition to the group-point test locations, an "operational" test was performed intended to replicate the kind of transit through Long Island Sound (LIS) that a mariner might undertake. This test is also designed to showcase the performance of the network-

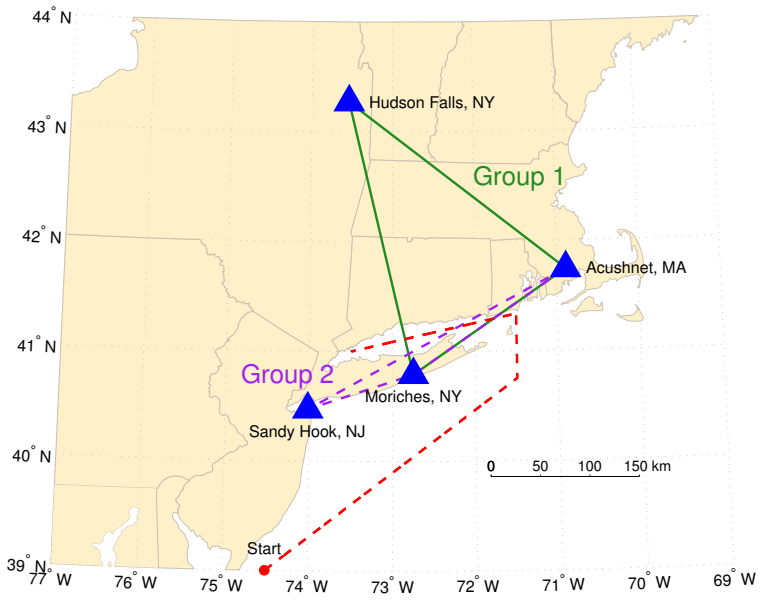

Figure 3.3: Map of a mariner's Long Island Sound transit, as an operational test, on the simulator. Lambert projection.

ing algorithms as the rover passes through a variety of distances, azimuths, and spatial orientation vectors from the beacon groupings. Fig. 3.3 shows this transit.

In order to understand the behavior of each networking algorithm, visualizations were generated using the Group 1 beacon set and the same geographic region and similar time window represented in Fig. 3.1. Fig. 3.4 shows the beacon grouping and associated PRCs overlaid on the PRC solution for each networking algorithm. Fig. 3.5 shows the SLI algorithm's behavior overlaid on the "actual PRC" plot from Fig. 3.1 (in gray mesh), as well as rover position D, demonstrating how the SLI hyperplane is extrapolated to the rover's position. Here, a 100 ms time difference is introduced so that the difference between the "actual PRC" grid and the SLI hyperplane may be observed more clearly as a slight vertical offset between the two.

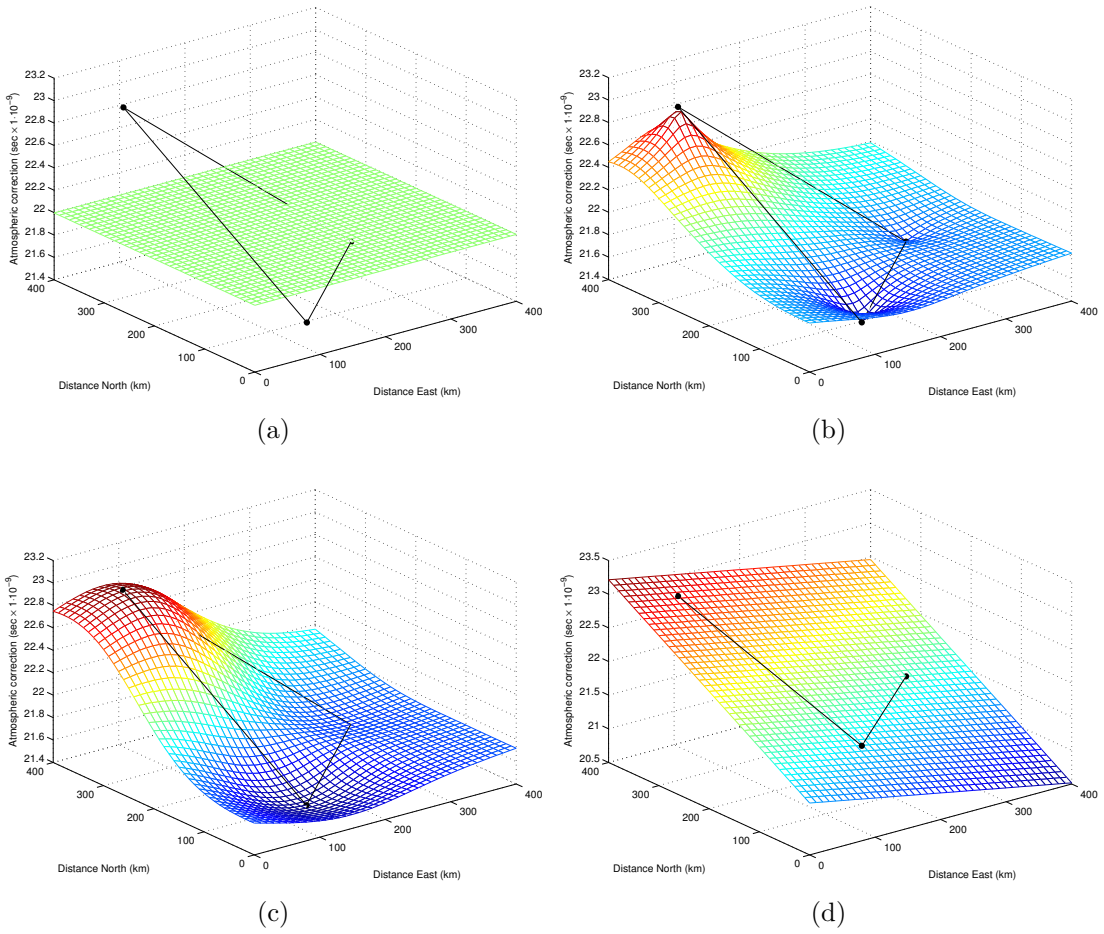

Figure 3.4: Representations of the networking methods, plotted with respect to the area covered by Fig. 3.2 and Group 1 beacons: (a) simple-averaging, (b) inverse-range, (c) inverse-range-squared, (d) spatial linear interpolation.

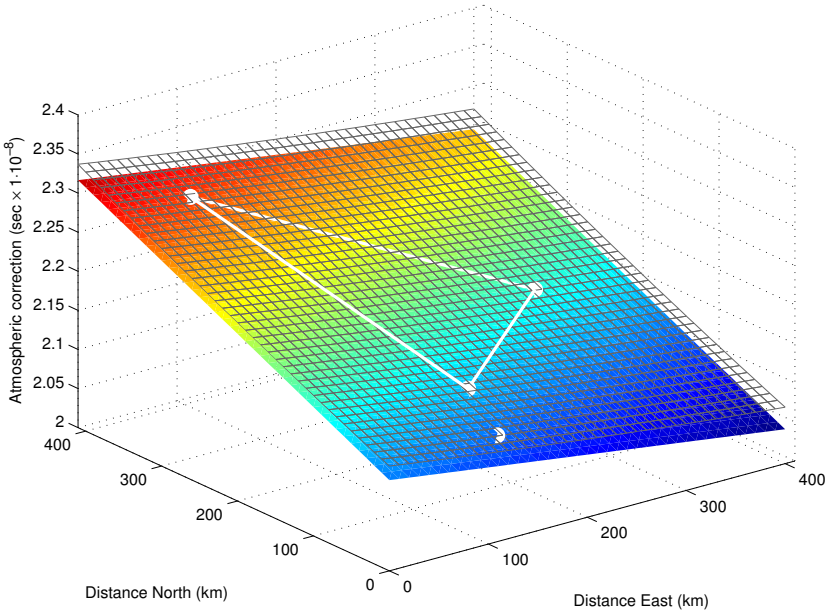

Figure 3.5: Representation of SLI's hyperplane (colored) overlaid on the "actual PRC" plot from Fig. 3.1 (gray grid), with DGPS beacon triangle and rover position D plotted in white on the SLI hyperplane.

3.3 Simulator testing results

When evaluating performance, the networking algorithms should be compared against each other and then again to single-beacon position solutions. Of particular interest are three values: (1) the time-averaged position bias length; (2) the radius containing 95% of the position solutions from the bias length, termed the scatter radius; and (3) the 2 × distance-root-mean-squared (2DRMS) value for each method's 2-dimensional position solutions. The bias length is the distance between the mean position solution and the true position. The scatter radius, with respect to the bias length, helps determine the precision of the solution method. Note: this is not the commonly-known R95 measure, which describes the radius including 95% of positions with respect to true position. The third measure of performance, 2DRMS, describes a common measure of horizontal accuracy (m), referencing both true position and position precision, given by:

$$2\text{DRMS} = 2\sqrt{\sigma_x^2 + \sigma_y^2} \tag{3.1}$$

where σ_x and σ_y (m) are the standard deviations of the x and y position values, respectively.

The positions for the DGPS beacon groups and rover locations are plotted in Figs. 3.6 through 3.14. Also plotted are the time-averaged bias lengths, denoted with a large dot placed at the center of mass of positions, the 95% radius (denoted with a dotted circle, and the true position (0, 0) point overlaid with thick black crosshairs.

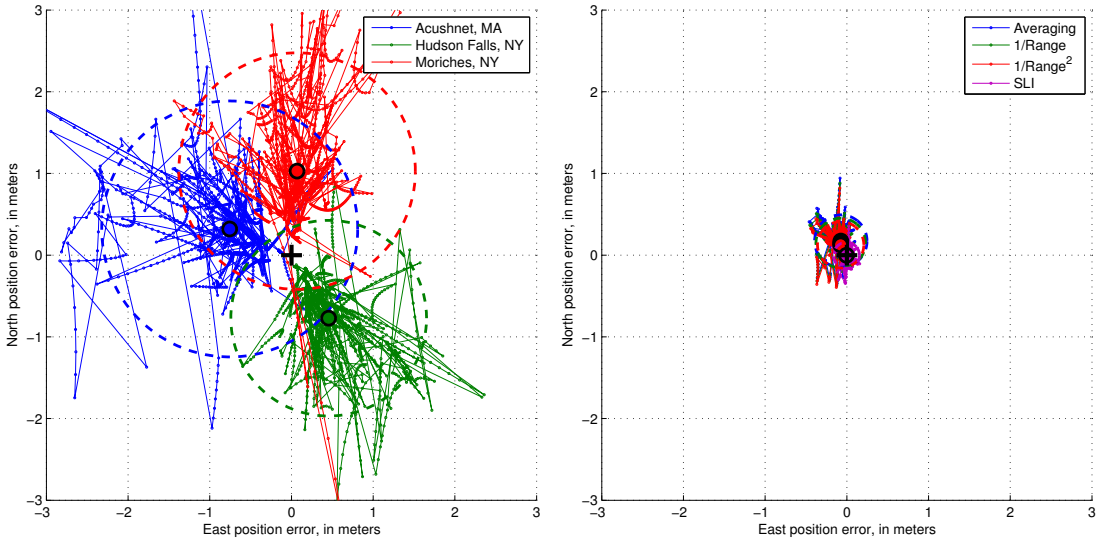

(a) Single-beacon. (b) Networked beacons.

Figure 3.6: Simulator position plots for Beacon Group 1, Rover Position A.

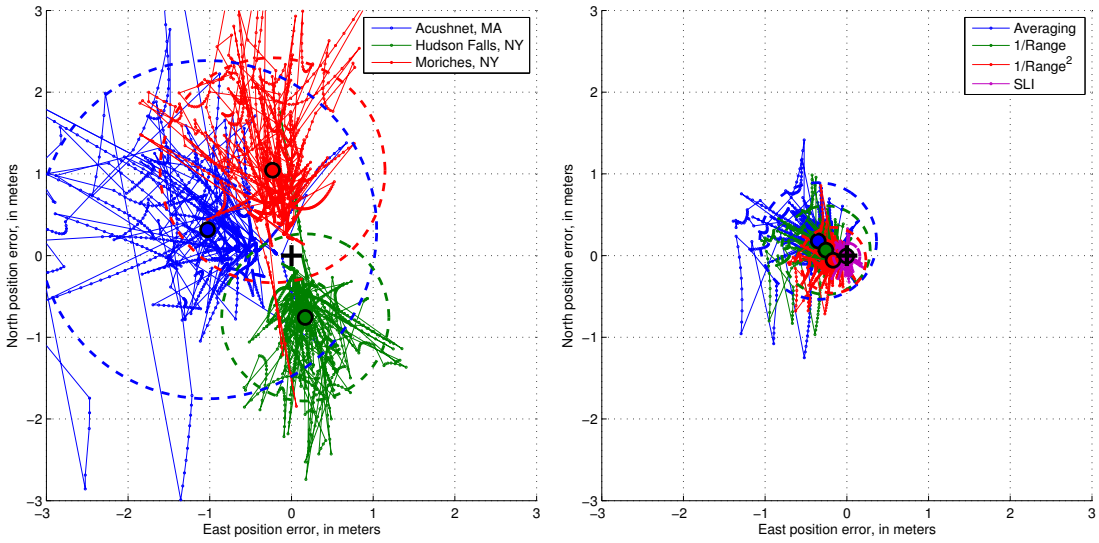

(a) Single-beacon. (b) Networked beacons.

Figure 3.7: Simulator position plots for Beacon Group 1, Rover Position B.

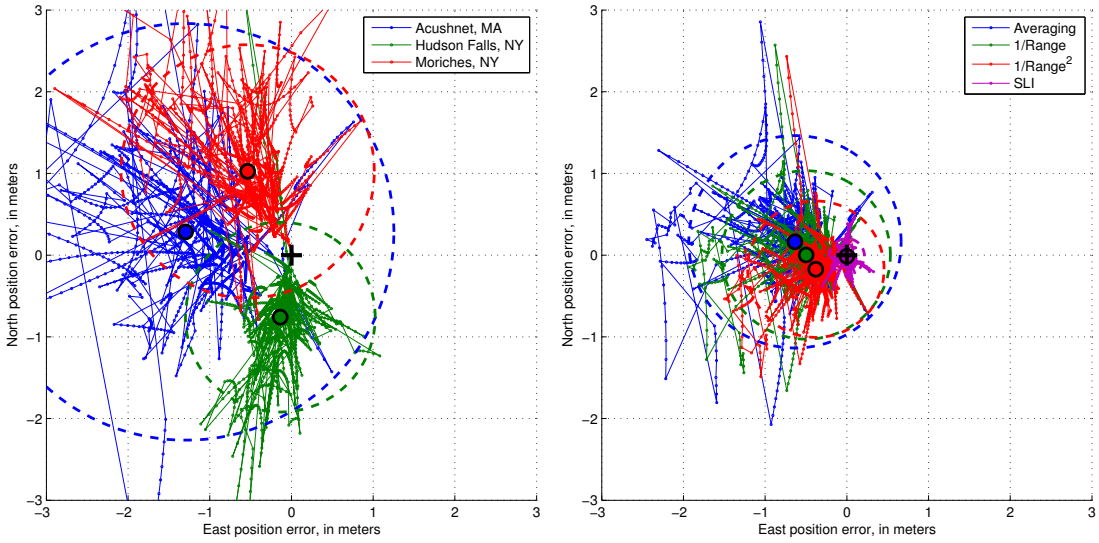

(a) Single-beacon. (b) Networked beacons.

Figure 3.8: Simulator position plots for Beacon Group 1, Rover Position C.

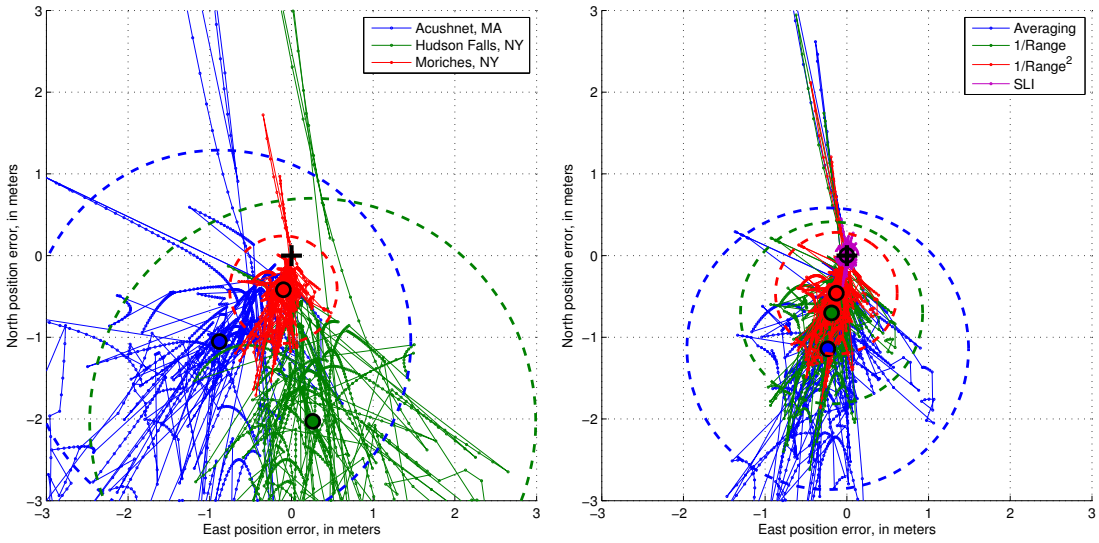

(a) Single-beacon. (b) Networked beacons.

Figure 3.9: Simulator position plots for Beacon Group 1, Rover Position D.

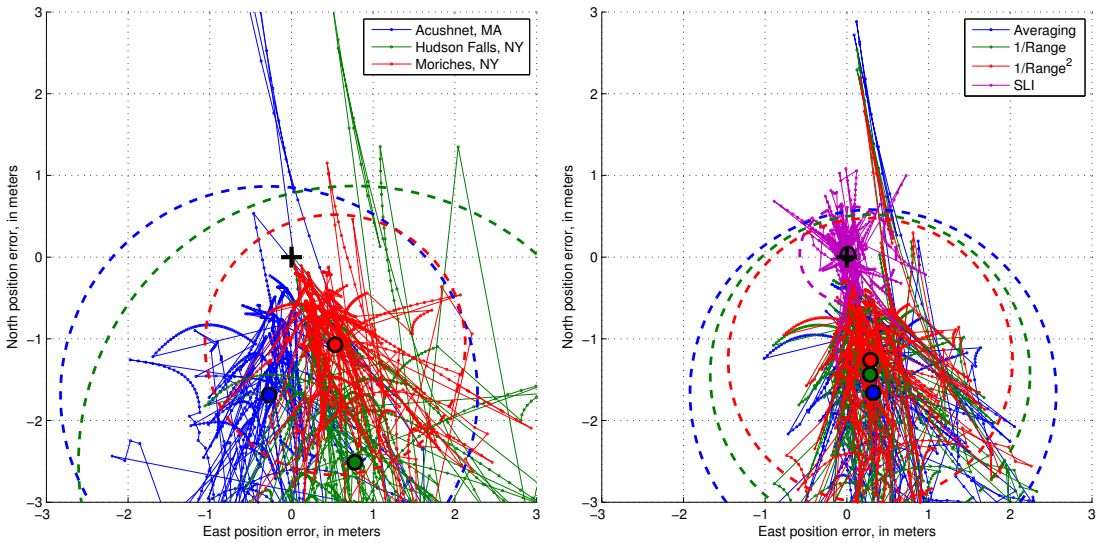

(a) Single-beacon. (b) Networked beacons.

Figure 3.10: Simulator position plots for Beacon Group 1, Rover Position E.

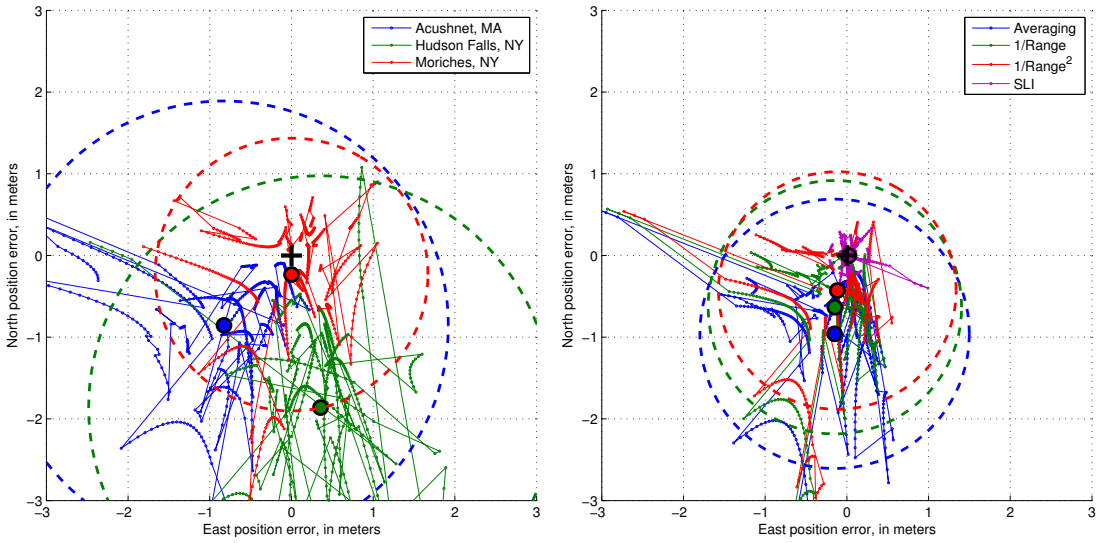

(a) Single-beacon. (b) Networked beacons.

Figure 3.11: Simulator position plots for Beacon Group 1, Rover Transit through Long Island Sound.

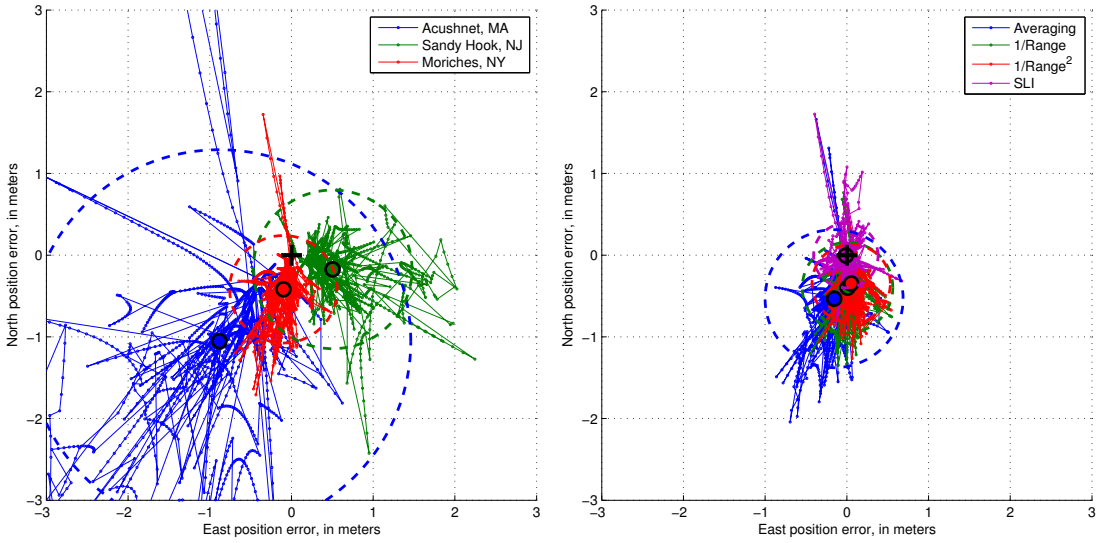

(a) Single-beacon. (b) Networked beacons.

Figure 3.12: Simulator position plots for Beacon Group 2, Rover Position D.

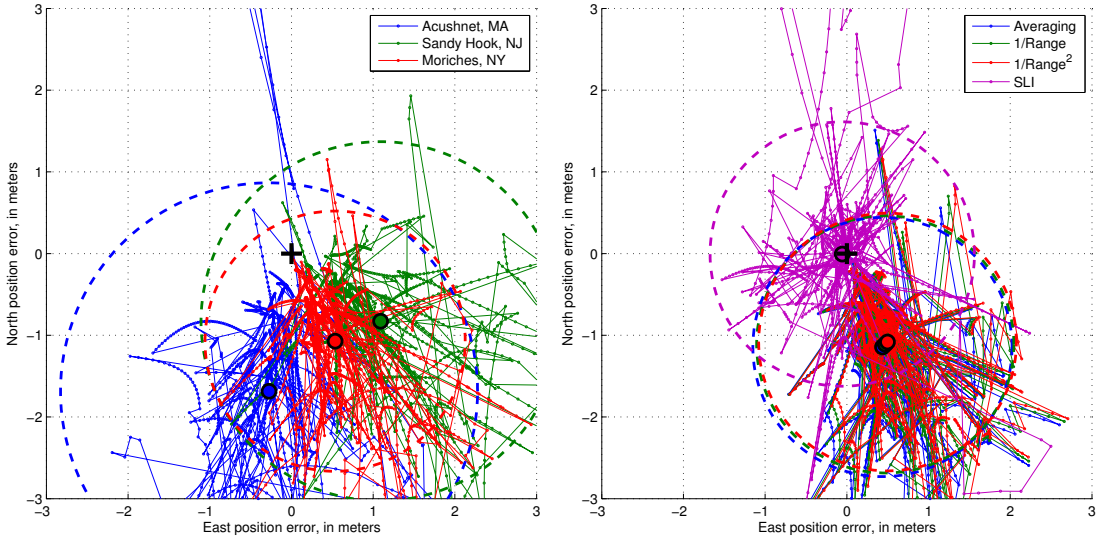

(a) Single-beacon. (b) Networked beacons.

Figure 3.13: Simulator position plots for Beacon Group 2, Rover Position E.

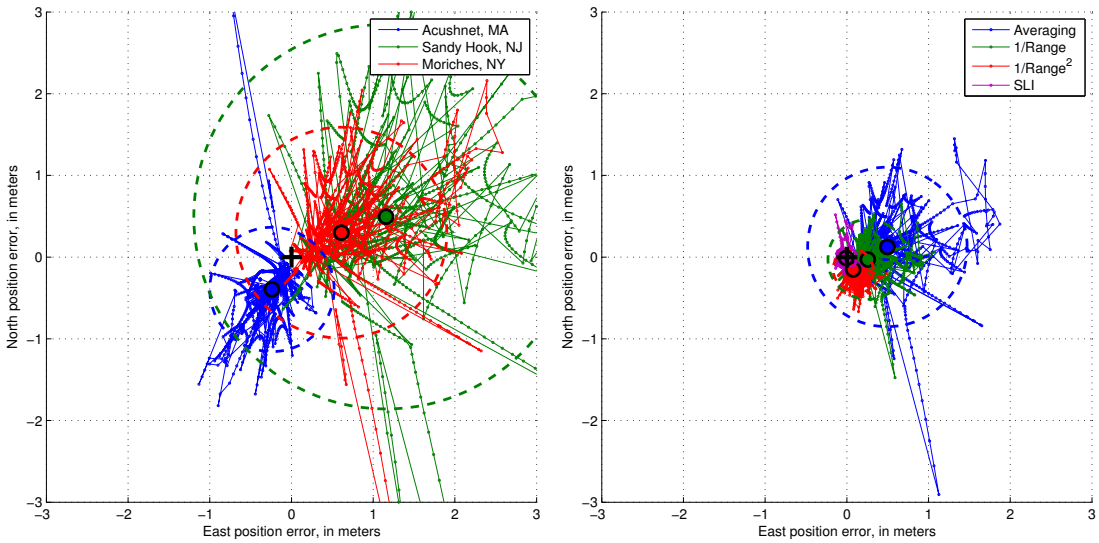

(a) Single-beacon. (b) Networked beacons.

Figure 3.14: Simulator position plots for Beacon Group 2, Rover Position F.

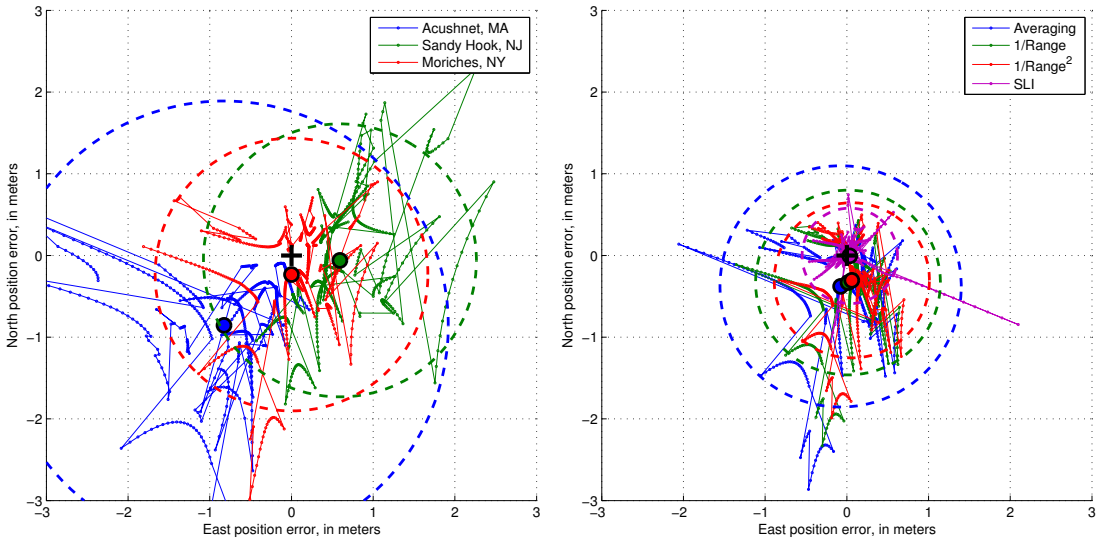

(a) Single-beacon. (b) Networked beacons.

Figure 3.15: Simulator position plots for Beacon Group 2, Rover Transit through Long Island Sound.

3.4 Discussion of simulator results

Fig. 3.16 demonstrates the performance metrics for each of the single-beacon and networked-beacon algorithms, categorized by Group-Point. As expected, the position solutions using corrections from a single DGPS beacon exhibit a bias away from the beacon. This is evident in every test case, with the magnitude of the bias being proportional to the distance away from the beacon. The azimuth of the bias remains constant, as expected. The 95% scatter radii magnitudes are also proportional to the distance away from the beacon. 2DRMS values suffer for those beacons that are far away from the rover. These results corroborate the results from previous work on DGPS bias.

Position solutions generated from networked-beacon algorithms tend to be better than those generated from single-beacon solutions in terms of all three performance metrics. In unique cases where the rover is very close to a beacon (within $\sim$50 km), however, single-beacon solutions perform very similarly to networked-beacon solutions.

Among the four networked-beacon algorithms, the simple-averaging method shows the greatest average values of bias length, scatter radius, and 2DRMS in all cases. We expect this because the simple-averaging method does not take into account the rover's position relative to the beacon, nor the beacon group geometries—it simply accounts for differences in beacon PRCs, which may be useful in an especially noisy environment or when the beacons are very close together. This method exhibits a very obvious bias away from the beacons, only mitigated when the rover is located equidistant to and in the center of all three beacons (see Group 1 Point A, denoted "1A"). As can be surmised, this method's 2DRMS values approximate an average among the three single-beacon 2DRMS values.

In all three metrics, the inverse-range and inverse-range-squared methods performed as well or better than the simple-averaging method. Again, this is to be expected, as these methods de-weight the beacons farther away and thus remove the greater biases (both length and scatter radius) from the position solutions. Consequently, the 2DRMS values for the inverse-range and inverse-range-squared methods are lower than those obtained from simple averaging. Performance of all three metrics is better for the inverse-range-

squared method than for the simple inverse-range because the squaring exponent places a greater emphasis on the closest beacon, even when all three are approximately the same distance from the rover (see position plot for Group 2 Point E). However, in all cases, these two methods exhibit a definite bias away from the beacons, caused by the algorithms' indifference to the beacon geometry. Because of the use of range, these methods are more precise than the simple-averaging method, and retain a slight bias.

The spatial linear interpolation method performs uniquely when compared against both single-beacon and other networked-beacon networking methods. In all cases, the bias length value for this method is smaller than for all other solution methods and the 2DRMS value is almost always the smallest. In any case, the 2DRMS values are significantly lower than almost all single-beacon solutions. This is particularly expected due to the calculated SLI hyperplane closely approximates the near-planar "actual" atmospheric correction grid from the first simulator test. However, the 95% scatter radius exhibits interesting properties when the beacon geometry is nearly linear and the rover is located at a tangent to the beacon line. In this case, the SLI solution is accurate, but with a greater scatter radius, and a 2DRMS value lower than all other solutions. In that peculiar arrangement, SLI's large scatter radius is caused by the orientation of the GPS constellation to the beacon group: as the satellites rise and fall, they come into and disappear from each beacon's view at different times. Because GPS position calculations require at least four satellites and, during this time, this may not be the case, the SLI correction may be, briefly, based entirely on a single satellite, and the position solutions behave with the bias of a single-beacon solution. A satellite count for group-point 1E, the rover-beacon orientation least likely to contain overlapping views of satellites, is shown in Fig. 3.17. However, a GPS constellation of only four visible satellites is unlikely to occur for a long time period except at high latitudes. Based on these results, the SLI method produces, in most cases, the best 2DRMS performance when compared with other networked-beacon and single-beacon solution methods.

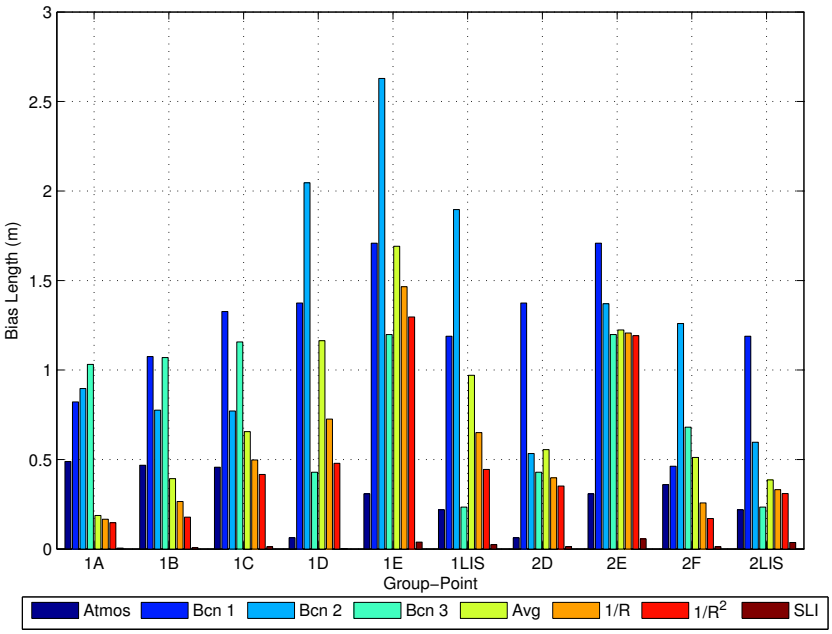

(a) Bias length comparison.

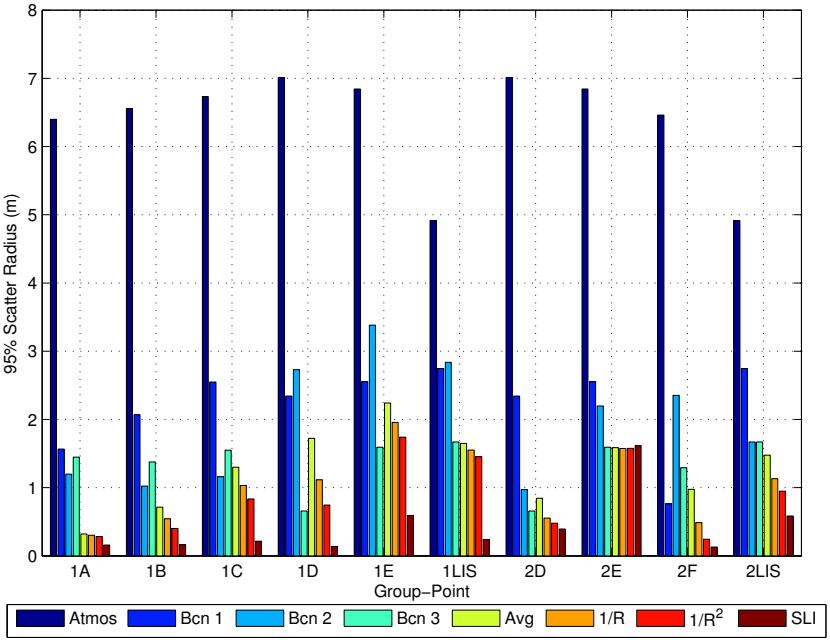

(b) 95% scatter radius comparison.

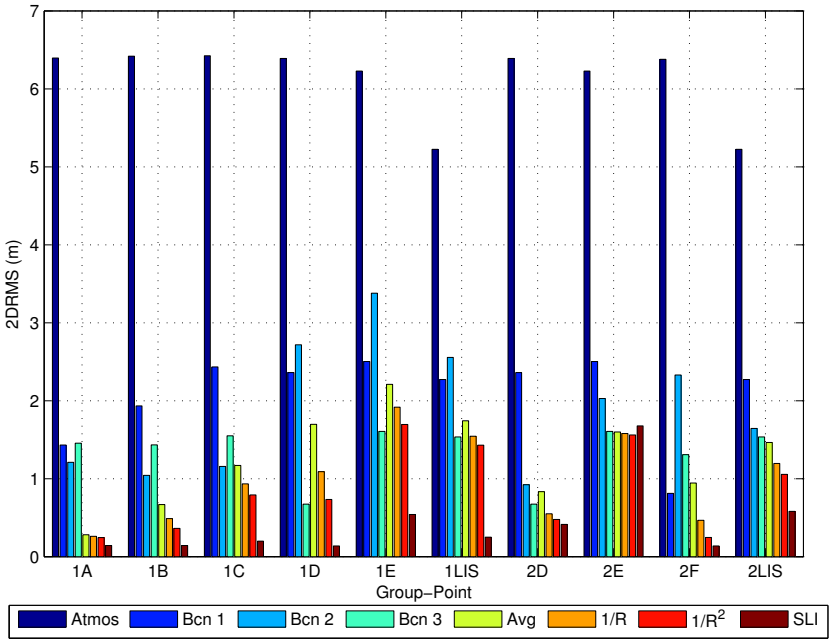

(c) 2DRMS comparison.

Figure 3.16: Bar graphs of bias length, scatter radius containing 95% of the positions, and 2DRMS. Bcn 1 is Acushnet, MA; Bcn 2 is Sandy Hook, NJ or Hudson Falls, NY, as appropriate; Bcn 3 is Moriches, NY; and LIS is Long Island Sound.

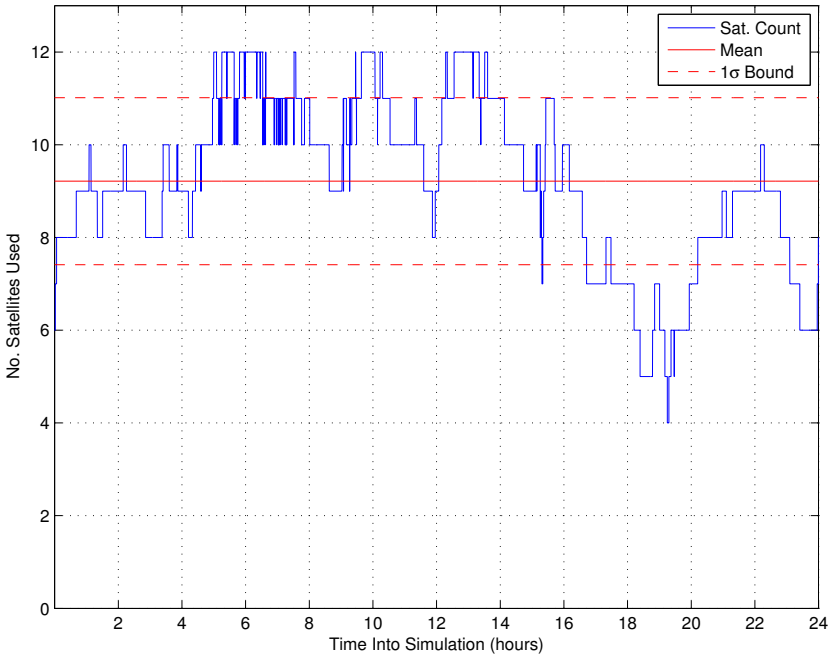

Figure 3.17: Satellite count for Point-Group 1E. The mean SV count is 9.21 and the standard deviation (1σ) is 1.81. The lowest count of usable satellites, four, was present for three minutes out of 24 hours.

List of References

[1] J. P. Collins, "Assessment and development of a tropospheric delay model for aircraft users of the Global Positioning System," M.S. thesis (Tech. Report No. 203), Dept. Geodesy, Geomatics Eng., Univ. New Brunswick, Fredericton, New Brunswick, Canada, Sept. 1999.

CHAPTER 4

Characterizing Networked DGPS Algorithm Performance

4.1 Overview

Thus far, we have introduced the concept of networking DGPS, proposed various methods of combining multiple beacons, and implemented those algorithms at various locations in New England. Because the previous chapter examined distinct points, those results are not sufficient to conclude that networked-beacon solutions offer improved performance over a complete DGPS coverage region. Characterizing the regional behavior of networked DGPS algorithms is necessary to accurately gauge overall performance.

We characterize algorithm behavior by examining two topics. First, we discuss the performance of each algorithm as a function of spatial orientation. We distinguish the performance of each algorithm by testing each algorithm with respect to distance and azimuth from the beacon groupings. Second, we consider each of the assumptions made up to this point. In particular, the effect of noise on performance of networked DGPS is introduced and examined.

4.2 Characterizing spatial behavior

A review of the previous chapter's simulations shows that at each point tested, networking algorithms yield position performance improvements over single-beacon solutions. Moreover, the user's position relative to the beacon grouping and the selection of the beacon grouping somehow impacts the performance of each networking algorithm. Less clear, however, is how the aforementioned factors relate to the performance of the algorithms.

In this section, we seek to characterize algorithm performance by examining the spatial behavior of the networking algorithms on the simulator. In particular, we evaluate 2DRMS performance relative to the spread of the beacon grouping, the beacon grouping geometry, and the user's position relative to the beacon grouping. We test the performance of each networking method over distance and azimuth to the beacon groupings.

4.2.1 Performance versus distance

First, we evaluate algorithm performance versus distance to a beacon grouping. Beacon Group 2 is used to evaluate networked DGPS performance versus user positions located every 50 km from 0 km to 400 km due south and east of Moriches, NY. Fig. 4.1 shows the points tested, in addition to the beacon triangles' centroids, marked with crosshairs.

The first comparison is performance versus distance south relative to the choice of beacon grouping. Fig. 4.2 demonstrates the 2DRMS performance of each algorithm on the run south, broken down by beacon grouping. In this case, the only difference between the two data sets is the choice of the third beacon: where Group 1 uses Hudson Falls, NY, and has a beacon grouping that is geographically diverse, Group 2 uses Sandy Hook, NJ, and has a linearly distributed beacon grouping oriented along a northeast axis. In this scenario, the starting point is nearly co-located with the Group 2 centroid, but is offset from the Group 1 centroid by approximately 120 km. In both graphs, the 2DRMS performance degrades linearly with the user's distance from the Moriches beacon, an effect known as *spatial decorrelation*. We observe the following:

1. Networked Group 1 beacons exhibit a wide variation between the linear spatial decorrelation coefficients, whereas networked Group 2 beacons exhibit similar coefficients.

2. Averaging and range-based networked Group 1 beacons exhibit equivalent or poorer 2DRMS performance than single-beacon solutions using Moriches, NY. Group 1 SLI performs significantly better than all other algorithms.

3. Networked Group 2 beacons offer no significant performance improvement over what is typically the closest beacon (Moriches, NY) in this direction.

4. Group 2 SLI performs slightly better than the single-beacon solution of the closest beacon. In both scenarios, the single-beacon solution with the lowest 2DRMS values provides the upper bound on the SLI algorithm's 2DRMS performance.

The second comparison is performance versus distance east relative to the choice of beacon grouping. Fig. 4.3 demonstrates 2DRMS performance on the run east, again broken down by beacon grouping. In this scenario, we expect that the networked Group 1 beacons will perform similar to the southerly direction and that the networked Group 2 beacons will perform better than in the southerly direction. In this test, we compare the 2DRMS performance runs east and runs south for each beacon grouping.

1. Group 1 east to Group 1 south. In an easterly direction, networked Group 1 beacons performed similarly to those in the southerly direction. That is: the lines of best fit exhibit similar rates of spatial decorrelation. Only the range-based networking algorithms showed an improvement, attributable to the decreased distances from the beacons and a finding that is informative. As expected, the SLI algorithm maintained the lowest spatial decorrelation coefficients.

2. Group 2 east to Group 2 south. For Group 2 beacons in an easterly direction, the networking algorithms exhibit a much greater diversity of spatial decorrelation coefficients than in the southerly direction. Again, SLI provides the lowest 2DRMS values at all distances. Of note is that the 2DRMS performance appears to improve when traveling in a direction better approximating the beacon line.

3. Group 2 east to Group 1 east. The networked DGPS algorithms' performances appear very similar to the Group 1 beacons in the easterly direction. Of interest is that Group 2 SLI shows excellent 2DRMS improvement over single-beacon up to 200 km and Group 1 SLI shows excellent improvement over single-beacon for all distances.

Table 4.1 documents the coefficients for each algorithm's performance over distance, assuming the performance is approximately linear. Nonlinear 2DRMS performance is evident in those single-beacon solutions where the user's azimuth to the beacon changes quickly and are noted as such in table.

In evaluating the 2DRMS performance versus distance, all graphs exhibit a characteristic degradation of performance over distance. This behavior is expected, since

Table 4.1: Linear coefficients of 2DRMS performance over distances south and east from Moriches, NY, by beacon grouping. Nonlinear data is noted and excluded from comparison due to high azimuthal rate of change. Note that beacons 1 and 2 are not located at Moriches, NY, and exhibit an initial offset. Beacon 1 is Acushnet, MA, Beacon 2 is Hudson Falls, NY, for Group 1 and Sandy Hook, NJ, for Group 2, and Beacon 3 is Moriches, NY.

Algorithm	Direction	Group	Coefficient (cm/100 km)	Group	Coefficient (cm/100 km)
Beacon 1	South	1	67.341	2	67.341
Beacon 2	South	1	69.252	2	Nonlinear
Beacon 3	South	1	87.647	2	87.647
Average	South	1	73.643	2	81.109
1/Range	South	1	93.903	2	85.233
$1/\text{Range}^2$	South	1	94.629	2	83.792
SLI	South	1	33.006	2	78.051
Beacon 1	East	1	Nonlinear	2	67.341
Beacon 2	East	1	Nonlinear	2	81.134
Beacon 3	East	1	87.785	2	87.785
Average	East	1	Nonlinear	2	80.183
1/Range	East	1	74.691	2	75.814
$1/\text{Range}^2$	East	1	69.240	2	67.839
SLI	East	1	24.866	2	57.576

single-beacon DGPS solutions exhibit the same characteristic spatial decorrelation (see Chapter 1). If we combine the corrections from each DGPS beacon, we expect to reduce the magnitude of single-beacon spatial decorrelation. We note that single-beacon algorithms using corrections from beacons farther from the user tend to have the highest 2DRMS values. In each scenario, the averaging algorithm exhibited 2DRMS performance comparable to an average of the three beacons' 2DRMS values. Inverse-range and inverse-range-squared algorithms performed better in every case than the simple averaging. The SLI algorithm had the lowest 2DRMS values of all the algorithms, and was bounded from higher 2DRMS values by the best-performing single-beacon solutions. Note that the SLI solution's 2DRMS performance is highly dependent on the beacon geometry and the direction of travel relative to the beacon grouping's axis. We examine this aspect is further in the next section.

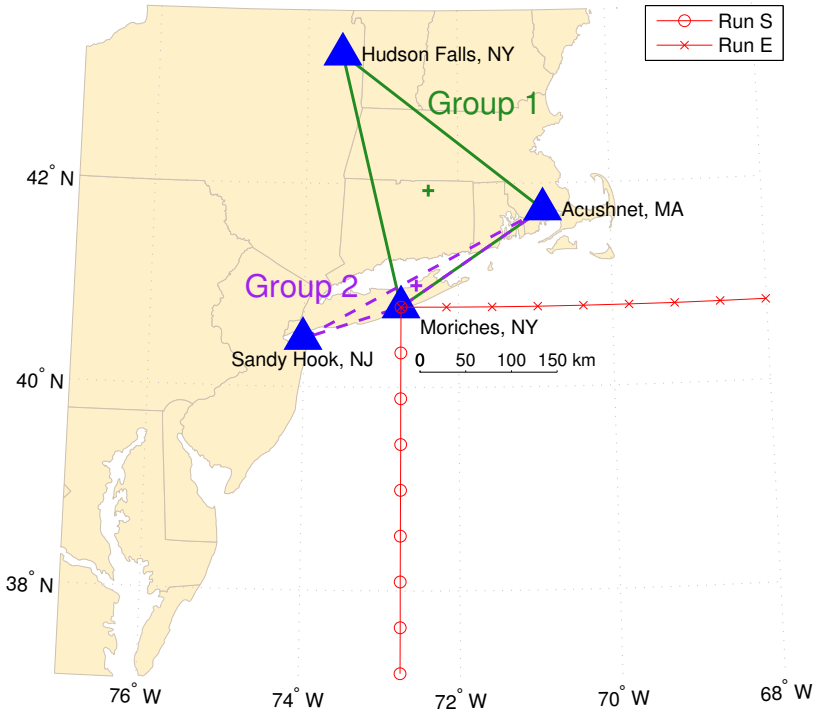

Figure 4.1: 2DRMS performance testing locations due south and east of Moriches, NY. Locations are spaced every 50 km from the origin. Lambert projection.

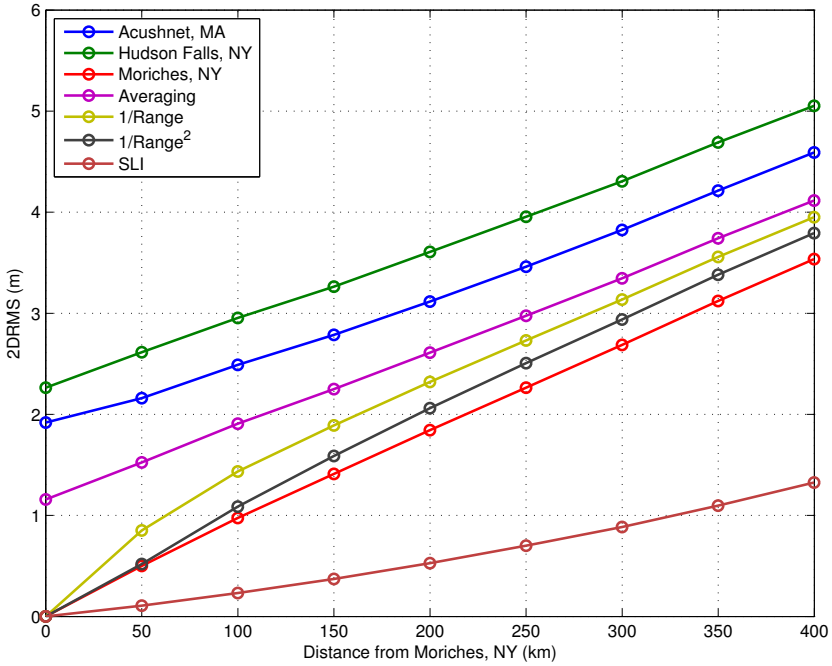

(a) Using Group 1 beacons.

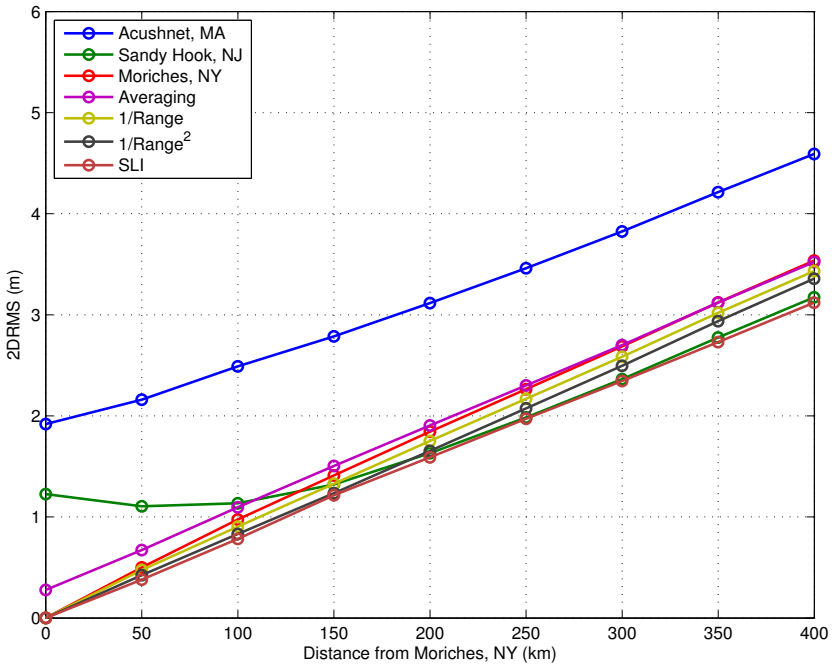

(b) Using Group 2 beacons.

Figure 4.2: 2DRMS performance vs. distance south of Moriches, NY.

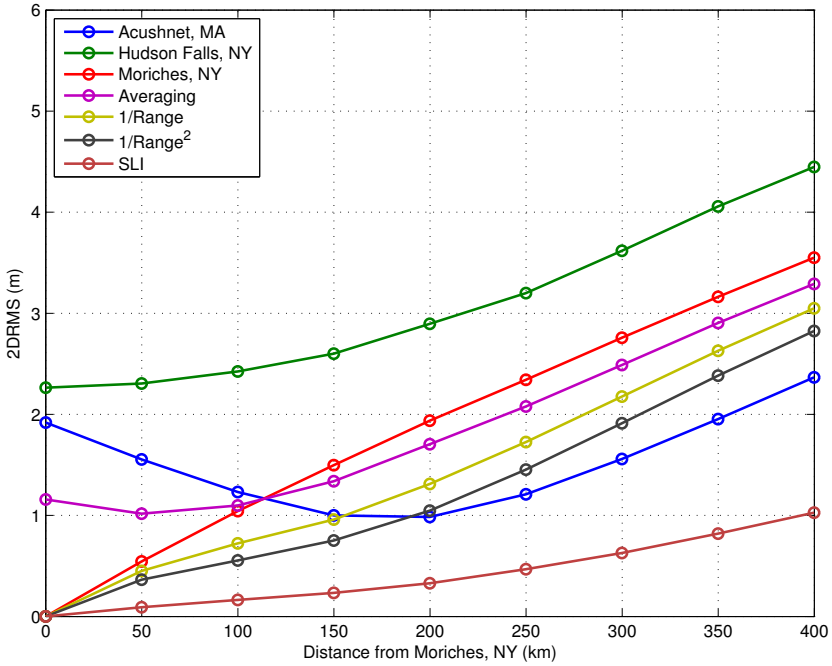

(a) Using Group 1 beacons.

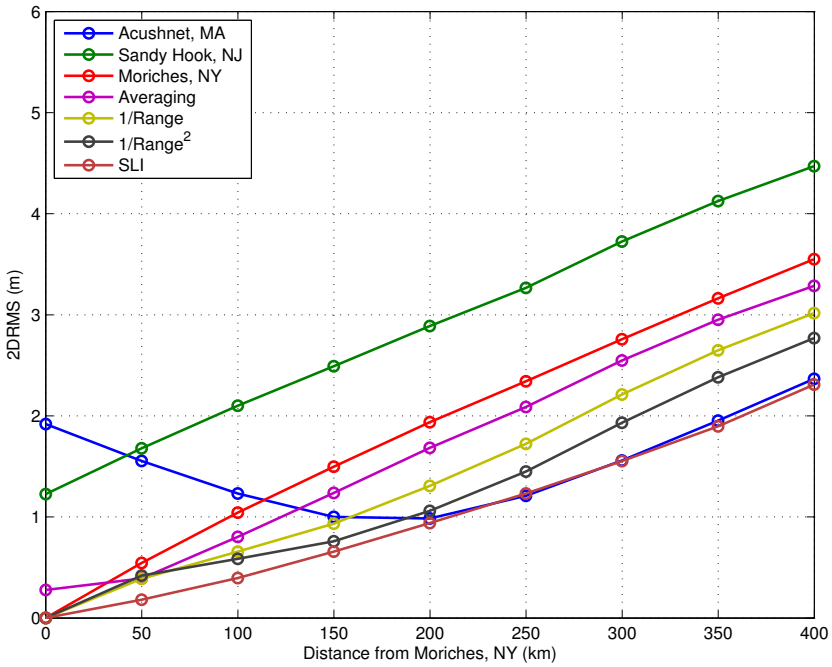

(b) Using Group 2 beacons.

Figure 4.3: 2DRMS performance vs. distance east of Moriches, NY.

4.2.2 Performance versus azimuth

The point-group and performance versus distance tests from Chapter 3 and Section 4.2.1 indicate that networked DGPS 2DRMS performance changes with the user's azimuth to the beacon set. We now evaluate the second performance category: networked DGPS performance versus the user's azimuth to the beacon grouping. Each beacon grouping was tested at locations every 30° from the grouping's centroid at various radii. Beacon grouping 2 was tested at Moriches, NY, because it is approximately co-located with the centroid. Beacon grouping 1 was tested at radii of 200 km and 400 km, and Group 2 was tested at radii of 100 km and 200 km. Figs. 4.4 and 4.6 indicate the geographic locations of the test radials, and include the beacon triangles' centroids marked with crosshairs.

The first scenario considers 2DRMS performance versus azimuth relative to the Group 1 centroid. This establishes a baseline of 2DRMS performance by using a spatially diverse beacon grouping. Figs. 4.5(a) and 4.5(b) plot the 2DRMS performance versus azimuth at radii of 200 km and 400 km, respectively. The networked algorithms have 2DRMS values that are lower than the single-beacon solutions for both radial distances in this scenario. At both distances, the SLI algorithm performs significantly better at all angles than any other correction algorithm. Of interest from Figs. 4.5(a) and 4.5(b) are the following observations:

- The averaging algorithm smoothes the apparent bias directions from the single-beacon solutions.

- The range-based algorithms exhibit the poorest 2DRMS performance along a Northeast axis (angles 240° and 60°), which corresponds to the greatest sum of user distances to each beacon.

- The 2DRMS values of SLI are nearly equal at all angles, suggesting that this algorithm de-weights the proximity of the user to the nearest beacon more so than the other networking algorithms. This behavior is more evident in Fig. 4.5(b).

- In 4.5(b), where the user is well outside of the beacon triangle, the range-based algorithms perform nearly equally to the averaging algorithm. This behavior confirms what can be expected from (2.6) and (2.7), where as $r \to \infty, \boldsymbol{a} \to \left[\frac{1}{3}, \frac{1}{3}, \frac{1}{3}\right]^\top$. Recall that $\boldsymbol{a}$ is the weighting coefficient vector for each beacon.

The second scenario considers 2DRMS performance relative to the beacon geometries for both Group 1 and Group 2, using test locations concentric about Moriches, NY. Fig. 4.6 shows the testing locations both 100 km and 200 km from the Moriches DGPS beacon. Again, because Moriches, NY, is very close to the Group 2 centroid, the difference between these positions and their 2DRMS values is negligible, so Moriches may be considered equivalent to the triangle centroid. 2DRMS values are plotted using Group 1 and Group 2 beacons in order to differentiate the performance by beacon grouping and geometry. Fig. 4.7 compares azimuthal 2DRMS performance between Group 1 and Group 2 at 100 km from Moriches, NY. The following is observed:

- As expected, the networking algorithms perform better than single-beacon solutions.
- At all angles, the SLI algorithm maintains the lowest 2DRMS values.
- From Fig. 4.7(a), when applying Group 1 beacon corrections, the 2DRMS values are elliptical, with the best performance where the user is inside the beacon triangle.
- From Fig. 4.7(b), using Group 2 beacons, the range- and spatial-based networking algorithms exhibit a "figure-8" pattern, where the 2DRMS lobes extend perpendicularly to the beacon line axis and the best performance is in line with the beacon grouping axis.

Fig. 4.8 shows the azimuthal 2DRMS performance over a 200 km radius about Moriches, NY, so that the rover's location extends outside of the Group 2 beacon triangle. Of interest in Fig. 4.8(b) is that the range-based algorithms no longer exhibit the "figure-8" pattern, but the SLI 2DRMS plot does. Here, the SLI algorithm does not change its behavior whether the user is inside or outside the beacon triangle because the 2DRMS

behavior is directly linked to the beacon's geometry. At all angles, Group 1-corrected positions exhibit 2DRMS values lower than Group 2-corrected positions. This confirms that the qualities of the beacon geometry play a direct role in the SLI algorithm's 2DRMS behavior.

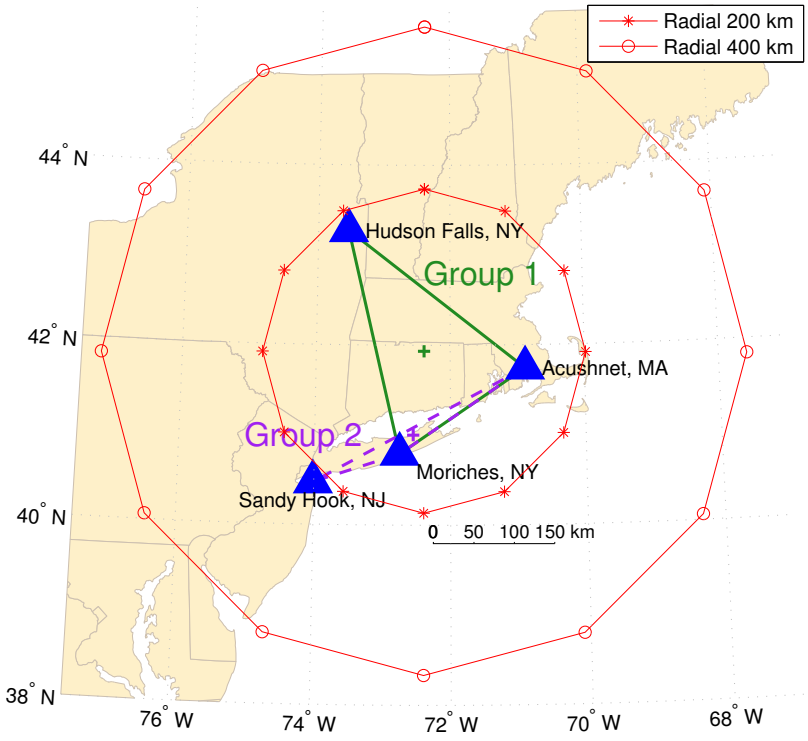

Figure 4.4: 2DRMS performance testing locations at radii of 200 km and 400 km from Group 1 centroid. Locations are spaced every 30° from true North (0°). Lambert projection.

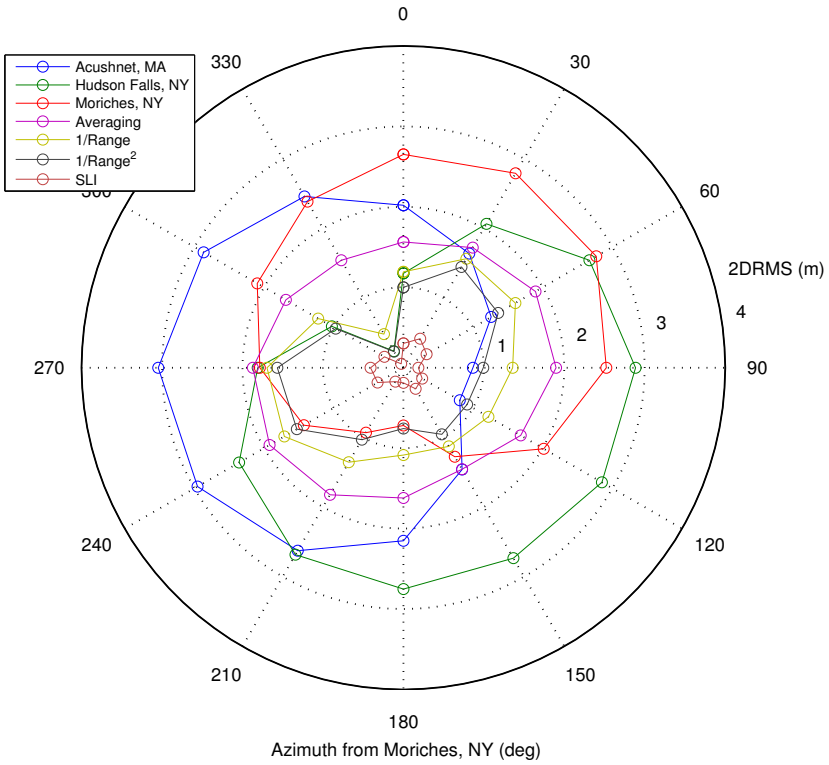

(a) 200-km radii.

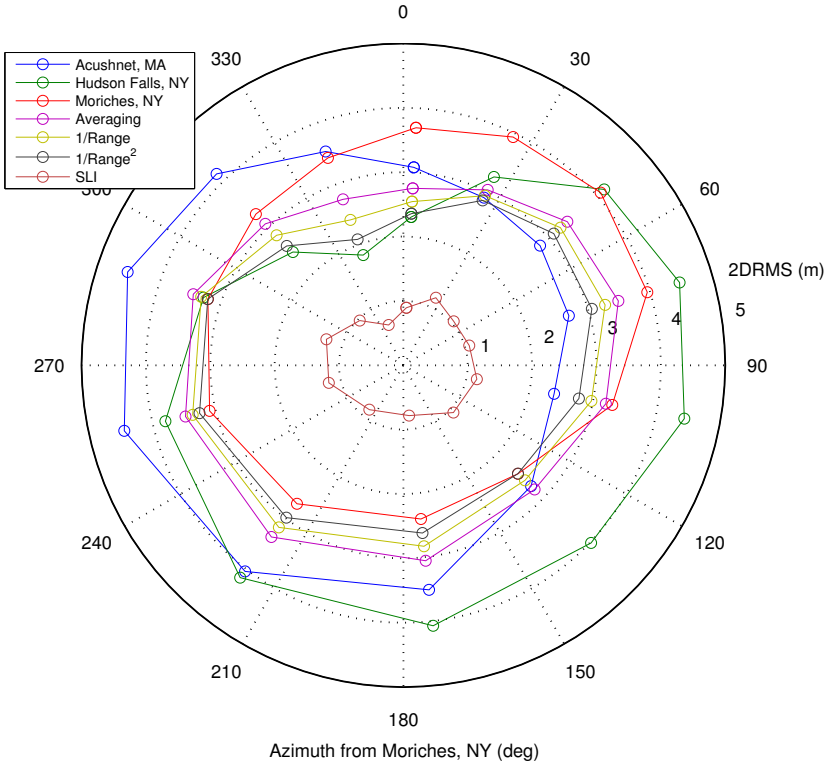

(b) 400-km radii.

Figure 4.5: 2DRMS performance vs. azimuth from Group 1 centroid using Group 1 beacons. Performance is shown by radius to the centroid.

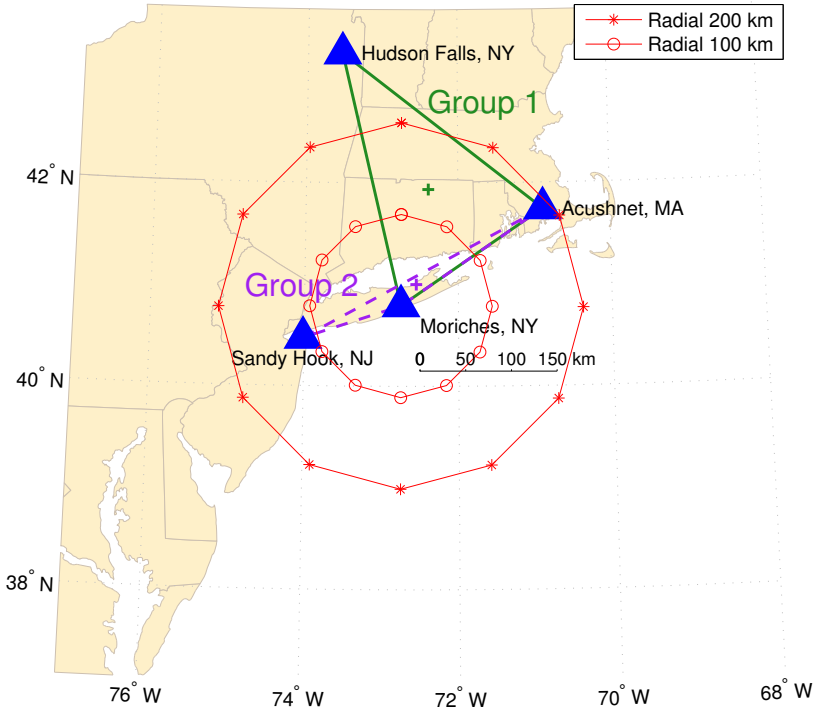

Figure 4.6: 2DRMS performance testing locations at radii of 100 km and 200 km from Moriches, NY (approximately the Group 2 centroid). Locations are spaced every 30° from true North (0°). Lambert projection.

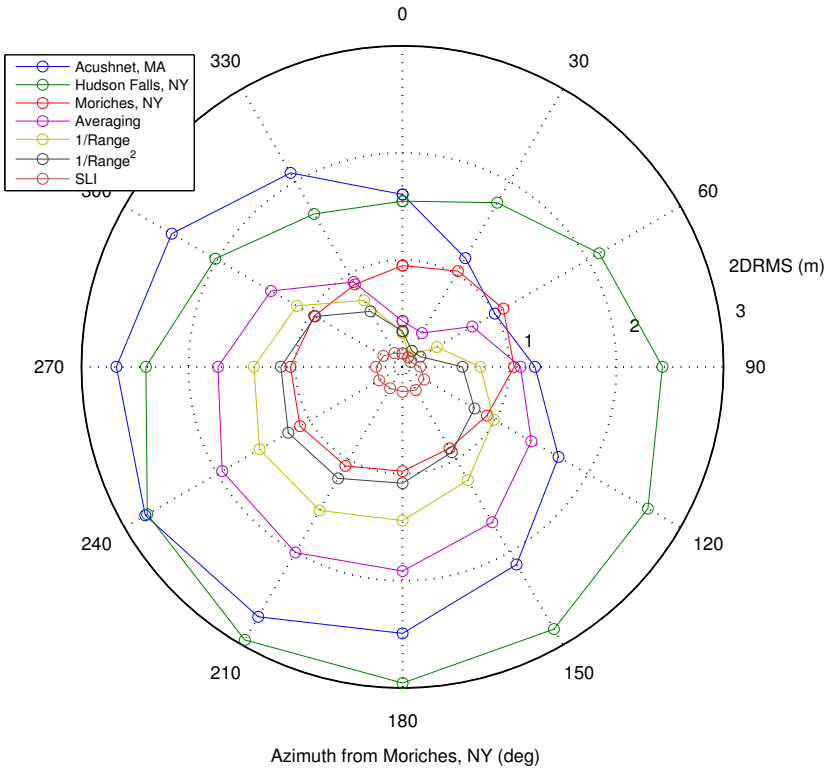

(a) Using Group 1 beacons.

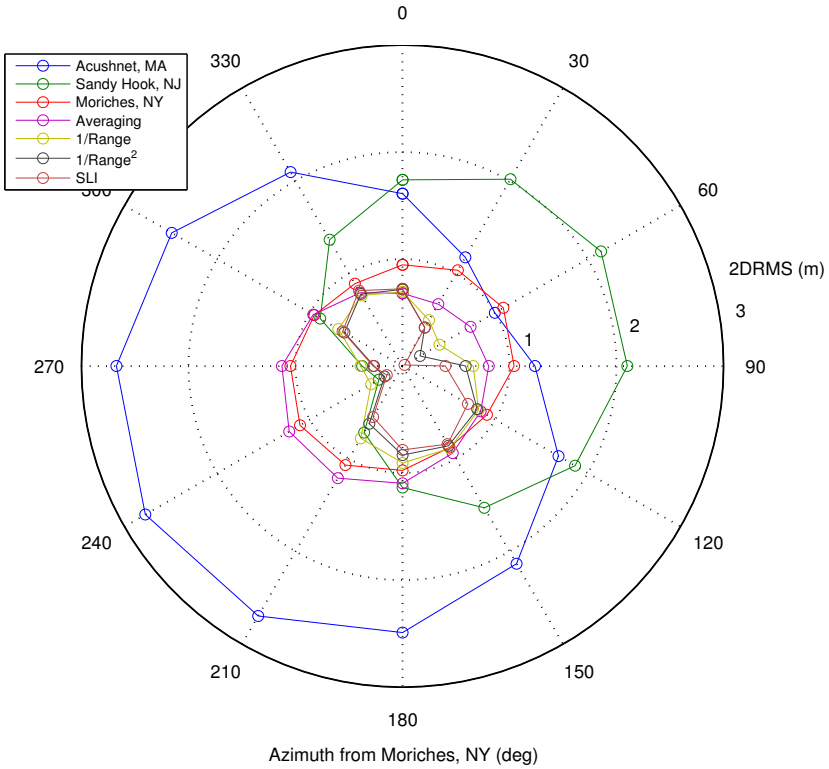

(b) Using Group 2 beacons.

Figure 4.7: 2DRMS performance vs. azimuth from Moriches, NY at radii of 100 km.

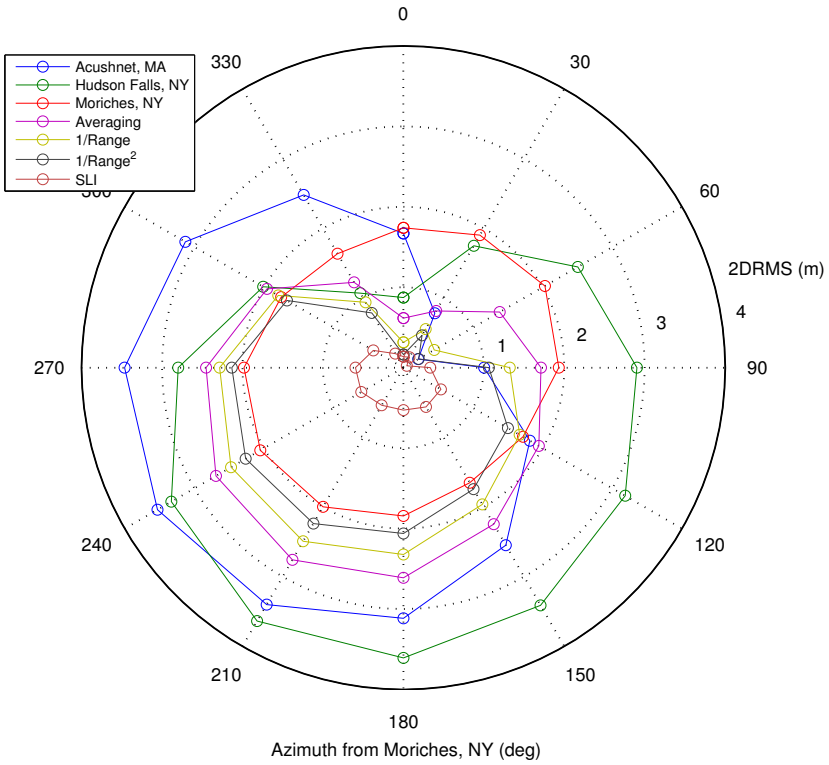

(a) Using Group 1 beacons.

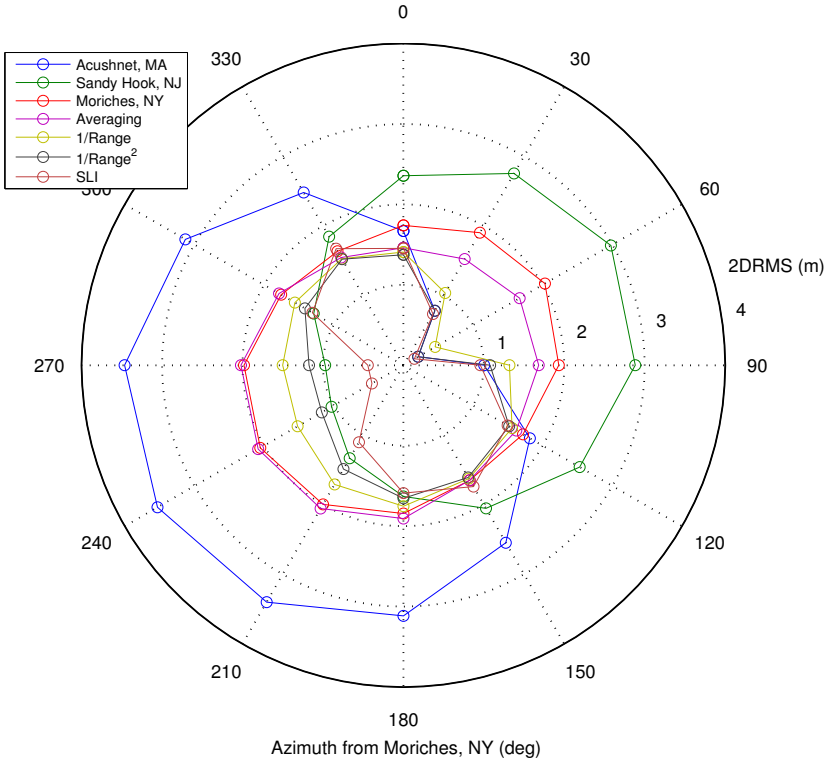

(b) Using Group 2 beacons.

Figure 4.8: 2DRMS performance vs. azimuth from Moriches, NY at radii of 200 km.

4.3 Consideration of assumptions

When calculating user positions, we have made certain assumptions hitherto about the kinds of signals that would be transmitted and received, as well as the behavior of environmental and geographic factors. We consider and evaluate those assumptions in this section to determine the potential impacts on the results and discussions so far.

Consider the standard model for calculating the pseudorange to a satellite, modified from [1]:

$$\hat{\rho}_s = \rho_s + \mathrm{c}\,(dt_\mathrm{R} - dt_s + T_s + I_s + m_s) + e_s \tag{4.1}$$

where :

$\hat{\rho}_s$: calculated pseudorange (m)

s : satellite number

ρ_s : true range to the satellite (m)

c : speed of light, $2.997\,924\,58 \cdot 10^8\,\mathrm{m{\cdot}s^{-1}}$

dt_R : receiver's clock bias (s)

dt_s : satellite's clock bias (s)

T_s : tropospheric path time delay (s)

I_s : ionospheric path time delay (s)

m_s : satellite multipath error (s)

e_s : additional observational error (m)

For the simulation trials, we made the following assumptions about the pseudorange calculation terms: (1) true ranges to satellites are known because the orbits are known; (2) receiver and satellite clock biases are zero; (3) Klobuchar ionospheric and NATO STANAG 4294 tropospheric models accurately represent the atmospheric terms; (4) there is no satellite multipath error; and (5) there is no additional observational error (noise). The first four assumptions are acceptable, within reason, and are discussed in turn below.

4.3.1 Assumption 1: Known satellite orbit

We assume that we know the true ranges to each satellite because we know their published orbits. In reality, a user's true range to any satellite in the GPS constellation is unknown and remains unknowable. While the U.S. Air Force attempts to position each satellite in a very precise orbit, exterior forces such as gravitational pull cause small perturbations in the orbits travelled. However, the Air Force mitigates the effects of orbital error by regularly updating the content in the satellite navigation message broadcasts with new ephemeris data [1, 2]. The International GNSS Service (IGS) tracks satellite orbital error for scientific purposes, which can then be used for very precise post-processing of GPS data. With updated ephemeris data, each satellite's orbit is known to within several meters. With respect to DGPS beacons, each site has been surveyed to sub-centimeter accuracy. Consequently, for users near a DGPS beacon, the orbital error contribution to the pseudorange is nearly the same. As a user moves farther from a beacon, the orbital error contribution is expected to become less similar. For the purposes of simulator testing, the user's true range to satellite is known deterministically because it was generated by the simulator.

4.3.2 Assumption 2: Zero clock bias

Receiver and satellite clock biases are assumed to be zero. However, satellite clocks, DGPS beacon clocks, and user receiver clocks are all subject to clock drift and phase noise in some manner. Each GPS satellite carries multiple high-quality caesium and rubidium clocks onboard so that satellite clock biases are usually very small, exhibit excellent phase noise characteristics, and have very slow drift rates, usually within 10 ns of Coordinated Universal Time (UTC) [2, 3]. A user's equipment, however, is usually of much poorer quality and exhibits poor clock bias and drift. The clock bias of the DGPS beacons themselves also acts as a source of clock error. Described in Chapter 1, Last *et al.* conducted research into whether clock biases would affect the user when employing a combination of DGNSS beacon pseudorange corrections and determined that this effect would be minimal [4]. While pseudorange corrections are subject to calculation time

and the beacons' own clock biases, they are slow to change (see Fig. 4.9), the user will experience a minimal offset when combining beacon clock bias.

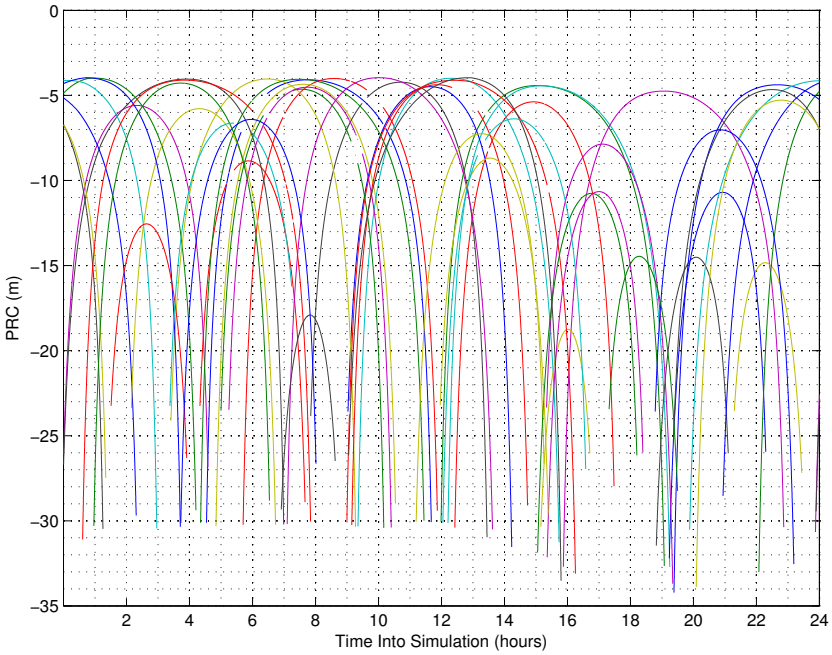

Figure 4.9: Pseudorange corrections for a 24-hour period at simulator Group-Point 1E. Most SVs are visible for several hours at this rover's latitude and longitude. Compare to actual PRCs at Moriches, NY, in Fig. 5.15.

4.3.3 Assumption 3: Sufficient atmospheric models

The atmospheric models used by the simulator are limited in scope, since the Klobuchar ionospheric model is intended to be a simplified model for ease of calculation and exhibits very smooth geographic behavior [5]. GPS satellites transmit Klobuchar ionospheric coefficients in the navigation message which are used by single-frequency (L1 band) GPS receivers to correct SV pseudoranges [6]. There are numerous models available that can estimate ionospheric conditions more accurately, such as the Naval Research Laboratory's new SAMI3 model, [7], which take into account a variety of ion species for the purpose of three-dimensional modeling and are designed for use with space-based communications. However, those models are not available for this simulator and many require a supercomputer to run. Because the user and beacon groupings are assumed to be confined to a small geographic region (less than 1000 km across), the at-

mospheric models are likely to behave smoothly under normal atmospheric conditions. Abnormal solar activity generates significant atmospheric electron activity, such as the SED events discussed by Skone *et al.* which can significantly alter the ionospheric delays (and, consequently, the pseudorange corrections) in an unpredictable way [8, 9]. The tropospheric model from NATO STANAG 4294 has been in use since the mid-1990s and is the standard for modeling lower atmosphere thermal effects [10, 11]. Typically, tropospheric effects are significant only for low-elevation satellites. Therefore, this model's errors are mitigated by the use of multiple higher-elevation satellites. Because the user can expect to see at least eight satellites in various constellations at any given time, these modeling errors play a minimal role here.

4.3.4 Assumption 4: Zero multipath error

Satellite multipath errors are assumed to be zero, but are actually present anywhere a GPS receiver is located near reflective surfaces. This thesis focuses on the marine and littoral environments, which are effectively free from multipath as long as the user's antennas are located away from other objects. DGPS beacons' antennas are sited specifically to mitigate the majority of multipath sources by placement far from reflective objects (such as buildings) and on local high grounds. Fig. 4.10 shows this siting arrangement at Moriches, NY. For the beacon, then, multipath can be considered negligible. Therefore, the major source of multipath errors would be at the user's location. However, multipath is very difficult to model and a well-studied effect, but also outside the scope of this thesis. Consequently, we can assume the user's multipath errors are zero, provided that the antenna has been placed to mitigate those effects.

4.3.5 Assumption 5: Zero thermal noise

Of all the sources of error in (4.1): orbital error, clock bias, atmospheric models, and multipath can be considered negligible. The last assumption, which disregards thermal noise, requires consideration and is discussed in depth in section 4.4.

(a) DGPS transmitter.

(b) GPS receiver equipment.

Figure 4.10: Moriches, NY, DGPS beacon and GPS receiver equipment.

4.4 Consideration of noise

It is well established that black-body radiation and thermal noise are present everywhere. This section examines the effects of thermal noise relative to GPS and networked DGPS position solutions. Specifically, we consider how noise affects the networked DGPS algorithms and the user's horizontal position solution. In order to do this, we determine how noise is introduced to the PRC weighting equation (2.4), which is accomplished by reviewing the position equation and distinguishing its networked DGPS inputs.

4.4.1 Derivation of noise effects on DGPS

We begin by introducing a specific point on Earth to the standard pseudorange calculation equation (4.1), which yields the non-linear position calculation equation. Here, the pseudorange calculation from a position to a specific satellite described in [1] and [2] are given by:

$$\hat{\rho}_s = \sqrt{(x_s - x)^2 + (y_s - y)^2 + (z_s - z)^2} + e \tag{4.2}$$

where $\hat{\rho}_s$ is the calculated pseudorange to a target satellite, s, (x_s, y_s, z_s) are the satellite coordinates broadcast in the ephemeris data from the navigation message, (x, y, z) are the user coordinates to be determined, and e is an additional error.

The position equation is typically modified by examining the *residuals*, or position errors, introduced into the above equation when solving with an estimated user position. The resultant residual equation reduces (4.2) to a simple non-linear, over-determined Pythagorean sum of squares minimization problem. Here, the position-time vector $[x, y, z, t]^\top$ is found that minimizes:

$$\sum_{s=1}^{S} \left(\sqrt{(x_s - x)^2 + (y_s - y)^2 + (z_s - z)^2} + e \right)^2 \tag{4.3}$$

where S is the number of satellites visible and the other variables are represented in the same manner as (4.2).

The minimization problem (4.3), usually found using a least-squares method, is linear when the difference between estimated position and true position is small [12]. The linearized pseudorange residuals equation is given by (4.4):

$$\delta\boldsymbol{\rho} = \boldsymbol{H} \cdot \delta\boldsymbol{x} \tag{4.4}$$

where $\delta\boldsymbol{\rho}_{S\times 1}$ is a small difference between true and calculated pseudoranges, $\boldsymbol{H}_{S\times 4}$ is the *visibility* matrix defined by (4.5), and $\delta\boldsymbol{x}_{4\times 1}$ is a small difference between true and estimated position-time ($\boldsymbol{x}$ is the user's position-time vector $[x, y, z, t]^\top$, expressed in

ECEF coordinates) [1, 2].

$$\boldsymbol{H} = \begin{bmatrix} \cos\theta_{1x} & \cos\theta_{1y} & \cos\theta_{1z} & 1 \\ \cos\theta_{2x} & \cos\theta_{2y} & \cos\theta_{2z} & 1 \\ \cos\theta_{3x} & \cos\theta_{3y} & \cos\theta_{3z} & 1 \\ \cos\theta_{4x} & \cos\theta_{4y} & \cos\theta_{4z} & 1 \\ \vdots & \vdots & \vdots & \vdots \\ \cos\theta_{Sx} & \cos\theta_{Sy} & \cos\theta_{Sz} & 1 \end{bmatrix} \tag{4.5}$$

where θ is the angle from the receiver to each satellite in the subscripted x, y, z directions along the earth-centered, earth-fixed (ECEF) coordinate axes and S is the number of satellites visible.

We prefer to understand the effects of noise on positioning in the horizontal position domain, rather than satellite pseudoranges, so we rearrange the linearized pseudorange residuals equation (4.4) and expand it to show the difference estimated and true positions:

$$\hat{\boldsymbol{x}} - \boldsymbol{x}_0 = \left(\boldsymbol{H}^\top \boldsymbol{H}\right)^{-1} \boldsymbol{H}^\top \left(\hat{\boldsymbol{\rho}} - \boldsymbol{\rho}_0\right) \tag{4.6}$$

where $\hat{\boldsymbol{x}} - \boldsymbol{x}_0$ is the difference between the x, y, z rover's estimated and true position at time t and $\hat{\boldsymbol{\rho}} - \boldsymbol{\rho}_0$ is the difference between the rover's estimated and true pseudoranges to each satellite at the rover's position at time t.

Now, we add the $S \times 1$ size vectors of atmospheric corrections ($\mathring{\boldsymbol{\rho}}_\mathrm{R}$ and $\mathring{\boldsymbol{\rho}}_\mathrm{B}$) and thermal noise ($\boldsymbol{n}_\mathrm{R}$ and $\boldsymbol{n}_\mathrm{B}$) at the rover and beacon, respectively, to (4.6):

$$\hat{\boldsymbol{x}} - \boldsymbol{x}_0 = \left(\boldsymbol{H}^\top \boldsymbol{H}\right)^{-1} \boldsymbol{H}^\top \left(\hat{\boldsymbol{\rho}} - \boldsymbol{\rho}_0 + \mathring{\boldsymbol{\rho}}_\mathrm{R} + \boldsymbol{n}_\mathrm{R} - \mathring{\boldsymbol{\rho}}_\mathrm{B} + \boldsymbol{n}_\mathrm{B}\right) \tag{4.7}$$

For ease of observation, we isolate the three terms from (4.7). Here, we can see the estimation error and the individual bias and noise terms:

$$\left(\boldsymbol{H}^\top \boldsymbol{H}\right)^{-1} \boldsymbol{H}^\top \left(\hat{\boldsymbol{\rho}} - \boldsymbol{\rho}_0\right) \Rightarrow \delta\boldsymbol{x} \tag{4.8}$$

$$\left(\boldsymbol{H}^\top \boldsymbol{H}\right)^{-1} \boldsymbol{H}^\top \left(\mathring{\boldsymbol{\rho}}_\mathrm{R} - \mathring{\boldsymbol{\rho}}_\mathrm{B}\right) \Rightarrow \text{bias} \tag{4.9}$$

$$\left(\boldsymbol{H}^\top \boldsymbol{H}\right)^{-1} \boldsymbol{H}^\top \left(\boldsymbol{n}_\mathrm{R} + \boldsymbol{n}_\mathrm{B}\right) \Rightarrow \text{noise} \tag{4.10}$$

where (4.8) is the estimation error and goes to zero after several iterations, (4.9) describes the mean bias inherent in any corrected GPS position solution, and (4.10) describes the combined effect of noise from the beacon and rover.

Now, thermal noise may be applied to the PRC weighting equation (2.4), which provides insight into the unitless PRC noise domain for each satellite. At the beacon, thermal noise is assumed to be a white Gaussian noise random variable given by a normal distribution with zero mean and variance σ^2:

$$\mathring{\rho}_s = \sum_{b=1}^{B} a_b \left(\mathring{\rho}_b + n_b\right), \quad n_b \sim \mathcal{N}(0, \sigma_b^2) \tag{4.11}$$

$$= \sum_{b=1}^{B} a_b \mathring{\rho}_b + \sum_{b=1}^{B} a_b n_b \tag{4.12}$$

The expected value term is examined:

$$\mathrm{E}\left[\mathring{\rho}_s\right] = \mathrm{E}\left[\sum_{b=1}^{B} a_b \mathring{\rho}_b + \sum_{b=1}^{B} a_b n_b\right] \tag{4.13}$$

$$= \sum_{b=1}^{B} a_b \mathring{\rho}_b \tag{4.14}$$

$$= \boldsymbol{a}^\top \mathring{\boldsymbol{\rho}} \tag{4.15}$$

The variance term is examined:

$$\mathrm{var}\left(\mathring{\rho}_s\right) = \mathrm{var}\left(\sum_{b=1}^{B} a_b \mathring{\rho}_b + \sum_{b=1}^{B} a_b n_b\right) \tag{4.16}$$

$$= \sum_{b=1}^{B} a_b^2 n_b^2 \tag{4.17}$$

$$= \left(\boldsymbol{a} \odot \boldsymbol{a}\right)^\top \boldsymbol{\sigma}^2 \tag{4.18}$$

where $\odot$ is the element-wise multiplication of two vectors. The resulting pseudorange correction random variable is given by:

$$\mathring{\rho}_s \sim N\left(\boldsymbol{a}^\top \mathring{\boldsymbol{\rho}}, \left(\boldsymbol{a} \odot \boldsymbol{a}\right)^\top \boldsymbol{\sigma}^2\right) \tag{4.19}$$

Now, we can glean some useful information from (4.19). For a weighted sum of pseudorange corrections, the expected value is simply the sum of weighted PRC errors between the rover and beacon, and the variance is the sum of the square of the weights multiplied by the beacon variances. Consequently, the PRC calculated at the rover's position is highly dependent on the quality of the beacon. The quality of the GPS

receivers and PRC calculation equipment in use at fielded DGPS sites is assumed to be much higher than a typical user's equipment, and is therefore much less subject to thermal noise error. As a result, the noise variance terms are minimized by the DGPS station.

However, (4.19) is represented in the unitless PRC noise domain, so we convert it to the horizontal position domain which is more useful to the user. For legibility, we combine the weighted beacon PRC and noise terms into one correction noise term, $\boldsymbol{n}_{\mathrm{C}}$; we shorten the visibility matrix manipulation term, $\left(\boldsymbol{H}^{\top}\boldsymbol{H}\right)^{-1}\boldsymbol{H}^{\top}$, into $\boldsymbol{G}_{4\times S}$; and evaluate the total noise, $\boldsymbol{n}_{S\times 1}$, from the rover and the correction.

$$\boldsymbol{n}_{\mathrm{C}} = \mathring{\boldsymbol{\rho}}_{\mathrm{B}} + \boldsymbol{n}_{\mathrm{B}} \tag{4.20}$$

$$\boldsymbol{G} = \left(\boldsymbol{H}^{\top}\boldsymbol{H}\right)^{-1}\boldsymbol{H}^{\top} \tag{4.21}$$

$$\boldsymbol{n} = \boldsymbol{G}\left(\boldsymbol{n}_{\mathrm{R}} + \boldsymbol{n}_{\mathrm{C}}\right) \tag{4.22}$$

$$= \boldsymbol{G}\boldsymbol{n}_{\mathrm{R}} + \boldsymbol{G}\boldsymbol{n}_{\mathrm{C}} \tag{4.23}$$

The spatial domain expected value is examined:

$$\mathrm{E}\left[\boldsymbol{n}\right] = \mathrm{E}\left[\boldsymbol{G}\boldsymbol{n}_{\mathrm{R}} + \boldsymbol{G}\boldsymbol{n}_{\mathrm{C}}\right] \tag{4.24}$$

$$= \mathrm{E}\left[\boldsymbol{G}\boldsymbol{n}_{\mathrm{R}}\right] + \mathrm{E}\left[\boldsymbol{G}\boldsymbol{n}_{\mathrm{C}}\right] \tag{4.25}$$

$$= \boldsymbol{G}\mathring{\boldsymbol{\rho}}_{\mathrm{B}} \tag{4.26}$$

The spatial domain covariance is examined:

$$\mathrm{cov}\left(\boldsymbol{n}\right) = \mathrm{cov}\left(\boldsymbol{G}\boldsymbol{n}_{\mathrm{R}}\right) + \mathrm{cov}\left(\boldsymbol{G}\boldsymbol{n}_{\mathrm{C}}\right) \tag{4.27}$$

$$= \boldsymbol{G}\mathrm{cov}\left(\boldsymbol{n}_{\mathrm{R}}\right)\boldsymbol{G}^{\top} + \boldsymbol{G}\mathrm{cov}\left(\boldsymbol{n}_{\mathrm{C}}\right)\boldsymbol{G}^{\top} \tag{4.28}$$

$$= \boldsymbol{G}\mathbf{I}\left(\sigma_{\mathrm{R}}^{2} + \sigma_{\mathrm{C}}^{2}\right)\boldsymbol{G}^{\top} \tag{4.29}$$

$$= \left(\sigma_{\mathrm{R}}^{2} + \sigma_{\mathrm{C}}^{2}\right)\boldsymbol{G}\boldsymbol{G}^{\top} \tag{4.30}$$

Now, the effect of thermal noise is described in the horizontal position domain and defined with a mean and covariance. The mean position error from (4.26) denotes the position offset stemming from the original position bias term (4.9). The spatial covariance is dependent on the rover's noise variance, σ_{R}, which is unknown and the beacon's

noise variance, σ_{C}, which is assumed to be small due to the quality of the beacon's receiving equipment. The term describing the temporal satellite visibility, $\boldsymbol{G}\boldsymbol{G}^{\top}$, assumes the standard *dilution of precision* (DOP) form [2]. DOP defines the precision of a position solution by taking into account the orientation of the satellite constellation. For example, a constellation of eight satellites spaced evenly across the sky will have a low DOP, considered good, and a constellation of four satellites in line and low on the horizon will have a high DOP, considered to be poor. DOP is expressed in two dimensions as Horizontal DOP, or HDOP, and typically takes on values around 1.0 for a 24-hour period [13]. Because HDOP varies by time but is expressed as the norm of the east, north standard deviations, it is effectively a constant scale factor for the noise mean and covariance, which we can now write as d:

$$\mathrm{E}\left[\boldsymbol{n}\right] = d\mathring{\boldsymbol{\rho}}_{\mathrm{B}} \tag{4.31}$$

$$\mathrm{cov}\left(\boldsymbol{n}\right) = d^2\left(\sigma_{\mathrm{R}}^2 + \sigma_{\mathrm{C}}^2\right) \tag{4.32}$$

Since σ_{R} and d are dependent on user's equipment and satellite constellation they are determined experimentally. Expanding the simplified mean and covariance equations, (4.31) and (4.32), the additive effect of noise on the user's horizontal position is:

$$\boldsymbol{n} \sim d \cdot \mathcal{N}\left(\mathring{\boldsymbol{\rho}}_{\mathrm{B}}, \sigma_{\mathrm{R}}^2 + \sigma_{\mathrm{C}}^2\right) \tag{4.33}$$

$$\text{where } \sigma_{\mathrm{C}}^2 = \left(\boldsymbol{a} \odot \boldsymbol{a}\right)^{\top} \boldsymbol{\sigma}_{\mathrm{B}}^2 \tag{4.34}$$

4.4.2 Spatial representations of bias magnitude and noise covariance

Now that the behavior of the pseudorange corrections has been mathematically determined, we plot the effects of bias and noise variance over a region of New England. We evaluate (4.19) using the standard beacon groups 1 and 2 for bias magnitude and noise variance based on rover position with the GPS simulator. Fig. 4.11 indicates the testing locations, an area approximately 400 km by 400 km extending north and east from 40.0° N and 74.5° W. Each test location was sampled at intervals of 60 s for 24 hours.

The bias magnitude and noise variance plots are calculated differently using (4.19). Because the bias is dependent on the actual PRCs, these values are time-dependent and calculated using 24 hours of data averaged with a temporal mean. Because we are interested in how the beacon noise affects the user's equipment, we set the user's noise variance, $\sigma_R^2 = 0$. The beacon variances are experimentally determined, so they are assumed constant over time and the variance vector set to $\boldsymbol{\sigma}_{\mathrm{B}}^2 = \mathbf{1}$. Since the scale factor, d, is also experimentally determined and constant, it is set to $d = 1$. The noise variance is not based on the pseudorange corrections (and therefore, in conjunction with our assumption of constant variances, not time-dependent); these values are calculated using a single time and displayed over a larger area (1000 km by 1000 km) so as to better show the variance behavior. Figs. 4.12 and 4.13 show the bias magnitudes and variance when using Group 1 beacons, Figs. 4.14 and 4.15 show the bias magnitudes and variance when using Group 2 beacons. For the purpose of direct comparison, SLI variance figures are plotted on a unitless scale from 0 to 35.

The simple averaging plots showed poor bias magnitude performance over a region and good noise-reduction in variance. The minimum bias magnitudes are located at the centroids of the beacon triangles (see Figs. 4.12(a) and 4.14(a)) and increase linearly as the rover departs from the centroids. This is expected because the averaging weights only accurately represent the PRC when the rover is located at the "average" triangle position (the centroid). The noise variances for both beacon groupings are equal and constant over the entire region, since the variance term depends on the weights, which are constant. The constant weight vector, $\boldsymbol{a} = \left[\frac{1}{3}, \frac{1}{3}, \frac{1}{3}\right]^\top$, drives the variance term to $\frac{1}{3}$, constant for all rover locations. Thus, the simple averaging algorithm is maximally subject to bias magnitude and minimally subject to beacon PRC noise.

The inverse-range and inverse-range-squared plots confirm the data collected in Chapter 3: that the areas near each beacon would exhibit decreased bias when close to the beacon grouping. From Figs. 4.12(b) and 4.12(c), these algorithms' bias magnitudes are lowest at and in between the beacons. Note the bias in the areas immediately surrounding each beacon is much lower in the inverse-range-squared plots than the inverse-range plots.

This characteristic is also visible in the Group 2 plots. With respect to noise variance (and as mentioned in Section 4.2.2), the expected behavior for both algorithms as the rover's range to the beacons increases will drive the variance to $\frac{1}{3}$. This behavior is noted in the applicable plots. Also notable in Figs. 4.13(c) and 4.15(c) is that the inverse-range-squared algorithm exhibits larger regions of higher noise variance around the beacons. Again, this is expected, since this algorithm weights closer beacons more highly when compared to the inverse-range algorithm. Thus, the inverse-range and inverse-range-squared algorithms have good bias magnitude performance near to and inside the beacon groupings and poor bias magnitude performance outside the beacon groupings. With respect to noise variance, the inverse-range and inverse-range-squared algorithms have high variance susceptibility near to and inside the beacon groupings and low variance susceptibility outside the beacon groupings.

The SLI algorithm plots clarify what was observed in Chapter 3: that the bias magnitude performance is excellent and the noise variance is highly dependent on the rover's location and beacon geometry. Geographically-distributed beacons in an equilateral formation are expected to have the optimal geometry to maximize this algorithm's regional accuracy. Also expected is that beacons forming a line will have good performance (both bias and variance) in the direction of the beacon line and poor performance at a tangent to the beacon line. This expectation is based on the fact that the spatial linear interpolation algorithm has the most data about the PRCs along the beacon line and little data at the beacon line's tangent. A mean of nearly zero bias magnitude is observed for Groups 1 and 2 (Figs. 4.12(d) and 4.14(d)) as well as noise variance matching expectations (Figs. 4.13(d) and 4.15(d)).

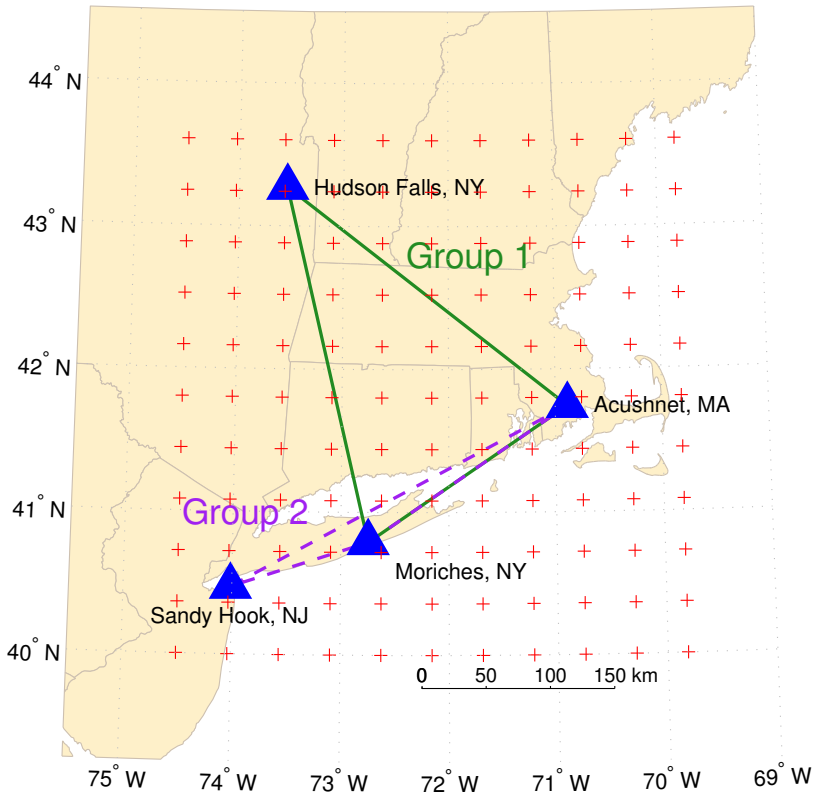

Figure 4.11: Noise variance map grid, at constant latitudes and longitudes stemming 40 km east and north of 40.0°N and 74.5°W.

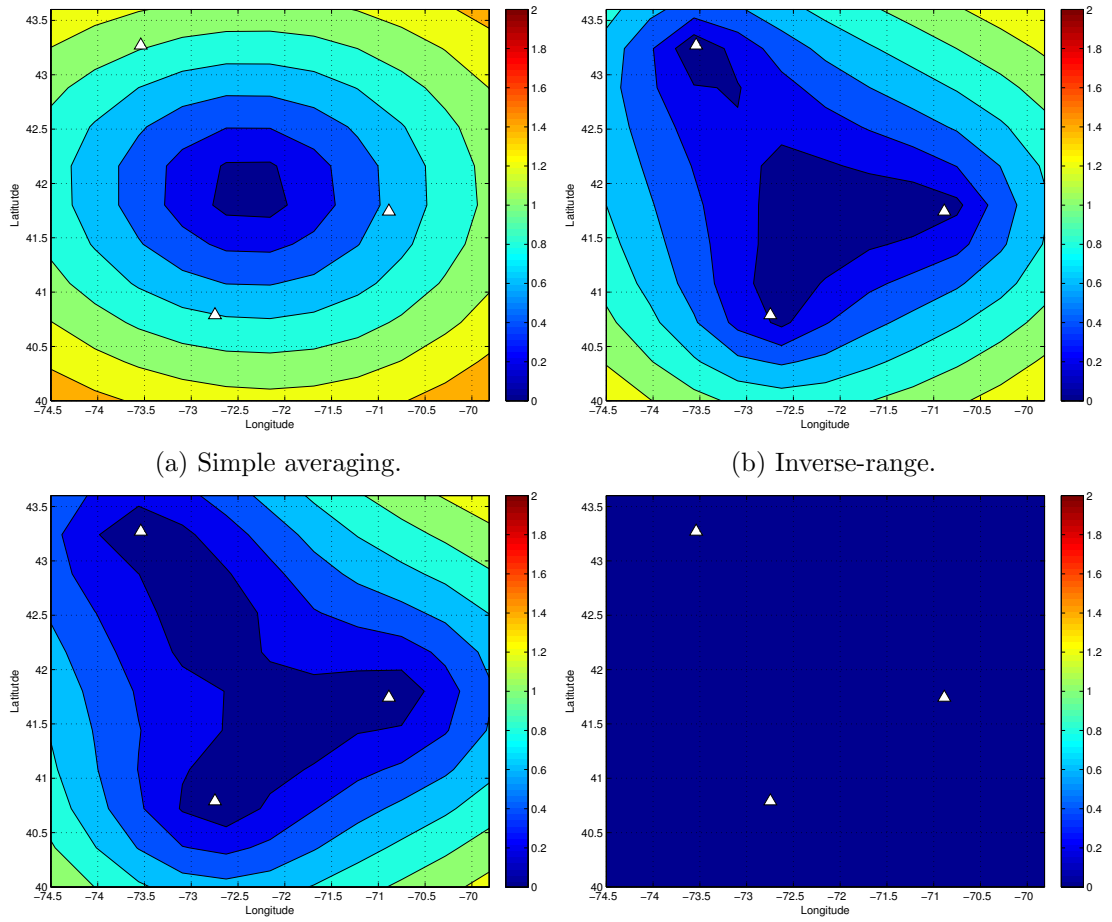

(a) Simple averaging.

(b) Inverse-range.

(c) Inverse-range-squared.

(d) SLI.

Figure 4.12: Bias magnitude over New England using Group 1 beacons. Beacon locations are plotted with white triangles.

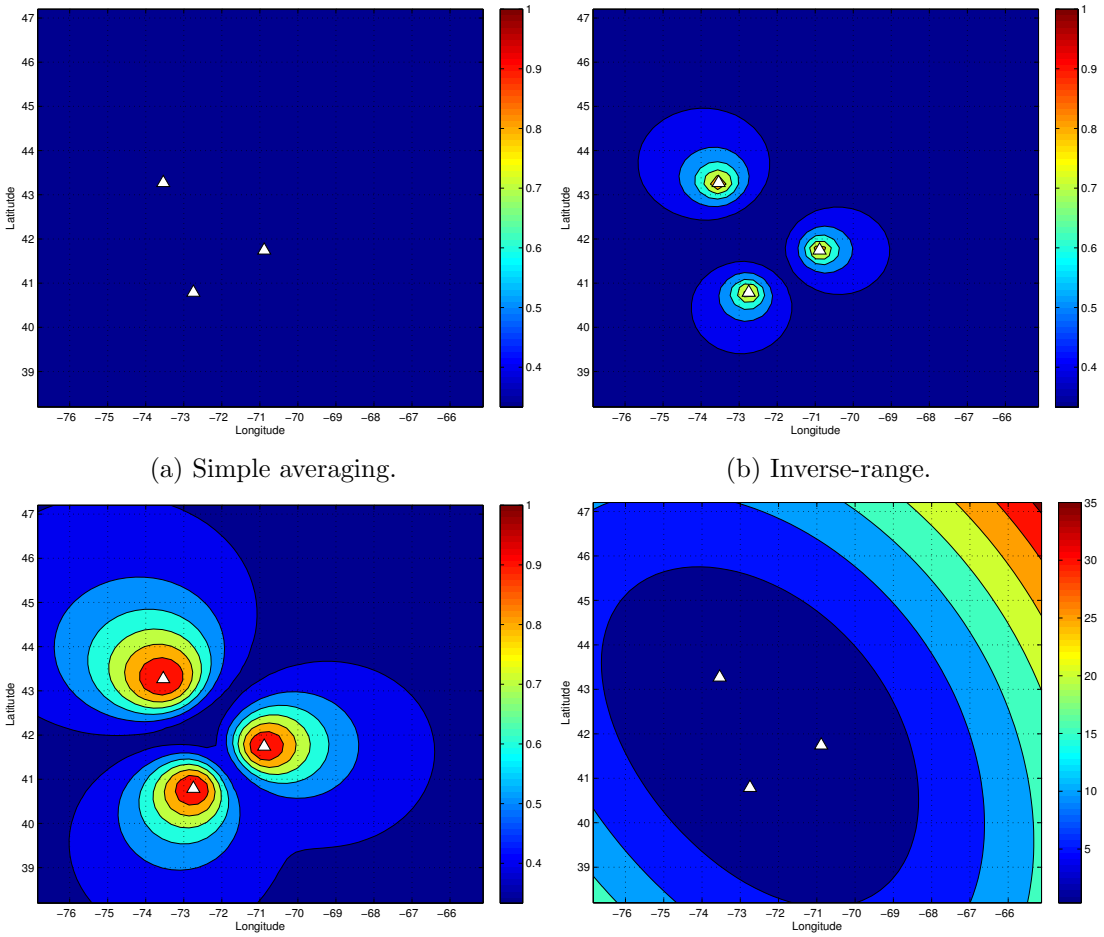

(a) Simple averaging.

(b) Inverse-range.

(c) Inverse-range-squared.

(d) SLI.

Figure 4.13: Noise variance over New England using Group 1 beacons. Note the different SLI color scale. Beacon locations are plotted with white triangles.

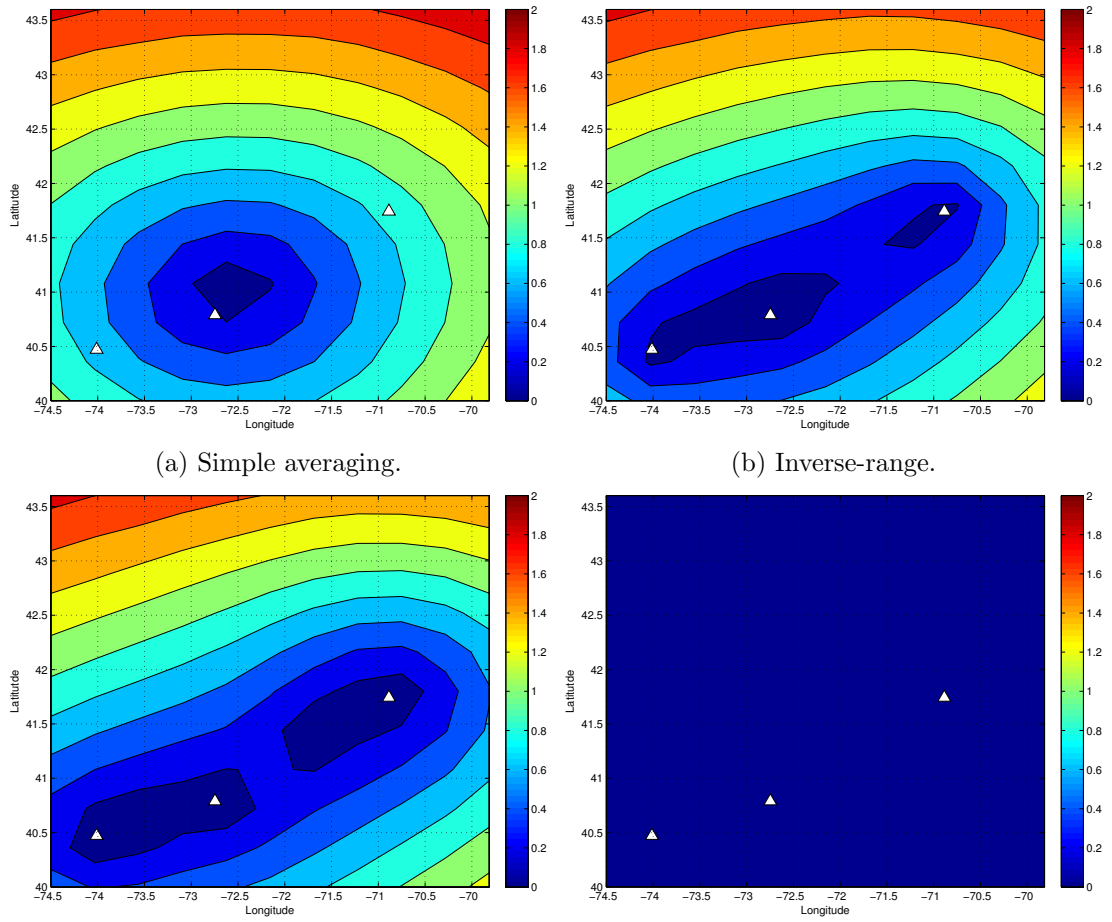

(a) Simple averaging.

(b) Inverse-range.

(c) Inverse-range-squared.

(d) SLI.

Figure 4.14: Bias magnitude over New England using Group 2 beacons. Beacon locations are plotted with white triangles.

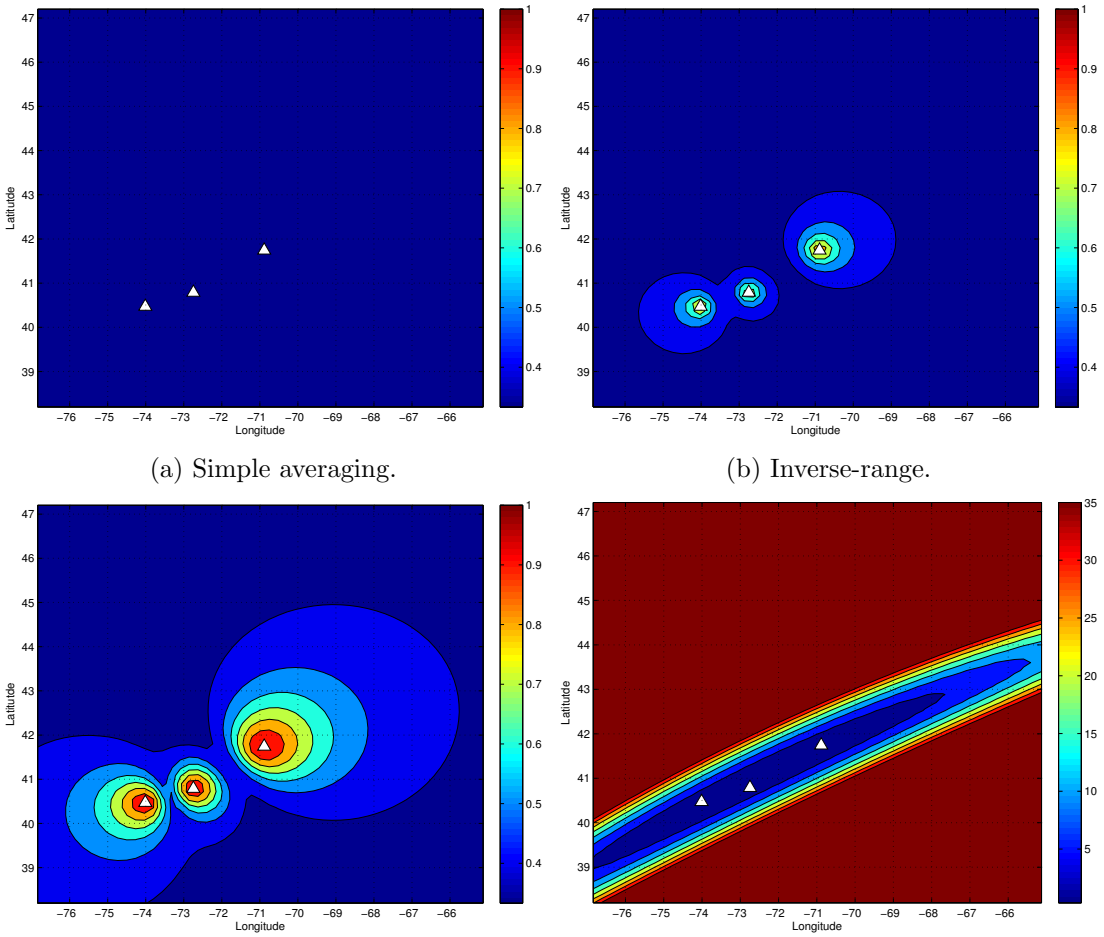

(a) Simple averaging.

(b) Inverse-range.

(c) Inverse-range-squared.

(d) SLI.

Figure 4.15: Noise variance over New England using Group 2 beacons. Note the different SLI color scale. Beacon locations are plotted with white triangles.

4.5 Beacon grouping quality and selection criteria

A user is interested in selecting the best DGPS beacons available. When using a single-beacon solution, the user typically selects the beacon by some selection criteria, such as highest SNR. The selection criteria, or quality factors, have been discussed in depth in [14, 4]. Attention is now given to assigning similar quality factors to networked-DGPS beacon groupings. However, these concepts are new and different for the use of combined beacon groupings. We propose one method of assessing beacon grouping quality and selecting an appropriate beacon grouping for the user.

Beacon grouping quality

So far, we have determined that the bias magnitude and variance (and, ultimately, the total 2DRMS) performance is dependent upon the beacon geometry and the user's position relative to the beacon geometry. We now define quality factors for each algorithm, with regards to these factors.

Simple averaging: the bias magnitude is related to the user's distance to the beacon triangle centroid and the noise variance is constant. Therefore, the quality factor is dependent only on the bias magnitude:

$$Q_{\text{Avg}} = \left\| \boldsymbol{x}_{\text{R}} - \boldsymbol{x}_{\text{C}} \right\| \tag{4.35}$$

where $\boldsymbol{x}_{\text{R}}$ is the rover's x, y position vector and the mean of $\boldsymbol{x}_{\text{C}}$ is the beacon grouping centroid x, y position vector.

Inverse-range: the bias magnitude is more dominant than noise variance. The bias magnitude is dependent upon the sum of the user's ranges to each beacon. Likewise, the inverse-range-squared algorithm is based on the square of the user's ranges to the beacons:

$$Q_{\text{IR}} = \sum_{b=1}^{B} \left\| \boldsymbol{x}_{\text{R}} - \boldsymbol{x}_b \right\| \tag{4.36}$$

$$Q_{\text{IR}^2} = \sum_{b=1}^{B} \left\| \boldsymbol{x}_{\text{R}} - \boldsymbol{x}_b \right\|^2 \tag{4.37}$$

Spatial linear interpolation: the bias magnitude is constant and the noise variance is the term of interest. The noise variance term from (4.19) takes into account the user's

spatial orientation to the beacon and the beacon grouping's geometry, and is ideal to represent the quality factor of this algorithm:

$$Q_{\mathrm{SLI}} = (\boldsymbol{a} \odot \boldsymbol{a})^{\top} \boldsymbol{\sigma}^2 \tag{4.38}$$

Selection criteria

A user should select the beacon grouping that provides the best overall performance given a location, i.e.: the beacon grouping with the lowest Q for the intended networking algorithm. Q is evaluated using three different beacon sets in order to illustrate the geographic boundaries between optimal grouping performance. The three possible beacon groupings are shown in Fig. 4.16.

Fig. 4.17 shows the selection zones between Group 1 and Group 2 or 3, respectively. The selection zones based on Q for the averaging, inverse-range, and inverse-range-squared algorithms are the same and plotted only once as Figs. 4.17(a) and 4.17(c). The selection zones for the SLI algorithm conform to the axial Q behavior discussed in the previous section. With respect to SLI, when selecting between Groups 1 and 3, the margin for selecting Group 3 is limited to a narrow band in the direction of the beacon line. Likewise, when comparing two similarly geographically-distributed beacon groupings, such as Groups 1 and 2, the selection zones are similar.

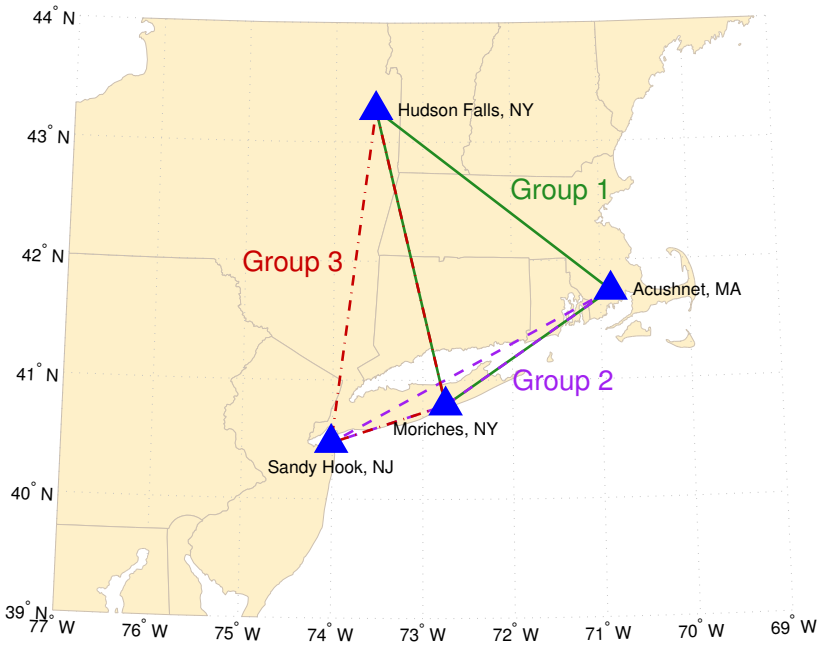

Figure 4.16: Map of quality factor beacon groupings. Lambert projection.

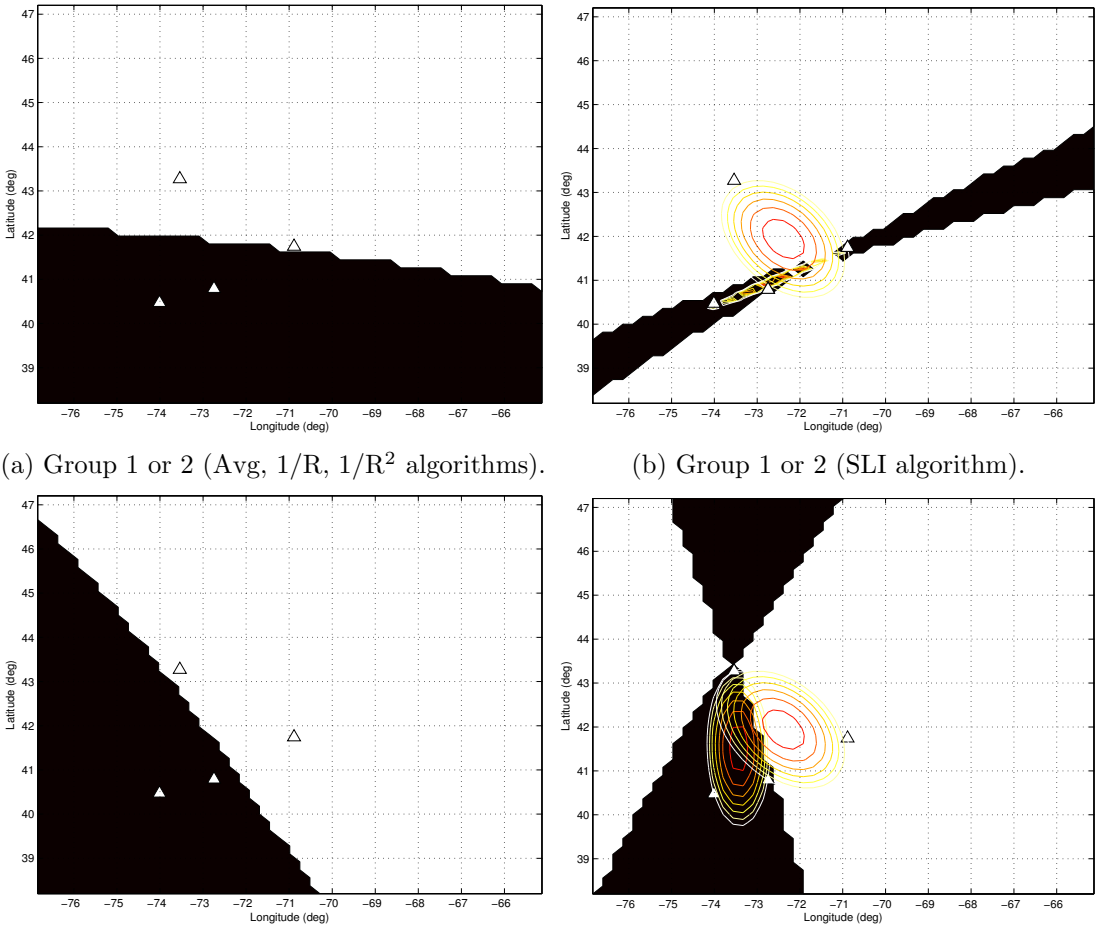

(a) Group 1 or 2 (Avg, 1/R, $1/R^2$ algorithms).

(b) Group 1 or 2 (SLI algorithm).

(c) Group 1 or 3 (Avg, 1/R, $1/R^2$ algorithms).

(d) Group 1 or 3 (SLI algorithm).

Figure 4.17: Beacon selection zones between Group 1 or 2 and Group 1 or 3. Group 1 beacons would be selected in the zones colored white, Group 2 or 3 beacons would be selected in the zones colored black. Beacons are plotted in white triangles and the SLI algorithm's Q contour lines are plotted for clarity. (Note: the selection borders appear jagged due to sampling interval—the actual borders behave linearly.)

4.6 Discussion of Networked DGPS character

This chapter reviews the character of each networked DGPS algorithm in order to establish it's behavior over a region of application. Here, a parallel link can be made to single-beacon DGPS: knowing that spatial decorrelation is a factor in the quality of a user's position solution, that information can be used to determine the "best" beacon available and give the user a measure of solution quality.

Evaluating the 2DRMS performance by distance reveals that as a rover travels farther from a beacon grouping, the performance degrades nearly linearly, but with coefficients dependent on the algorithm in use. Traveling in a different direction produces the same type of linear degradation, but with different decorrelation coefficients. Typically, the SLI algorithm produces the lowest 2DRMS values and has an upper limit bounded by the best-performing single-beacon.

Comparing networked DGPS algorithms' 2DRMS performance by azimuth, we determine that performance is not constant at all azimuths and is primarily dependent on the geometry of the beacon grouping. With respect to a line of beacons, the performance is best along the direction of the line and poor at a tangent to it. Those beacon groupings that are arranged in a well-spaced and nearly-equilateral layout offer, in comparison to a beacon line, better 2DRMS performance in all directions.

When beacon noise is introduced to the pseudorange correction equation, the expected value indicates the mean bias magnitude and the noise variance term describes the zones of performance. Here, the expected value and noise variance are based on the weights attributed to the pseudorange corrections from each beacon. The lowest mean bias magnitude for simple averaging is observed to be co-located with the beacon grouping centroid; and the zones of best bias performance are located within the beacon groupings for the inverse-range and inverse-range-squared algorithms. SLI has nearly constant bias magnitude over the region of interest. Simple averaging is observed to have a constant noise variance over the region of interest; and the noise is maximized about each beacon for the inverse-range and inverse-range-squared algorithms. These three algorithms exhibit good noise averaging at a distance from the beacon grouping.

SLI noise variance is shown to be a function of the user's location relative to the beacon grouping geometry.

We introduce a quality factor, Q, to describe a function with which a user's multi-beacon DGPS receiver may select the optimal beacon grouping. We propose quality factors for each networking algorithm. Interestingly, the selection line between two beacon groupings for the range-based algorithms' quality factor does not pass along the beacon border, but through the beacon sets. The proposed quality factor for SLI is simply the noise variance equation; this takes into the beacon groupings' zones of best performance. Again, the selection zones exhibit some interesting behavior: when selecting beacons west of Group 2, the Q_{SLI} chooses Group 1 even though Group 2 is nearer. This occurs because the variance is lower for Group 1 than Group 2 at this location. However, if the user also employed some form of position averaging, it is likely that the Q factor would be similar for both beacon groupings over this entire area and the user would be able to select either grouping with confidence.

List of References

[1] K. Borre, D. M. Akos, N. Bertelsen, P. Rinder, and S. H. Jensen, *A Software-Defined GPS and Galileo Receiver: a Single-Frequency Approach.* Boston, MA: Birkhäuser, 2007.

[2] P. Misra and P. Enge, *Global Positioning System: Signals, Measurements, and Performance.* Lincoln, MA: Ganga–Jamuna Press, 2006.

[3] C. Hackman and D. Matsakis, "Accuracy and precision of USNO GPS carrier-phase time transfer," in *Proc. 42nd Annu. Precise Time and Time Interval (PTTI) Meeting*, Reston, VA, Nov. 2010, pp. 197–214.

[4] D. Last, A. Grant, A. Williams, and N. Ward, "Enhanced accuracy by regional operation of Europe's new radiobeacon differential system," in *Proc. 15th Int. Tech. Meeting Satellite Division Inst. Navigation (ION GPS 2002)*, Portland, OR, Sept. 2002, pp. 2723–2732.

[5] J. A. Klobuchar, "Ionospheric time-delay algorithm for single-frequency GPS users," *IEEE Trans. Aerosp. Electron. Syst.*, vol. 23, pp. 325–331, May 1987.

[6] *Navstar GPS Space Segment/Navigation User Segment Interfaces*, Global Positioning Systems Directorate Specification IS-GPS-200, Rev. F, Sept. 2011.

[7] J. D. Huba, G. Joyce, and J. Krall, "Three-dimensional equatorial spread F modeling," *Geophys. Res. Lett.*, vol. 35, pp. 325–331, May 2008, doi:10.1029/2008GL033509.

[8] S. Skone, R. Yousuf, and A. Coster, "Performance evaluation of the Wide Area Augmentation System for ionospheric storm events," *J. Global Positioning Syst.*, vol. 3, no. 1–2, pp. 251–258, 2004.

[9] S. Skone, R. Yousuf, and A. Coster, "Combating the perfect storm: improving marine Differential GPS accuracy with a wide-area network," *GPS World*, pp. 31–38, Oct. 2004.

[10] *Navstar Global Positioning System (GPS)–System Characteristics, Part 1*, North Atlantic Treaty Organization Standardization Agreement (STANAG) 4294, Aug. 1990.

[11] J. P. Collins, "Assessment and development of a tropospheric delay model for aircraft users of the Global Positioning System," M.S. thesis (Tech. Report No. 203), Dept. Geodesy, Geomatics Eng., Univ. New Brunswick, Fredericton, New Brunswick, Canada, Sept. 1999.

[12] L. O. Lupash, "A new algorithm for the computation of the geodetic coordinates as a function of Earth-centered Earth-fixed coordinates," *J. Guidance, Control, Dynamics*, vol. 8, no. 6, pp. 787–789, Nov. 1985, doi:10.2514/3.20057.

[13] R. B. Langley, "Dilution of precision," *GPS World*, pp. 52–59, May 1999.

[14] A. J. Grant, "Availability, continuity, and selection of maritime DGNSS radiobeacons," Ph.D. dissertation, Sch. Informatics, Univ. Wales, Bangor, United Kingdom, 2002.

CHAPTER 5

Real-World Implementation of Networked DGPS

5.1 Overview

We designed a software-defined radio (SDR) system to capture and post-process DGPS data from multiple beacons. Because of its wide user base, ease of integration within the MATLAB environment, and system capabilities, we chose an Ettus Research Universal Software Radio Peripheral (USRP) model N210 as the vehicle for SDR. The system was installed on top of and in the laboratory space in McAllister Hall, at the U.S. Coast Guard Academy, which was chosen for its proximity to three DGPS beacons: Acushnet, MA; Moriches, NY; and Sandy Hook, NJ. The setup was also tested in New Haven, CT, atop the U.S. Coast Guard's Electronics Support Detachment building.

5.2 Networked DGPS system setup

The system setup consisted of a four-foot DGPS E-field antenna, low-loss coaxial cable (LMR-400), low-noise Krohn-Hite bandpass filter-amplifier, a USRP with low-frequency receiving front-end (capturing 0–30 MHz band), and a computer running MATLAB. Fig. 5.1 details the DGPS system diagram for post-processing with the USRP. While the USRP is capable of sampling rates up to 100 Msample·s^{-1}, a sampling rate of only 100 kHz is required to capture the entire DGPS band. Using the USRP system driver developed by Ettus and Mathworks, the device decimation was set to 400, effectively a 250 kHz sampling rate. These quantized data, now in MATLAB format, were then down-converted to baseband for each of the target DGPS station frequencies and processed through a Viterbi decoder set up to accommodate the 100 bit·s^{-1} and 200 bit·s^{-1} MSK modulation. The resulting bitstream was read by an RTCM SC-104 parser and output to the user. Additionally, the USRP was configured to synchronize and step its 10 MHz and 1 pulse-per-second (PPS) local oscillator to an HP 5071A caesium frequency standard to ensure accurate timing. Photographs of the equipment setup on the rooftop and in the laboratory are shown in Fig. 5.2. These subsystems are described in depth in

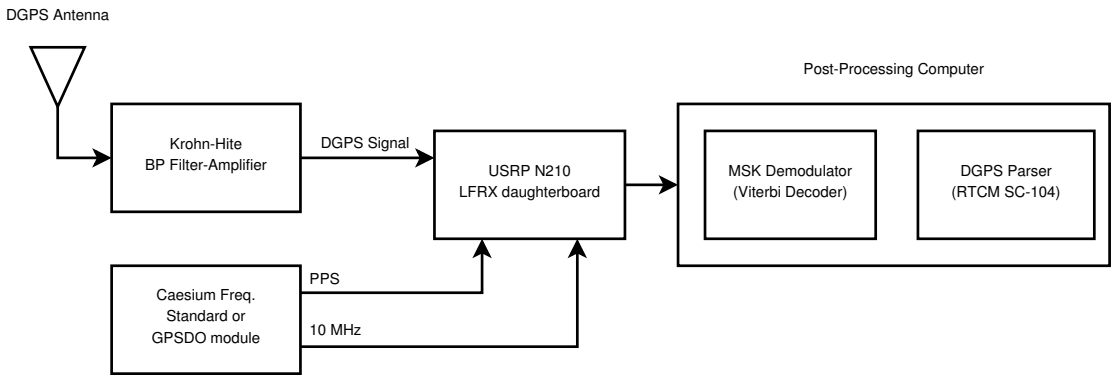

Figure 5.1: System diagram of real-world test using USRP to collect entire DGPS spectrum for post-processing.

the next two sections: a full description of the USRP and its capabilities may be found in Section 5.3; and the demodulation functions are described in Section 5.5.

(a)

(b)

Figure 5.2: DGPS post-processing system setup: (a) E-field whip antenna on the roof of McAllister Hall at the U.S. Coast Guard Academy, (b) bandpass filter, USRP, and blade server for post-processing.

5.3 The Universal Software Radio Peripheral

There are a variety of software-defined radio devices currently available in today's marketplace. One manufacturer, Ettus Research, based in Mountain View, CA, produces the Universal Software Radio Peripheral (USRP), which is available in a range of hardware configurations, from the entry-level B-series to the research-grade N-series. Ettus Research also manufactures a collection of daughterboards which are capable of receiving and transmitting on a variety of frequency bands, making the frequency bands used for GPS and DGPS easily accessible for research. All of the USRP models' hardware and firmware designs are open-source so the user can program and configure the device to meet specific needs [1]. Essentially, the USRP is a simple hardware conduit between an antenna and a computer. The hardware and software are described in the following two sections.

The USRP range was selected because of its large user base, variety of models, and large academic and professional user base. From the USRP range, the N210 model was selected for research because of its high sampling rate, networked capability, scalability, and FPGA adaptability. Because USRP hardware and software is designed and sold as open-source, a wide variety of free and open-source applications have been developed for

them. The majority of the work done in this thesis was conducted on the USRP N210, as it was an advanced platform which provided the requisite characteristics for receiving GPS, DGPS, and other desired signals.

5.3.1 USRP Hardware

The following sections describe the USRP hardware components used in this thesis, as well as their capabilities and relevant technical specifications.

Motherboard

USRP's N210 model was selected because of its high sampling rate, networked capability, scalability, and FPGA adaptability. The sampling rate of the N210 is higher than previous generations, now set at 100 Msample·s^{-1} (prior to decimation in time), allowing a wide maximum signal spectral bandwidth of 50 MHz. The USRP1 had a sampling rate of 64 Msample·s^{-1} prior to decimation, allowing a maximum signal bandwidth of 8 MHz [2, 3]. The N210 is a networked device that uses a Gigabit Ethernet[1] connection to communicate with host computers. Because it is networked, the USRP is free to be placed in an area most suitable for signal reception and the host computer may be located anywhere else within the network. Additionally, the USRP can support multiple simultaneous users when in broadcast mode. The N210 can support multiple users because it broadcasts IP packets on the subnet, although only one computer can "control" the USRP at any moment. Consequently, the device may be installed using existing Gigabit Ethernet infrastructure, both wired and wireless, without added expense of reconfiguring or installing infrastructure to support its use. The USRP N210 can also scale to include other N210 devices with its Multiple-Input, Multiple-Output (MIMO) data port, so that a user may benefit from two devices receiving, transmitting, or processing simultaneously within a small physical space and on the same reference clock. The USRP N210 also houses a configurable FPGA containing 3.4 million gates, programmable as required by the user to accomplish tailored high-speed signal processing.

[1] 1000BASE-T Ethernet, as defined in IEEE 802.3-2008.

Daughterboards

To receive or transmit RF information, the USRP motherboard must be connected to the system antenna via a radio-frequency (RF) front-end, provided as USRP daughterboards. Ettus produces three functional classes of daughterboards: receivers, transmitters, and transceivers. Each daughterboard contains the RF front-end for a specified frequency range and a memory chip identifying both itself and its capabilities to the USRP motherboard. The daughterboards simply provide an interface from the motherboard to the receiving equipment and do not perform any processing of the signal (except the high-frequency daughterboards); they can be thought of as band-pass RF filters. The high-frequency daughterboards, such as the DBSRX, modulate down to an intermediate frequency. Subsequently, all signal processing, including analog-to-digital and digital-to-analog conversion, occurs on the motherboard. Together, the daughterboard collection is capable of receiving and transmitting RF frequencies from direct-current (DC) to 5.9 GHz. Receiver and transmitter daughterboards have specific connectors and are mounted on opposite sides of the motherboard, while transceiver daughterboards occupy both the receiver and transmitter connectors. The daughterboards are connected to the front panel with MCX or SMA connectors and from the front and back panels to the antenna by SMA connectors. Table 5.1 provides information on the available daughterboards and their capabilities.

Table 5.1: USRP N210 daughterboards, types, and frequency range capabilities.

Name	Type	Frequency Range
BasicRX	Receiver	1–250 MHz
BasicTX	Transmitter	1–250 MHz
LFRX	Receiver	0–30 MHz
LFTX	Transmitter	0–30 MHz
WBX	Transceiver	50–2200 MHz
TVRX2	Receiver (×2)	50–860 MHz
SBX	Transceiver	400–4400 MHz
RFX900	Transceiver	750–1050 MHz
DBSRX2	Receiver	800–2350 MHz
RFX1200	Transceiver	1.15–1.45 GHz
RFX1800	Transceiver	1.5–2.1 GHz
RFX2400	Transceiver	2.3–2.9 GHz
XCVR2450	Transceiver	2.4–2.5 GHz, 4.9–5.9 GHz

GPS Disciplined Oscillator

In addition to the daughterboards, Ettus produces an accessory called the GPS-disciplined oscillator (GPSDO) module, which is designed to provide more accurate timing to the motherboard. It is intended for timing-sensitive applications where the motherboard's existing reference clock and 1 PPS timer may not be sufficiently stable. The GPSDO module synchronizes to a GPS L1 input signal and outputs a stable, synchronized 10 MHz reference clock and 1 PPS timer [4]. Unlike external clock sources, such as a caesium or rubidium clock, the GPSDO module is mounted inside the USRP N210 enclosure next to the motherboard.

Motherboard processing and capabilities

The USRP N210 motherboard performs all the signal conversion, hardware processing, and communication functions. The signal conversion block is comprised of dual 14-bit analog-to-digital converters (ADC) and dual 16-bit digital-to-analog converters (DAC). The ADC is capable of performing up to $105\,\text{Msample}\cdot\text{s}^{-1}$ but is limited to run at $100\,\text{Msample}\cdot\text{s}^{-1}$ simultaneously on the two channels [5]. The DAC runs at $160\,\text{Msample}\cdot\text{s}^{-1}$ without decimation and up to $400\,\text{Msample}\cdot\text{s}^{-1}$ with decimation [6]. This configuration results in two input channels and two output channels. Therefore, when specifying real data input, two input signals of real data can be run simultaneously (one on each input channel); or, when specifying complex data input, one signal of complex data will occupy both input channels. Because a complex data signal, $S(n)$, is stored as described in (5.1), the in-phase (real-valued I) and quadrature (imaginary-valued Q) values each occupy an individual channel.

$$S(n) = I(n) + \mathrm{j}Q(n), \quad n = 0, 1, ..., N-1 \tag{5.1}$$

The FPGA performs all high-speed digital signal processing calculations and passes the data to the communication port for external processing via computer. These calculations are performed on the USRP N210 by a Xilinx Spartan 3A-DSP 3400 FPGA, which, with the supplied FPGA firmware images, performs decimation in time, digital down-conversion, and digital up-conversion [7]. The routines that are performed by the

FPGA are executed on all input and output sequences and depend on the firmware image embedded, which is highly programmable. It is possible, therefore, to program the FPGA to perform a variety of signal processing functions, such as signal acquisition and tracking, at very high speed prior to sending processed information to the user's computer.

The basic FPGA functions of interest to the user are the high speed decimation, down-conversion, and up-conversion. Decimation in time can be set during run-time and effectively sets a different sampling rate, f_s, by capturing only samples at the decimation (D) interval, described in (5.2). Upon decimation, the FPGA performs digital down-conversion to reduce the intermediate-frequency (IF) signal to baseband (B) by modulating the IF signal, i.e. multiplying the IF signal by a complex sinusoid at the center frequency f_c, described in (5.3).

$$f_\mathrm{s} = \frac{100 \cdot 10^6 \,\mathrm{sample{\cdot}s^{-1}}}{D} \tag{5.2}$$

$$S_\mathrm{B} = S_\mathrm{IF} \cdot \exp\left(\mathrm{j}2\pi f_\mathrm{c}\right) \tag{5.3}$$

The USRP N210 has the capability to link two USRP N210s with the MIMO cable so that they may share reference clocks, time synchronization, and Ethernet connections. This setup allows a user to have multiple input and output connections for multi-band or multi-antenna applications. The MIMO setup is particularly useful when working with multi-band signals that are co-dependent on the same time base, such as GPS and DGPS. The connection between two MIMO-linked USRP N210s can support data bitrates of up to $2\,\mathrm{Gbit{\cdot}s^{-1}}$ [8].

The USRP N210 requires a Gigabit Ethernet connection due to the high sampling rates. However, the USRP N210 may be connected to a Gigabit Ethernet switch with other data rates on the other side, such as $10/100\,\mathrm{Mbit{\cdot}s^{-1}}$ Ethernet, but a throttled connection is not recommended unless the user is confident the USRP N210 will be transmitting data well below those speeds. For example, to avoid data overrun while receiving a signal and decimating by 4, the USRP N210 would require a connection speed greater than $340\,\mathrm{Mbit{\cdot}s^{-1}}$, not including additional TCP-IP packet and frame

header information. The USRP's standard frame length is set to 1472 bytes[2]. In order to reduce bandwidth requirements, the frame size may be set to be larger (reducing header information) if the communication environment is relatively noise-free. Likewise, the frame size may be specified smaller in noisy environments, increasing data bandwidth requirements.

5.3.2 USRP Software

While the USRP is capable of performing FPGA routines autonomously, the majority of the communication to and from the USRP was initiated, in this thesis, by a networked computer which also performed the signal post-processing. A variety of software is available on both Ubuntu Linux, Mac OS X, and Microsoft Windows 7 platforms to work with the USRP, both of which are used here. The Universal Hardware Driver (UHD) that controls communication to the N-series USRP is widely available for almost any platform, including Ubuntu, Mac OS X, and Windows 7.

Most USRP software is developed on and for Linux-based operating systems. Consequently, Ubuntu Linux is a good environment to implement the most up-to-date distributions of SDR-related software. In this thesis, Ubuntu Linux ran the UHD and GnuRadio. The UHD was used in Ubuntu to perform low-level functions on the USRP hardware itself, such as updating the FPGA firmware images and receiving-and-writing samples to file [7]. GnuRadio is a graphical front-end program and was used to display various representations of a signal, such as an oscilloscope or frequency spectrum scope [9].

USRP software is also in development for the Mac OS X and Windows 7 platforms and is typically adapted from Linux. MathWorks has developed a USRP blockset for its Simulink simulation toolkit that implements the UHD for easy communication with the USRP. When compared with Ubuntu, MATLAB and the USRP blockset are used here for the majority of the signal receiving and post-processing tasks.

Detailed information about the system configuration can be found in Appendix A. Installation guides for the UHD and GnuRadio software on Ubuntu Linux 12.04 x64 and

[2]ISO/IEC IEC 80000-13:2008–Part 13 definition 1 byte = 8 bits.

the SDRu Blockset for MATLAB on x64 operating systems can be found in Appendix B and Appendix C, respectively.

Universal Hardware Driver

The Universal Hardware Driver is written by Ettus and is a driver-level link between the user environment and the USRP. That is, MATLAB and GnuRadio use the UHD to "talk" to the USRP. The UHD also provides feedback to the user environment, such as throttling requested sampling rates. The MATLAB UHD is limited to the following decimation settings: 1 to 128, 128 to 256 (values in this range must be even), and 256 to 512 (values in this range must be evenly divisible by 4). In addition, the UHD comes with several useful programs, discussed in Appendix B.

GnuRadio and Companion

GnuRadio is a Linux-based graphical front-end and flow-graph editor for the UHD, which allows a user to customize functions for the USRP using a variety of signal processing blocks [9, 10]. To use the USRP with GnuRadio, the computer must be set up as described in detail in Appendix B. GnuRadio is capable of building advanced flow graphs, as well as executing flow graph scripts written in Python [11]. A basic receiver diagram used in this thesis is displayed in Fig. 5.3. When launched, the following blocks were dragged onto the flow graph: USRP Source, Variable ($\times 2$), File Sink, WX GUI Slider ($\times 2$), and WX GUI FFT Sink. The settings were modified by double-clicking each block as shown in Fig. 5.4.

MathWorks MATLAB and SDR Support Package

MathWorks MATLAB is a matrix-manipulation program also capable of communicating with the USRP through an SDR support package, which contains a version of the UHD. Appendix C describes the procedure for setting up an x64 computer to use the USRP with MATLAB (this assumes the USRP is already set up with the correct firmware images, a process performed easily in Ubuntu). A simple USRP Receiver model was set up in Simulink to capture GPS data, shown in Fig. 5.5.

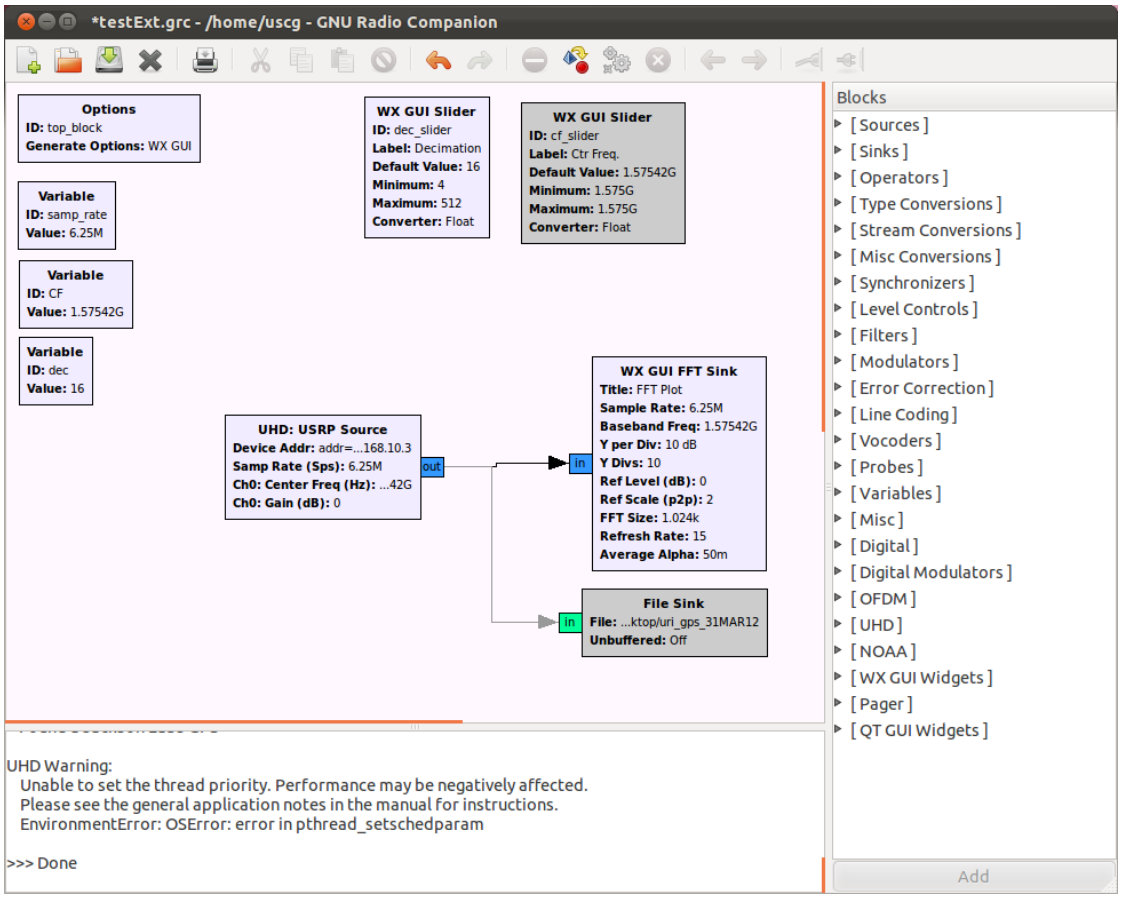

Figure 5.3: GnuRadio USRP GPS signal receiver.

The USRP settings were changed in the "SDRu Receiver" block. Note: if the UHD blockset successfully communicates with the USRP, the USRP's IP address is displayed in the Network menu and daughterboard information will be displayed in the "Hardware" section. The "sample time" was set to decimation/sampling frequency $\left(\frac{D}{f_s}\right)$. "Frame length" may be changed from the standard IP frame size 362 bytes to what is required and supportable by the infrastructure. Source and sink settings are shown in Fig. 5.6.

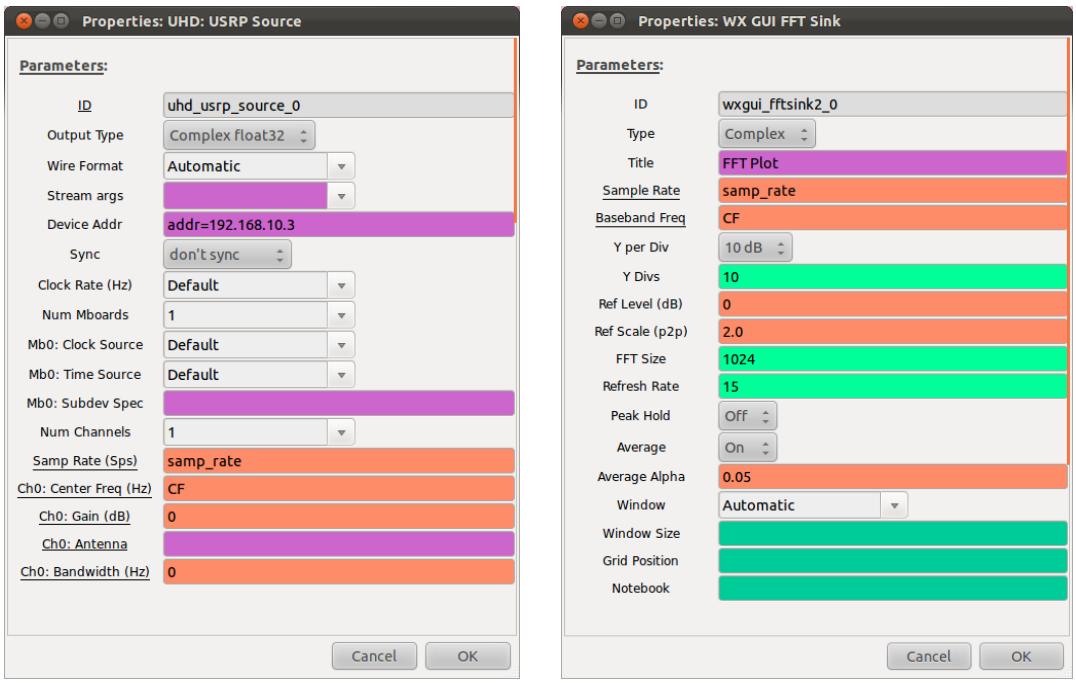

(a) GnuRadio USRP source settings. (b) GnuRadio FFT sink settings.

Figure 5.4: GnuRadio USRP blockset source and FFT sink settings.

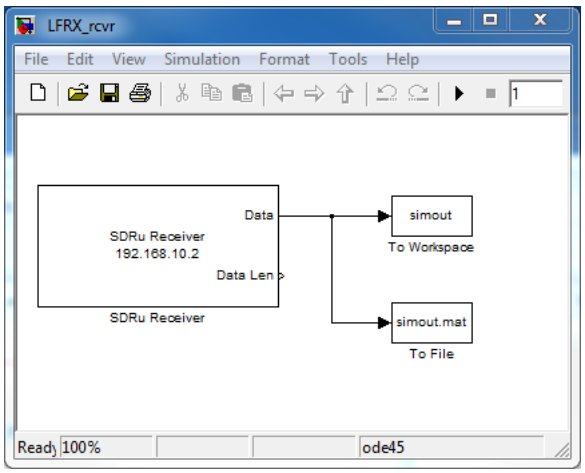

Figure 5.5: MATLAB USRP GPS signal receiver.

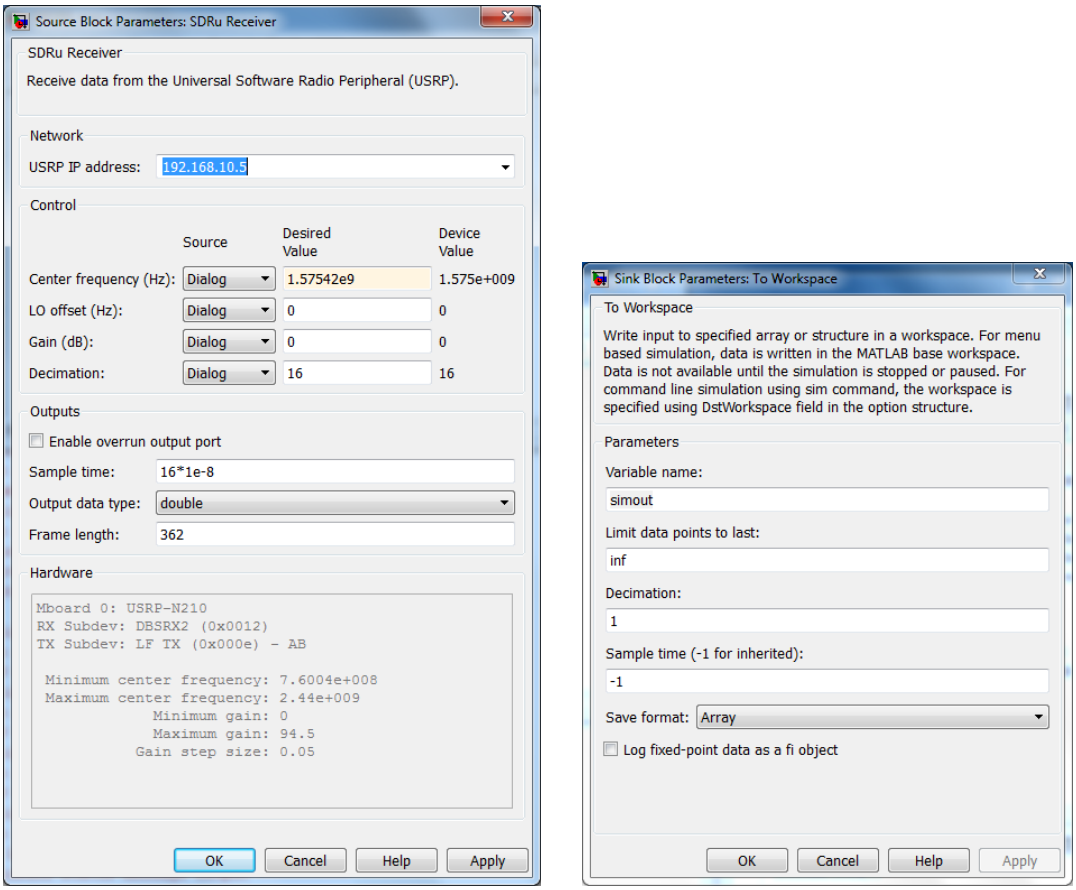

(a) Source. (b) Sink.

Figure 5.6: MATLAB SDRu blockset source and sink settings for GPS.

The USRP blockset default storage format is a "struct" object, and was simpler to set the "To Workspace" output block to "array" format for matrix manipulation. It is also possible to insert a "Frame Conversion" block prior to the storage block, which converts the frame-based information to a concatenated vector. Data from the USRP source is stored in a matrix of size "No. Frames × Frame Length" (i.e.: the first row is the first frame, the second row is the second frame, etc.). Note: using the "array" format restricts the data type to "double" which significantly increases data size. Typically, Simulink runs faster than the data is transmitted from the USRP, resulting in a recording time delay upon starting a Simulink model. This results in MATLAB padding the beginning data with zeros, unless instructed to disregard data frames of length zero. This expanded model is introduced in Fig. 5.7.

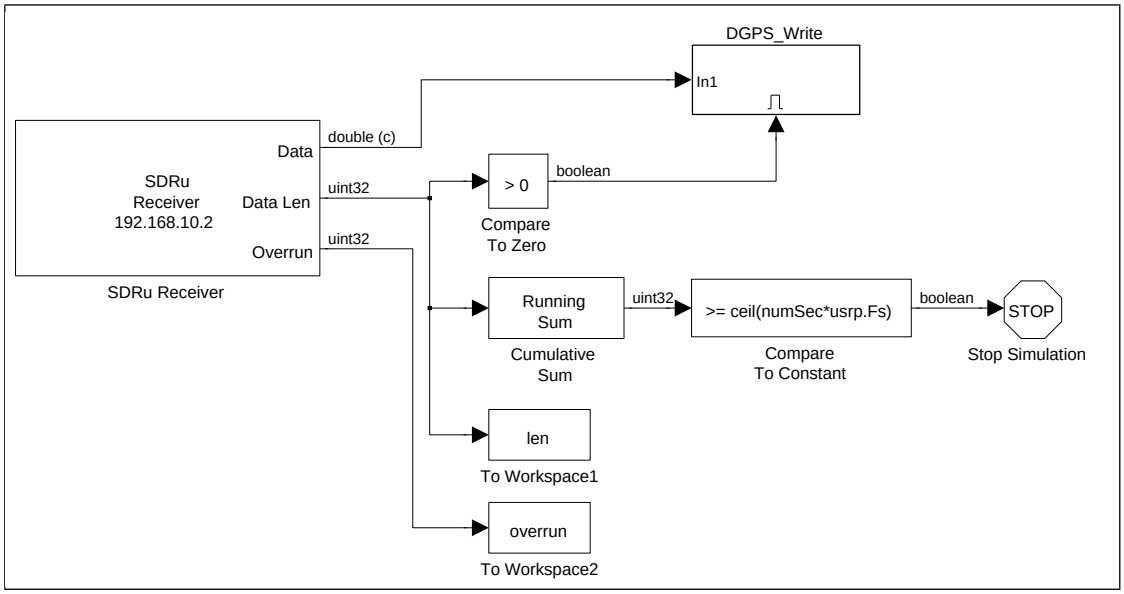

(a) DGPS receiver Simulink model.

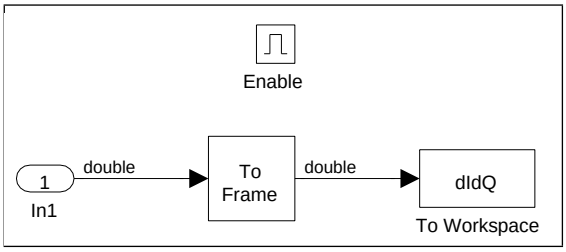

(b) DGPS receiver value-recorder subsystem.

Figure 5.7: Simulink DGPS receiver and subsystem.

5.4 Acquisition of DGPS and GPS signals

Upon setup of the software and USRP, the desired DGPS and GPS are observed from the SDR environment. Acquisition of DGPS and GPS signals is discussed below.

5.4.1 DGPS signal acquisition

As described in Chapter 1, DGPS stations broadcast signals at specific station frequencies between 285 kHz and 325 kHz, modulated with MSK at 100 bit·s^{-1} or 200 bit·s^{-1}. MSK is a constant-phase binary encoding scheme, where a 1 or 0 is represented by a corresponding ±90° phase shift. The bitstream is encoded in RTCM SC-104 format and arranged into messages. There are several message types, where the most common broadcast in the United States are Types 9-3, 7, and 6. Pseudorange corrections are broadcast in Type 9-3 messages, which contain PRCs for three satellites in each message. Type 7 messages are broadcast routinely every 10 minutes and contain information about the broadcasting beacon, such as location, health, and transmission characteristics. Type 6 are filler messages and contain only header data.

Messages are broken down into fields, where the number of fields in each message is based on the message type and amount of data to transmit. Every message type contains, at a minimum, header fields that denote the beginning of a message, transmitting beacon identifier, and message type identifier. A Type 9-3 message contains enough fields to describe the pseudorange corrections and range rate corrections (set to zero after SA was turned off) for three satellites. Message data bits are written to 30-bit words, such that there are 24 bits of data followed by 6 parity bits. Type 6 messages contain only a header and are 60 bits long; Type 9-3 messages contain more data and are 210 bits long. Parity bits are calculated with the same parity scheme used in GPS [12]. The actual construction of each message is discussed in depth in [13, 3] and is not reviewed here.

Here, we verify the USRP shows the expected DGPS signal characteristics and receives the expected beacons. We discuss extraction of the pseudorange corrections from the DGPS beacons in Section 5.5. To ensure the USRP received an MSK-modulated signal correctly, the USRP was set up to receive a 306 kHz signal from an Ashtech Z-12R

DGPS reference station. The reference station output actual corrections to a GPS signal from an antenna mounted on the roof of Kelley Hall at the University of Rhode Island. The MSK modulation can be seen from a GnuRadio screenshot in Fig. 5.8. To verify the USRP receives the expected DGPS stations, the GnuRadio and MATLAB environments were configured to display the DGPS frequency spectrum. A 60-second signal capture was taken at URI, shown in Fig. 5.9. Note: these graphs simply denote the presence of DGPS station signals, not the ability to successfully decode transmitted data.

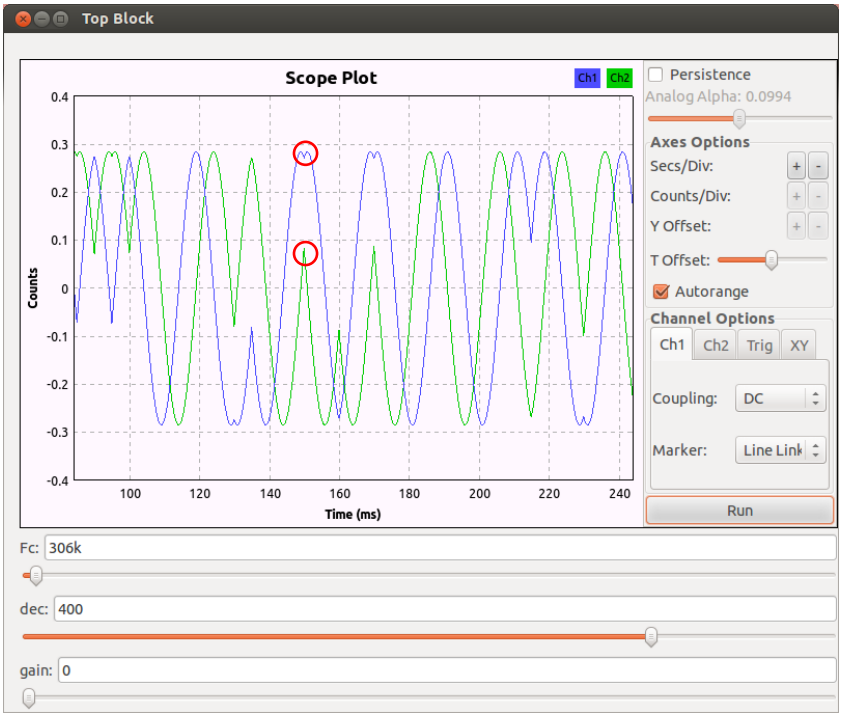

Figure 5.8: DGPS broadcast at 306 kHz showing MSK modulation generated by an Ashtech Z-12R reference station, viewed in GnuRadio oscilloscope block. Red circles indicate a bit transition, shown by 90° phase shifts on the in-phase and quadrature channels (1 and 2).

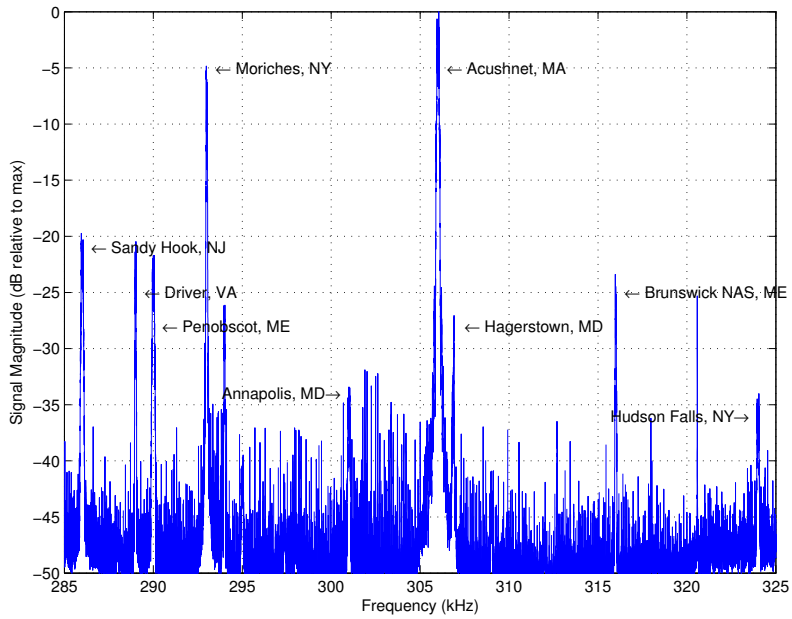

(a) URI

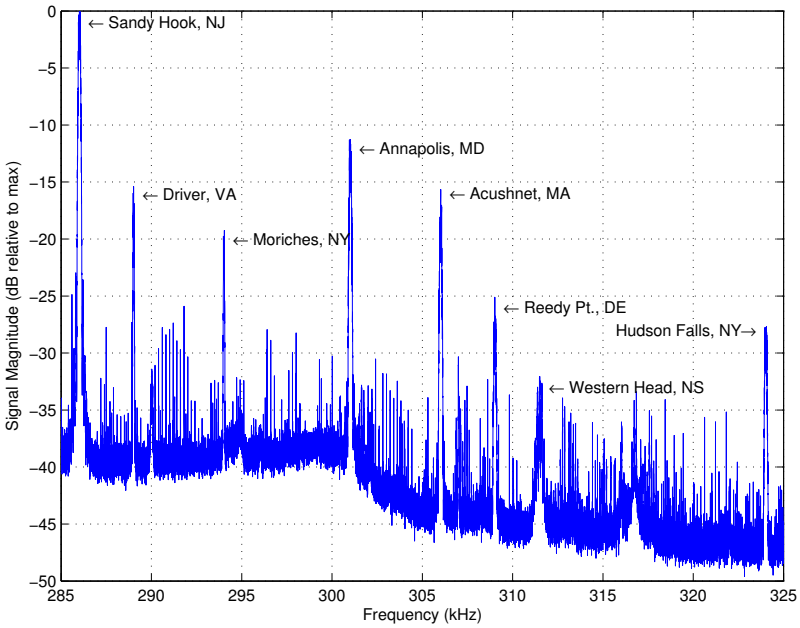

(b) New Haven, CT

Figure 5.9: Differential GPS spectra visible at URI and New Haven, CT, with visible stations labeled. Note: Moriches, NY, was broadcasting at low power during this capture.

5.4.2 GPS signal acquisition

To confirm that the USRP is capable of receiving single-frequency GPS C/A code necessary for DGPS corrections, the system was set up to collect and post-process over-the-air GPS data. A +20 dB inline amplifier was input to a USRP with a DBSRX2 daughterboard and split to the GPSDO module for higher-accuracy timing. Testing began on a Spirent GSS8000 simulator RF output; the frequency spectrum of the simulator can be observed in Fig. 5.11. The center frequency was set at 1575.42 MHz and the decimation set at 16, effectively a sampling rate of 6.25 MHz. Because GPS broadcasts 1000 PRN sequences per second, the USRP maintained a PRN sequence sampling rate of 6250 sample·s^{-1}.

A GPS satellite typically travels at speeds approximating 3.9 km·s^{-1} such that the broadcast signal is frequency modulated by as much as 10 kHz Doppler offset (typically, 5 kHz for land vehicles). A receiver will begin capturing GPS data for satellite acquisition somewhere in a PRN sequence. Therefore, the first stage in GPS signal acquisition is locking onto the PRN sequence by searching over frequency and code-phase.

Many methods of searching for PRN sequences have been proposed, this method employs the most basic method, sometimes called the serial-search algorithm. This method is diagrammed in Fig. 5.10. Essentially, the received GPS signal is compared against a known PRN sequence. The received signal is multiplied by the PRN sequence, the in-phase and quadrature components are then summed and squared individually, then summed for a final output cross-correlation value. This algorithm requires the input signal to be modulated by an appropriate Doppler offset and tested against each possible code-phase offset. While the serial-search algorithm is a time- and resource-consuming method of verifying the presence of a PRN sequence, the resultant "good" correlation peak is easily identifiable.

The Doppler offset ($\boldsymbol{\omega}$) is calculated by (5.4), typically in frequency steps (f_{step}) of 500 Hz. The frequency-offset GPS signal is given by (5.5), then searched over code-phase

(ϕ) by (5.6).

$$\boldsymbol{\omega} = 2\pi f_{\text{step}} n T_{\text{s}} \boldsymbol{t}, \quad n = \{-20, -19, \ldots, 20\} \tag{5.4}$$

$$\boldsymbol{d'} = \boldsymbol{d} \cdot \exp\left(\text{j}\boldsymbol{\omega}\right) \tag{5.5}$$

where n is the Doppler frequency bin, T_{s} is the sample time period, and $\boldsymbol{t}$ is the time vector from 0 to the length of the test signal, $\boldsymbol{d}$ is the sampled original GPS test signal, $\boldsymbol{\omega}$ is the Doppler frequency offset vector, $\boldsymbol{d'}$ is the Doppler-offset GPS signal.

The Doppler-modified GPS signal is then modified by code-phase, ϕ. This is accomplished with a circular shift for each sample, resulting in $\boldsymbol{d'_\phi}$, where ϕ is the number of samples shifted. The cross-correlation value, $c_{(\phi,\omega)}$, is obtained by (5.6) for a particular Doppler frequency offset and code-phase offset against a known PRN sequence.

$$c_{(\phi,\omega)} = \sum_{n=1}^{N-1} \left[\left(\boldsymbol{d'} I_\phi(n) \cdot p(n) \right)^2 + \left(\boldsymbol{d'} Q_\phi(n) \cdot p(n) \right)^2 \right] \tag{5.6}$$

where N is the bit-length of the test signal, $\boldsymbol{d'} I_\phi(n)$ and $\boldsymbol{d'} Q_\phi(n)$ are the nth bits in the respective in-phase and quadrature components of the modified GPS signal, and p is the PRN sequence upon which the GPS signal is being tested.

We tested the USRP for GPS signal acquisition with over-the-air transmissions using a GPS antenna mounted atop Kelley Hall at URI on 2012-04-05. Fig. 5.12 shows the results of a the serial search algorithm against a visible satellite broadcasting PRN 32 and non-visible satellite broadcasting PRN 3. The results of comparing this signal against all possible PRNs is documented in Table 5.2.

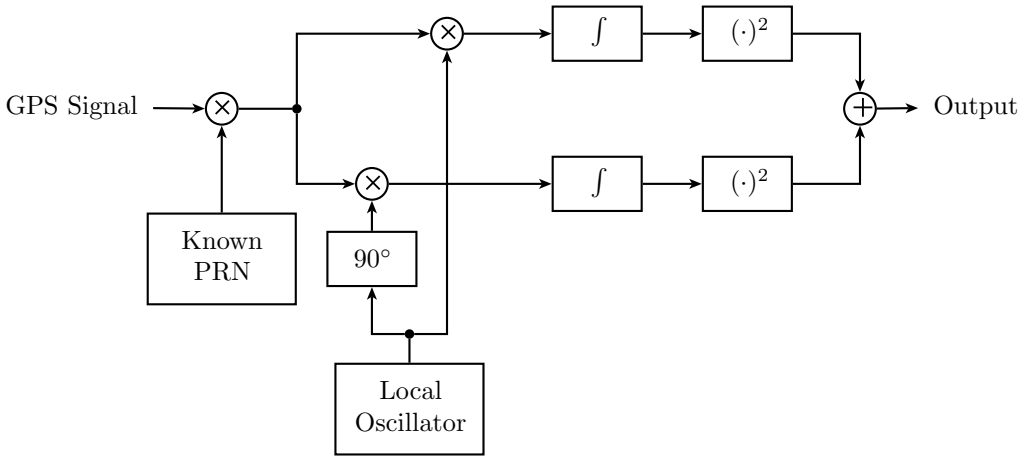

Figure 5.10: GPS serial search algorithm.

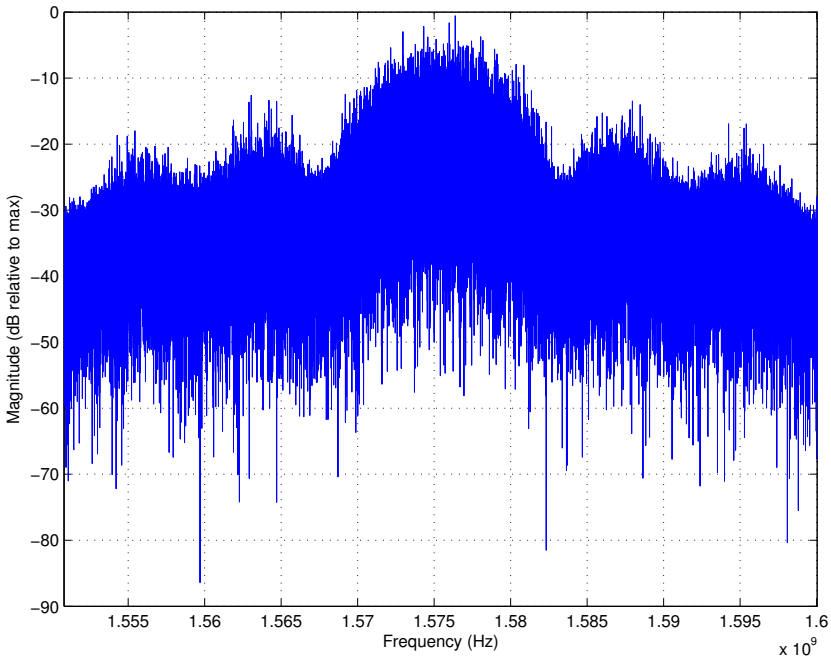

Figure 5.11: Spirent GSS8000 GPS simulator L1 signal spectrum. Signal amplified by GNSS +69 dB and inline amplifier +20 dB; captured in GnuRadio and imported into MATLAB.

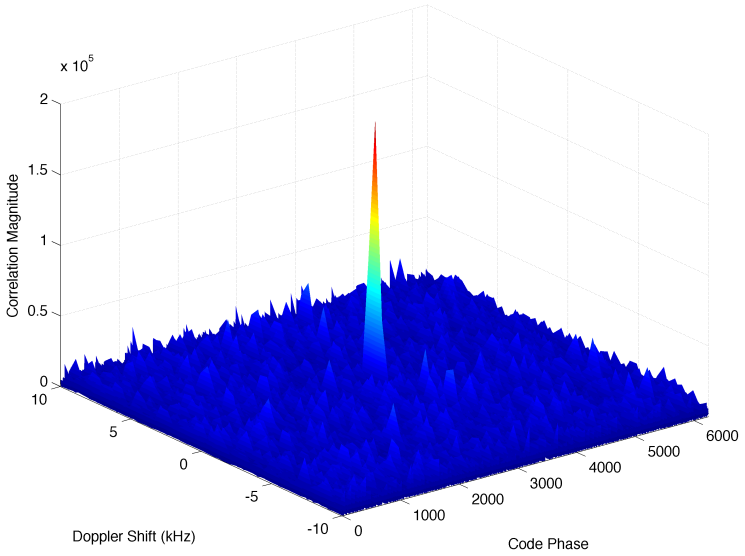

(a) Cross-correlation to visible SV, PRN 32.

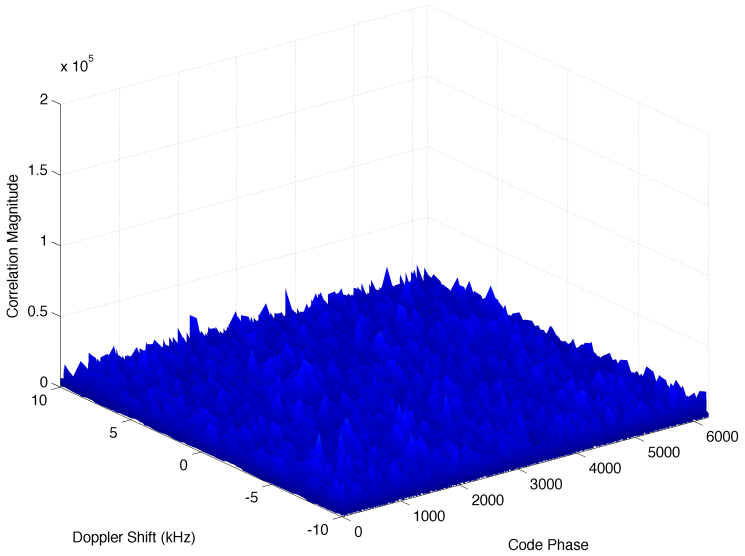

(b) Cross-correlation to non-visible SV, PRN 3.

Figure 5.12: Plots of cross-correlation to visible and non-visible satellites at URI. Note the relative difference in peak correlation magnitudes.

Table 5.2: GPS signal code-phase, Doppler shift, and correlation success to PRNs 1–32 captured at URI at 1600 (UTC-05) on 2012-04-05. PRN signal "Lock" indicates a maximum-to-mean ratio ≥ 20.0. Code-phase and Doppler shift values simply denote the highest peak; notice that for those satellites that exhibit a lock, their Doppler shift values are within the nominal range. SV visibility was confirmed with a co-located Ashtech Z-12R Differential GPS reference station.

PRN	Max:Mean	Lock	Code-Phase ϕ (Samples)	Doppler Shift ω (Hz)	Visible ($> 20°$ above Horizon)
1	14.9	-	3724	+9500	-
2	17.7	-	2014	-9500	-
3	11.8	-	5012	-3000	-
4	13.3	-	4134	+3000	-
5	11.9	-	187	+500	-
6	12.2	-	2106	-1500	-
7	11.0	-	3297	+7000	-
8	13.8	-	3768	+4500	-
9	13.3	-	3352	-8500	-
10	13.3	-	3883	-7000	-
11	13.2	-	817	+5000	-
12	12.1	-	2409	+3500	-
13	12.9	-	1769	-7000	-
14	62.8	Lock	3102	-1500	Yes
15	13.2	-	4348	-5000	-
16	16.6	-	5099	+4000	Yes[3]
17	11.0	-	3817	+1500	-
18	12.9	-	1202	+0	-
19	11.6	-	3659	-5500	-
20	23.5	Lock	4335	+2000	Yes
21	12.3	-	187	+1500	-
22	28.3	Lock	1463	-3500	Yes
23	11.4	-	1432	-6000	-
24[4]	64.1	Lock	2339	+0	Yes
25	81.5	Lock	1147	-2500	Yes
26	12.1	-	3260	-4500	-
27	13.5	-	798	+4000	-
28	13.6	-	3852	+10000	-
29	38.7	Lock	2568	+2000	Yes
30	50.6	Lock	2830	+3500	Yes
31	75.5	Lock	3047	+0	Yes
32	62.2	Lock	5702	+1000	Yes

[3]PRN 16 was re-tested using finer frequency steps of 250 Hz and 100 Hz and was locked at a maximum:average correlation ratio of 20.0 and Doppler shift of +3750 Hz. The low correlation-to-noise ratio may be attributed the correlation sequence occurring on a bit-edge transition.

[4]SVN 32 was listed as unhealthy and unusable, but was still broadcasting PRN 24 [14].

5.5 Networked DGPS with MATLAB

We created a MATLAB graphical user interface, building on related work by Wyman [3], to select and process DGPS information from multiple DGPS beacons, using the above system configuration. Fig. 5.13 shows a screenshot of this application, and displays two plots: a Fourier transform of the DGPS frequency band with DGPS frequencies of interest highlighted, and a scatterplot of satellites observed at each DGPS station for a time window of 15 seconds. These data were captured with an antenna placed atop the engineering building at USCGA, McAllister Hall.

A number of MATLAB functions were required to post-process decode the DGPS signal. The digitized signal from the USRP, in in-phase and quadrature format, was modulated down to baseband by multiplication with a complex sinusoid as in (5.4) and (5.5). The modulated signal is then passed to a function CPM_demod.m, where it is decimated further and passed to synch.m and vitdec.m. Synch.m synchronizes the input signal to the carrier bit-edge on 1-second intervals. This assists the decoding process because it assumes that the signal broadcast and receiving equipment have different sampling rates and those sampling rates drift with time. Vitdec.m is a modified Viterbi decoder that examines the trajectory of the carrier phase and determines, based on previous samples, if a bit transition has occurred. The output of CPM_demod.m is a bitstream which is then parsed by an RTCM SC-104 decoder, dgps_words.m. Because the DGPS parity check has the potential to pass invalid data as valid messages, the messages are then passed to sanitize.m, which checks the message headers against known beacon information, such as broadcast ID.

When the signal was decoded, the three closest beacons—Acushnet, MA; Sandy Hook, NJ; and Moriches, NY—were visible. Of particular note here is the reception of beacons much farther from the user's location, most likely from skywave propagation. At the USCGA recording location, beacons from as far as Driver, VA, and Annapolis, MD, are at high signal strengths, even higher than those from Sandy Hook, NJ. Later tests showed reception of up to 90% of the broadcast messages from Annapolis, MD. Because of this, a program designed to select the beacons with the three highest SNRs

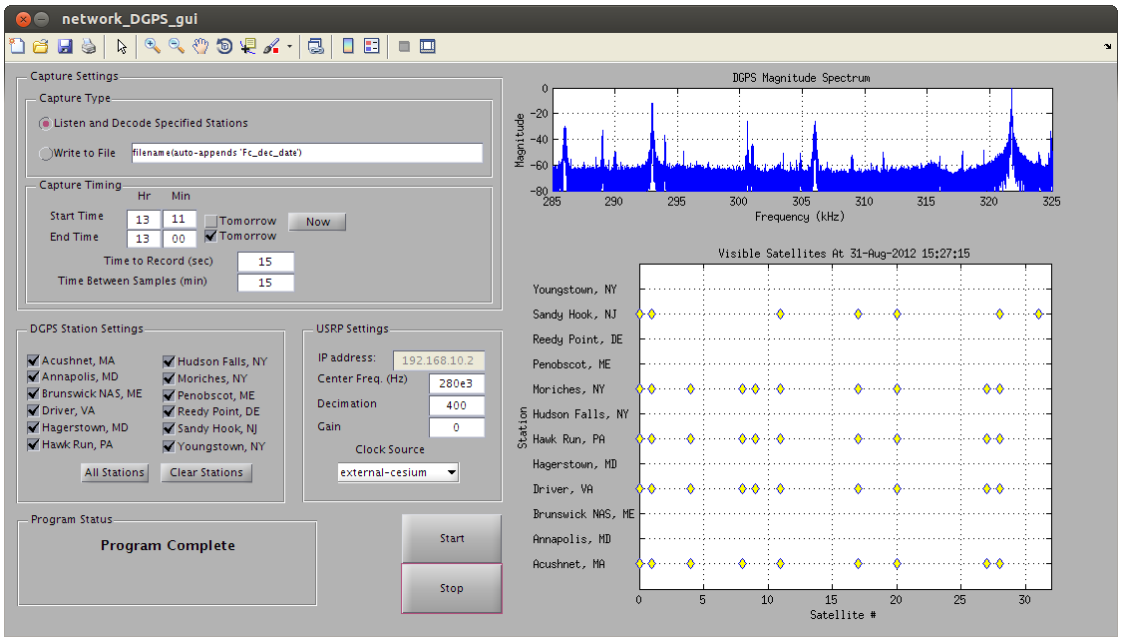

Figure 5.13: DGPS multi-beacon signal processing program.

might yield a surprising set of results. The following section describes application of over-the-air DGPS corrections to CORS GPS data.

5.6 CORS processing with MATLAB

We tested real-world networked DGPS performance by post-processing over-the-air pseudorange corrections with GPS data available through Continously Operating Reference Stations (CORS). The National Oceanic and Atmospheric Agency collects and stores pseudorange and ephemeris data from hundreds of CORS at locations around the world [15]. We collected and applied DGPS information from Group 2 beacons to GPS data from CORS sites within 250 km of Moriches, NY. Group 2 beacons include Moriches, NY; Acushnet, MA; and Sandy Hook, NJ. The CORS locations tested are shown in Fig. 5.14.

CORS sites in New England typically record data at intervals of 1, 5, and 30 seconds. Because PRCs are slow to change, we networked and applied those corrections within 40 seconds of a GPS record. We can now observe this behavior and compare real-world PRCs collected from Moriches, NY, shown in Fig. 5.15, to those from the GPS simulator, shown in Fig. 4.9.

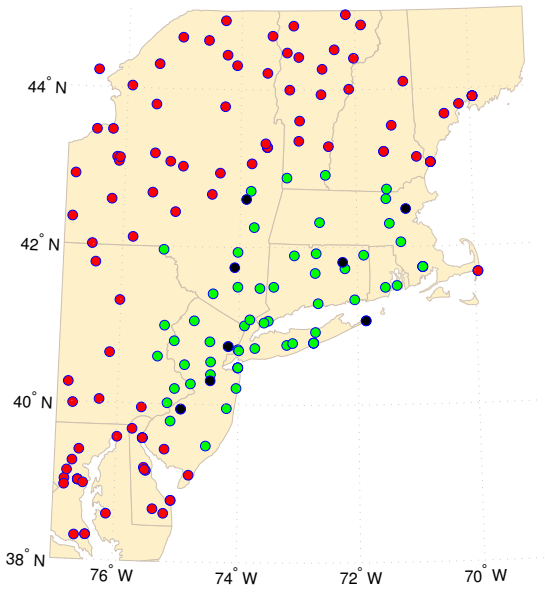

Figure 5.14: Map of CORS locations processed with networked DGPS. Tested sites were located within 250 km of Moriches, NY, colored in green. Non-operational sites within this radius are colored black, sites outside the radius are colored red. Lambert projection.

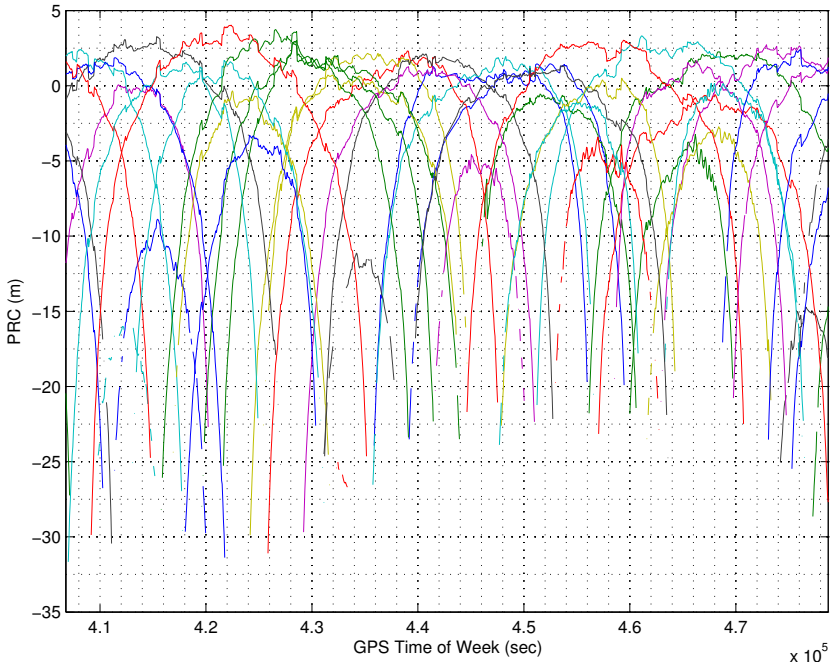

Figure 5.15: Pseudorange corrections broadcast by Moriches, NY, from 2013-03-14 to 2013-03-15. Compare to the GPS simulator's PRCs in Fig. 4.9.

The real-world tests break down algorithm performance by bias magnitude and 95% scatter radius, shown in Figs. 5.17 and 5.18, respectively. We expect to see similar performance between these real-world tests and the GPS simulator's spatial results, shown in Figs. 4.14 and 4.15. First, we select an arbitrary CORS site—YORK, located in York, PA—so we can see how the real-world effects are manifested on a position plot, shown in Fig. 5.16. Here, the noise, atmospheric delays, time delays, and ephemeris errors in the GPS data visibly distort the position plots and confirm the analyses from Chapter 4. Also visible is the hierarchy of performance between the networked DGPS algorithms found in Chapter 3.

Reviewing the plots in Figs. 5.17 and 5.18, we notice that the bias magnitude and scatter radii of the raw GPS positions varies widely between CORS sites. This is likely due to the difference in quality of GPS receivers and whether they employ some form of noise mitigation, such as position averaging.

With respect to the bias magnitude plots, each networking method appears in Fig. 5.17 exhibits the same spatial bias characteristics as those from the simulator trials, shown in Fig. 4.14. While the CORS sites are located only in directions north and west of the beacon grouping, we can see that the averaging method exhibits a linear increase in bias away from the beacon grouping's centroid. The inverse-range and inverse-range-squared plots show low bias within the beacon triangle, and bias magnitudes lower than simple averaging at the fringe CORS sites. As expected, the bias magnitude of SLI is the lowest of the four methods and constant across almost all test sites.

With respect to the 95% scatter radii, the real-world tests in Fig. 5.18 behave very similarly to the simulator tests in Fig. 4.15. Simple averaging exhibits a near-constant radius of about 2.3 m at all locations, excluding those outliers with poor raw GPS accuracy. Again, the range-based algorithms show higher variance at CORS sites close to beacons and averaging of the variance at locations farther away. SLI scatter radii behave as expected from Fig. 4.15(d) with low variance along the beacon line and higher variance at a tangent.

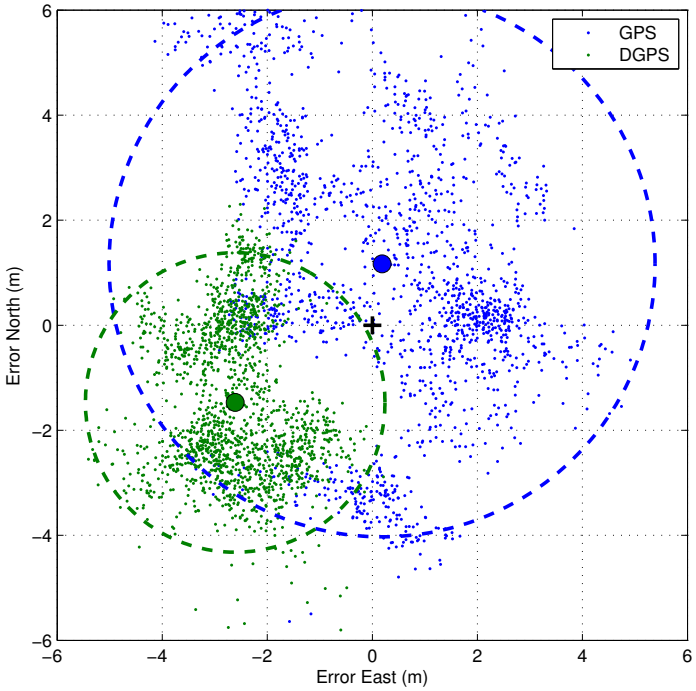

(a) GPS and single-beacon DGPS.

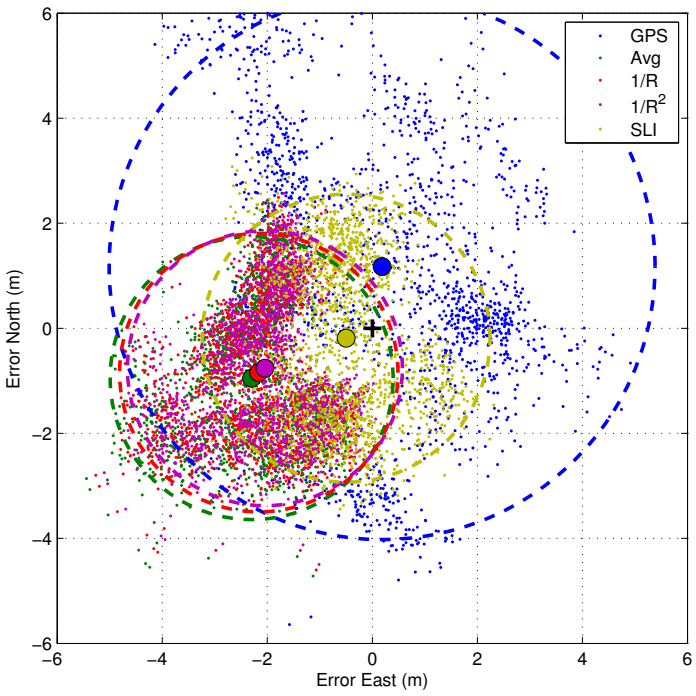

(b) GPS and networked DGPS.

Figure 5.16: Position plots for YORK CORS site, in York, PA. Single-beacon solutions use Sandy Hook, NJ, for pseudorange corrections; networked DGPS solutions use beacon grouping 2. YORK is located in line with Group 2 beacons and approximately 237 km southwest of Sandy Hook, NJ.

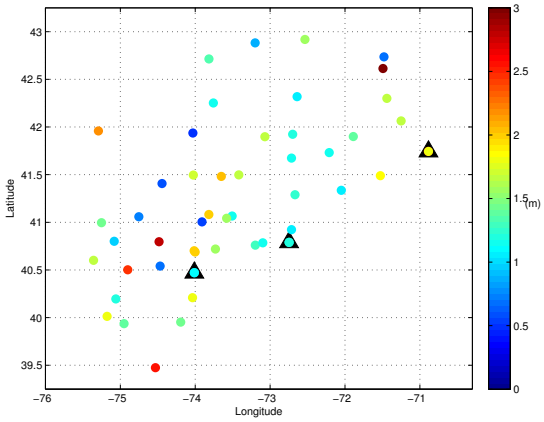

(a) GPS.

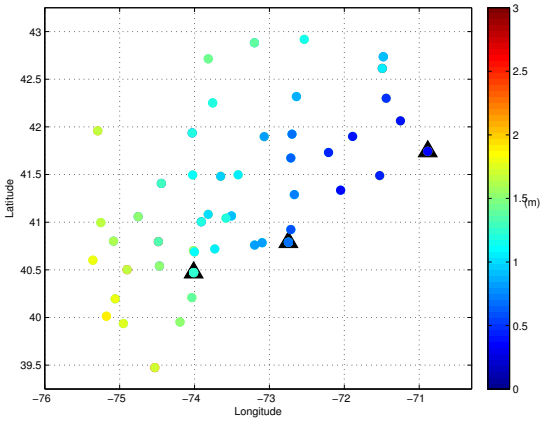

(b) Simple averaging.

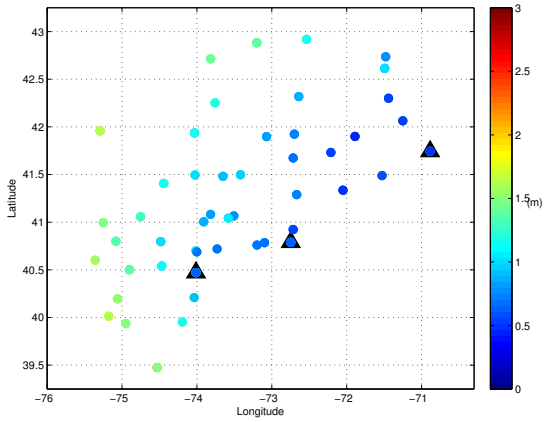

(c) Inverse-range.

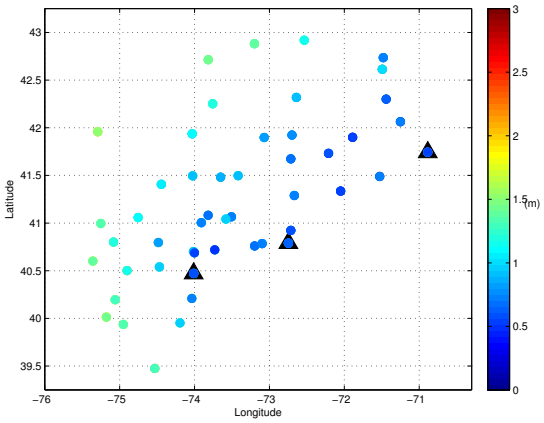

(d) Inverse-range-squared.

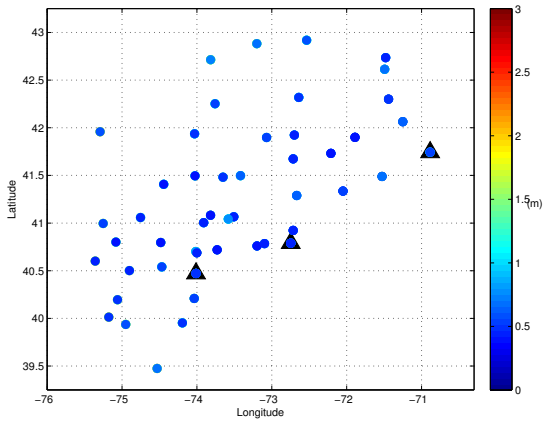

(e) SLI.

Figure 5.17: Bias magnitude plotted by CORS site. Networked DGPS positions are calculated with Group 2 beacons' corrections applied to CORS sites within 250 km of Moriches, NY. Beacon locations are plotted in black triangles.

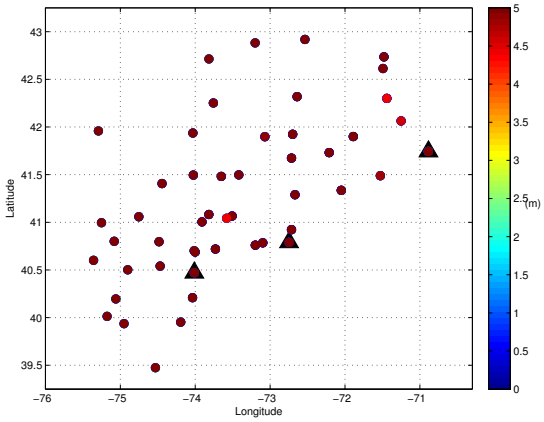

(a) GPS.

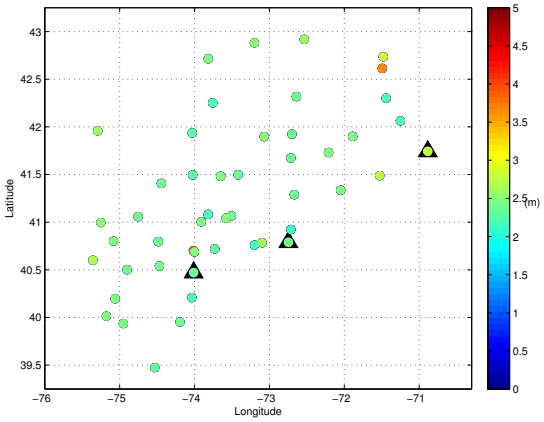

(b) Simple averaging.

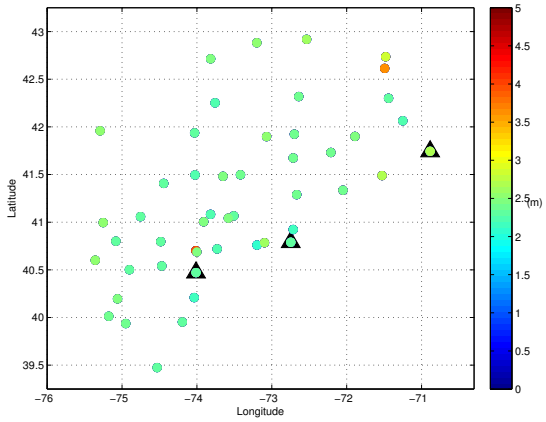

(c) Inverse-range.

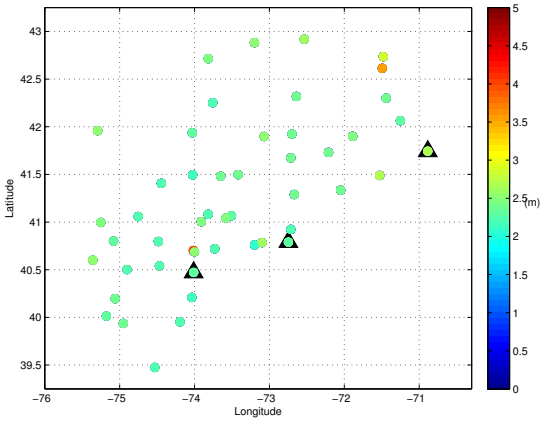

(d) Inverse-range-squared.

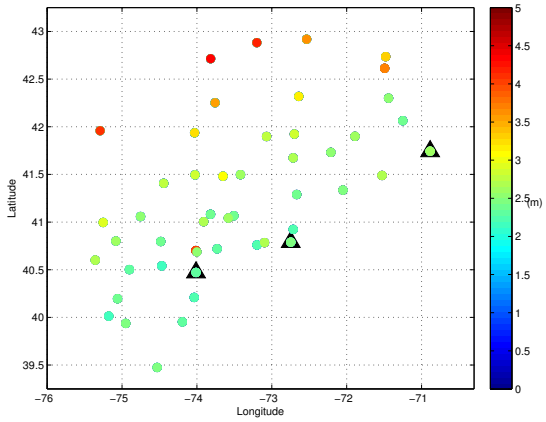

(e) SLI.

Figure 5.18: 95% scatter radius plotted by CORS site. Networked DGPS positions are calculated with Group 2 beacons' corrections applied to CORS sites within 250 km of Moriches, NY. Beacon locations are plotted in black triangles.

List of References

[1] Ettus Research. "USRP users mailing list." [Accessed: 1 Jul. 2011]. [Online]. Available: http://lists.ettus.com/pipermail/usrp-users_lists.ettus.com/

[2] *USRP N200/N210 Networked Series*, Ettus Research, Mountain View, CA, Jan. 2012, pp. 1–2.

[3] G. C. Wyman, "A software radio testbed for Coast Guard communication and navigation applications," M.S. thesis, Dept. Elect., Comput., Biomed. Eng., Univ. Rhode Island, Kingston, RI, 2010.

[4] *Installing the Ettus Research GPSDO Kit for USRP N200 Series & E100 Series*, 1st ed., Ettus Research, Mountain View, CA, Jan. 2012, pp. 1–2.

[5] *Dual Channel, 14-bits, 125/105/80/65 MSPS ADC with DDR LVDS/CMOS Outputs*, C ed., Texas Instruments, Dallas, TX, Feb. 2012, pp. 1–4.

[6] *16-Bit, 160 MSPS 2x/4x/8x Interpolating Dual TxDAC+ D/A Converter*, C ed., Analog Devices, Norwood, MA, Jan. 2006, pp. 5–8.

[7] "Loading firmware on the USRP N210." [Accessed: 18 Jul. 2011]. Apr. 2011. [Online]. Available: http://greencrest.blogspot.com/2011/04/loading-firmware-on-usrp-n210.html

[8] *TLK2701 1.6 to 2.7 Gbps Transceiver*, Texas Instruments, Dallas, TX, Mar. 2008, p. 1.

[9] E. Blossom, J. Corgan, M. Ettus, *et al.* GnuRadio. "GnuRadio wiki." [Accessed: 1 Jul. 2011]. [Online]. Available: http://gnuradio.org/redmine/projects/gnuradio/wiki

[10] GnuRadio. "GnuRadio mailing list." [Accessed: 25 Nov. 2011]. [Online]. Available: http://lists.gnu.org/archive/html/discuss-gnuradio/

[11] "Forum: GNU radio." [Accessed: 18 Jul. 2011]. Aug. 2011. [Online]. Available: http://www.ruby-forum.com/forum/gnuradio

[12] *Navstar GPS Space Segment/Navigation User Segment Interfaces*, Global Positioning Systems Directorate Specification IS-GPS-200, Rev. F, Sept. 2011.

[13] *RTCM Recommended Standards for Differential Navstar GPS Service*, Radio Technical Commission for Maritime Services (RTCM) Special Committee No. 104 Standard 2.1, Jan. 1994.

[14] United States Naval Observatory. "Current GPS constellation." [Accessed: 5 Apr. 2012]. Apr. 2012. [Online]. Available: http://tycho.usno.navy.mil/gpscurr.html

[15] National Oceanic and Atmospheric Agency. "Continuously operating reference station (CORS)." [Accessed: 14 Mar. 2013]. Mar. 2013. [Online]. Available: http://geodesy.noaa.gov/CORS/

CHAPTER 6

Considerations and Conclusions

6.1 Other considerations

There are a number of real-world conditions that complicate application of networked DGPS algorithms which we did not consider while testing on the simulator and are discussed below. Here, we discuss two types: sub-optimal and complex conditions. We define sub-optimal conditions as those events that cannot be controlled by the user and complex conditions as those things that the user (or receiver equipment) should take into consideration.

Sub-optimal conditions could include: reception of fewer than three beacons, poor GPS constellation, and ancillary noise sources. Of course, application of a spatial linear interpolation solution is predicated on receipt of three or more beacons. If receiving corrections from only two beacons, one potential solution would be two-dimensional linear interpolation. Effectively, this is the same as the proposed three-dimensional SLI, also taking into account beacon distance and azimuth. A poor constellation increases the dilution of precision for GPS solutions and is common in high-latitude regions such as the Arctic Ocean. This effect would be carried through when applying the transmitted DGPS corrections at the user's receiver. Ancillary noise sources, as discussed previously, can cause large variations in DGPS PRC accuracy. Particularly, SED events distort PRC accuracy across wide geographic areas. It is a potential strength of the networked DGPS algorithm, which can track and compensate-for those wide-area disturbances as they move through a beacon grouping. Consideration of these sub-optimal conditions presents itself as future work.

Complex conditions such as poor beacon geometry and areas with more than three DGPS beacons are interesting areas of further concentration. Poor beacon geometry is common in littoral areas, presenting issues with the 95% scatter radius discussed above. Sometimes, a beacon distinct from the grouping in use may be decoded; it is likely that, even though that beacon's PRCs may come in sporadically, storing and using

that beacon's PRCs may stabilize the variance of a networking algorithm like SLI. Poor beacon geometry can also include the geometry of the beacon group relative to the GPS constellation. For example, a case in which the beacons are lined parallel to a poor GPS constellation low on the horizon is likely to produce unfavorable correction behavior. In an area where four or more beacons are available to a user, the SLI solution could be applied to a number of different three-beacon groups. Most coastal areas nearby large seaports of in the U.S.A. can receive up to six beacons. In this case, should a three-beacon group be selected? Or should a least-squares hyperplane be fitted to all four-plus beacons? Perhaps a multi-dimensional plane could be considered. In addition, satellites low on the horizon tend to possess poor signal strengths, so it may be worth considering weighting each satellite based on SNR.

6.2 Future work

This thesis presents several methods of networking multiple DGPS beacons to improve horizontal position accuracy. However, discussion of three-dimensional positioning for each of these methods has not yet been discussed and presents a good area for further study, particularly for aviation applications. In this research we have assumed that the user is typically slow-moving and traveling along the water or in flat inland areas, but we know that other DGPS users include railroad, inter-state truck commerce, farm machinery, and airplane operators. Because aircraft travel at high speeds and experience different atmospheric conditions, it would be interesting to see how networked DGPS concepts differ from those discussed in this thesis.

We have demonstrated that DGPS information from multiple beacons can be captured simultaneously under real-life conditions; actual implementation of networked DGPS methods should be explored further. So far, our research has been limited to post-processing data, it would be useful to collect DGPS information from multiple beacons and apply them in real time to GPS data. The DGPS band can easily be captured, decimated, and processed into a bitstream on a single FPGA. The FPGA can also accept an *a priori* GPS position input and calculate the networked-DGPS pseudorange correc-

tions. Implementing this on the FPGA or in an SDR environment would be a low-cost implementation which could be used for further testing.

6.3 Conclusions

This thesis answers two questions about networking Differential GPS. The first is: "If available, how does one select the corrections to use from multiple sets of corrections?" We claim that "reception" of a beacon is a signal-to-noise ratio better than $37.5\,\mathrm{dB{\cdot}\mu V{\cdot}m^{-1}}$ provided that beacon can be decoded into RTCM SC-104 format. An examination of the desired qualities of a beacon grouping indicates that those beacons that are in a spatially-diverse and arranged in an equilateral shape are the highest-quality beacon groupings. We propose a Quality Factor, Q, to define the beacon grouping for each networking algorithm used. For the range-based algorithms, those beacon groups that are closest to the user's position are used; for the Spatial Linear Interpolation algorithm, the beacon group with the lowest noise variance term at the user's location are used.

The second question is: "Is it advantageous to combine pseudorange corrections in some way?" We determine that networking multiple DGPS beacons can provide marine and inland users with a greater degree of accuracy and precision in their position solutions than current single-beacon methods. For those users that are within a beacon triangle, all four methods will provide enhanced accuracy for whatever navigation application is needed. We have examined four different methods of combining multiple beacons and, given that DGPS has inherent biases dependent on the user's position, propose a novel solution which minimizes that bias. In particular, spatial linear interpolation is the first networked DGPS method that uses the beacon grouping's geometry to remove solution bias, and does so quite effectively. Both simulated and live-captured data analyses support this conclusion. Even though it was only 2011–2012 that we discovered DGPS-corrected positions are biased, we now have several solutions that are easy to implement.

The methods proposed and evaluated here are simple enough to be implemented on low-complexity, low-cost hardware and require nearly no changes to the user infrastruc-

ture and none to the DGPS broadcasting agency, which reduces the cost of potential improvement. It is also worth noting that the application of these methods would alter only one component of the typical DGPS-corrected system employed by users—the DGPS receiver—the DGPS antenna, GPS antenna, GPS receiver, and user interface require no changes!

APPENDIX A

System Configuration

A.1 Purpose

This appendix describes the configuration of the various hardware systems and physical connections used in this thesis to collect, control, and transmit information. It is intended for reproduction of the information and results gathered.

A.2 Ettus Research USRP

- USRP: Model N210 rev. 2 running FPGA firmware 003.002.003
- DBSRX2: a daughterboard for GPS work, modified to provide 3.3 V to in-line amplifier (jumper posts and jumper attached at J101)
- GPSDO: a disciplined oscillator module that synchronizes to a GPS signal and provides a 10 MHz clock signal to the USRP motherboard

Table A.1: Major components and capabilities of the USRP N210.

Use	Manufacturer	Model	Capacity	Ref.
FPGA	Xilinx	XC3SD3400A	$3.4 \cdot 10^6$ gates	[1]
A–D Converter	Texas Instruments	ADS62P44	100 Msample·s^{-1}	[2]
D–A Converter	Analog Devices	AD9777BSV	160 Msample·s^{-1}	[3]
MIMO Transceiver	Texas Instruments	TLK2701	160 Gbit·s^{-1}	[4]
Adjustable Reg. (DBSRX2)	Linear Technology	LT1085	-	[5]

A.3 Receiving equipment

- GPS antenna: TrueTime model 142-614-50
- GPS in-line amplifier: Raven/StarLink model LA-21-L1L2-B (+20 dB)
- DGPS antennas: Raven/StarLink model MBA-2, 9 VDC whip
- DGPS filter & amplifier: Krohn-Hite model 3905C

- DGPS antenna bias-tee: Minicircuits models ZFBT-4R2GW-FT+, ZFBT-6GW-FT+

Table A.2: Cable types and attenuations used in GPS signal capture.

Use	Type	Manufacturer	Length	Atten. @ 1500 MHz (dB/100 ft)	Total Atten.
Adapter	RG-58	-	1.5 ft	19.1	0.3 dB
Long-Run	LMR-400	Times Microwave	40 ft	5.1	2.1 dB
USRP	RG-58	Belden 7806R	1.5 ft	13.7	0.2 dB
				Total:	2.6 dB

A.4 USRP client computer

- Model: Apple MacBook Pro 8,2
- CPU: Intel i7-2635QM @ 2.00 GHz
- Memory: 8.00 GB
- Storage: Other World Computing model Mercury Electra 6G, solid-state, 240 GB capacity, SATA 6 Gbit·s^{-1} interface
- Platforms and software:
  1. Mac OS X (10.6.8) x64 with MathWorks MATLAB R2012b and UHD 003.002.003
  2. Ubuntu 12.04 x64 with GnuRadio and UHD 003.002.003

A.5 USRP blade server

- Model: Silicon Mechanics Rackform iServ R254
- CPU: Intel Xeon E5420 2×4 @ 2.50 GHz
- Memory: 24.0 GB DDR2 240-pin @ 667 MHz
- Hard drive: Hitachi model HDS723020BLA642, hard disk, 2.0 TB capacity, SATA 3 Gbit·s^{-1} interface

- Platforms and software: Ubuntu 12.04 x64 with MathWorks MATLAB R2012a, GnuRadio, and UHD 003.002.003

List of References

[1] *Spartan-3A DSP FPGA Family Data Sheet*, 3rd ed., Xilinx, San Jose, CA, Oct. 2010, pp. 2–3.

[2] *Dual Channel, 14-bits, 125/105/80/65 MSPS ADC with DDR LVDS/CMOS Outputs*, C ed., Texas Instruments, Dallas, TX, Feb. 2012, pp. 1–4.

[3] *16-Bit, 160 MSPS 2x/4x/8x Interpolating Dual TxDAC+ D/A Converter*, C ed., Analog Devices, Norwood, MA, Jan. 2006, pp. 5–8.

[4] *TLK2701 1.6 to 2.7 Gbps Transceiver*, Texas Instruments, Dallas, TX, Mar. 2008, p. 1.

[5] *7.5A, 5A, 3A Low Dropout Positive Adjustable Regulators*, G ed., Linear Technology, Milpitas, CA, pp. 1–5.

APPENDIX B

USRP N210 Setup on Ubuntu 12.04 x64

B.1 Purpose

This Appendix describes the procedure used in this thesis to control an Ettus Research USRP N210 from the Ubuntu 12.04 x64 operating system. It is intended to be performed with a new USRP N210 and performed in sequence. Starting with a previous build of the UHD or GnuRadio will likely cause problems; any other installations should be removed prior to proceeding. There are 4 steps to set up the USRP, described in detail in the sections below.

B.2 Install Ubuntu 12.04 x64

Perform a clean installation of Ubuntu 12.04 and install the most recent updates. Ubuntu can be downloaded and installed from `http://www.ubuntu.com`. Updates can be installed from "Top Panel > Power Menu > Software Up To Date".

Due to the variety of configurations, these steps are not included in this appendix. Many configuration setup guides can be found on the Ubuntu website.

B.3 Establish USRP IP-Layer Communication

The USRP N210 requires a Gigabit Ethernet connection which may be to the computer's network interface card (NIC) or a Gigabit Ethernet switch/router. In this guide, the USRP is connected directly to the computer's NIC. The default USRP IP address is 192.168.10.2 and a computer accessing it must be on the same subnet. The latest USRP manuals and instructions can be found on the Ettus site at `http://files.ettus.com/uhd_docs/manual/html/usrp2.html`

1. Connect the USRP to the computer: plug in the Ethernet cable between the USRP and the computer, then power on the USRP.

2. Access NIC IP settings: select "Top Panel > Network Menu > Edit Connections", then select the "Add".

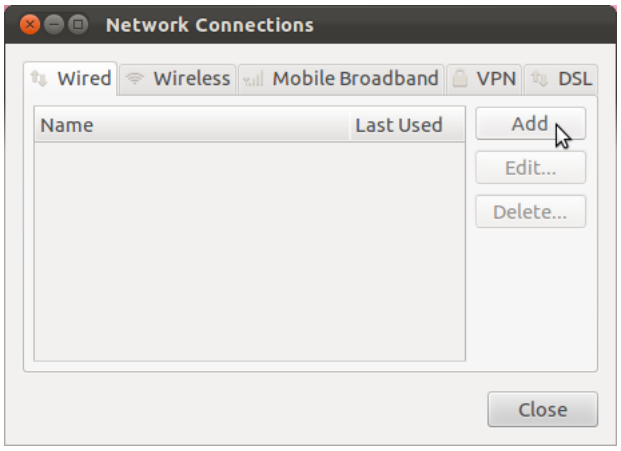

3. Create IP settings for the USRP: in the "Wired" tab, change the "Connection Name" as desired (in this case, `USRP 192.168.10.x`), select the "Device MAC address" of the NIC for use, then select "IPv4 Settings." Set the IP address to `192.168.10.1`, the netmask to `255.255.255.0`, and leave the gateway blank (optionally, set the gateway to `192.168.10.1`), then select "Save".

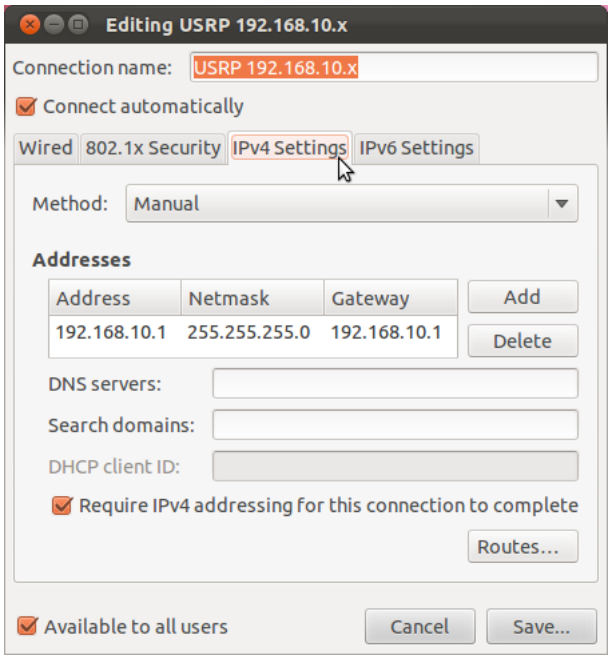

4. Select the newly-stored IP setting "USRP 192.168.10.x" from "Top Panel > Network Menu".

5. The USRP should now be recognized by the operating system. To test the connection between the host computer and USRP, in terminal, execute:

   ```
   $ ping 192.168.10.2
   ```

B.4 Build USRP UHD 003.002.003

The UHD enables device control. UHD version 003.002.003 was chosen specifically to support cross-platform functionality of the USRP in both the Ubuntu and Windows 7-MATLAB R2012a environment, which, as of installation, supports only UHD 003.002.003.

There are a variety of procedures that will build the UHD with numerous different configurations. The most up-to-date instructions can be found on the Ettus Research website at
`http://code.ettus.com/redmine/ettus/projects/uhd/wiki`.

1. Download and install UHD dependencies.

   (a) GnuRadio dependencies (from Ubuntu 11.04)[1], execute:

   ```
   $ sudo apt-get -y install libfontconfig1-dev \
   libxrender-dev libpulse-dev swig g++ automake autoconf \
   libtool python-dev libfftw3-dev libcppunit-dev \
   libboost-all-dev libusb-dev fort77 sdcc sdcc-libraries \
   libsdl1.2-dev python-wxgtk2.8 git-core guile-1.8-dev \
   libqt4-dev python-numpy ccache python-opengl libgsl0-dev \
   python-cheetah python-lxml doxygen qt4-dev-tools \
   libqwt5-qt4-dev libqwtplot3d-qt4-dev pyqt4-dev-tools \
   python-qwt5-qt4
   ```

   (b) Supplemental dependencies (for Ubuntu 12.04), execute:

   ```
   $ sudo apt-get -y install cmake python-tk
   ```

2. Download the UHD (specifically, version 003.002.003).

[1] Taken from `http://gnuradio.org/redmine/projects/gnuradio/wiki/UbuntuInstall`

(a) Use an Internet browser to download "release_003_002_003.tar.gz" from `https://github.com/EttusResearch/UHD-Mirror/tags`, then use the Archive Manager to extract the file to the home directory.

(b) Rename the folder to `uhd323`:

```
$ mv EttusResearch-UHD-Mirror-fb13983 uhd323
```

3. Install the UHD.

(a) Build a common source directory:

```
$ sudo chown $USER /usr/local/src
$ sudo chmod u+rwx /usr/local/src
```

(b) Copy uhd323 folder to the common source directory:

```
$ cp -r $HOME/uhd323 /usr/local/src && rm -rf $HOME/uhd323
```

(c) Install UHD:

```
$ cd /usr/local/src/uhd323/host
$ mkdir build
$ cd build
$ cmake ../
$ make
$ make test
$ sudo make install
$ export LD_LIBRARY_PATH=$LD_LIBRARY_PATH:/usr/local/lib
$ sudo ldconfig
```

4. Verify correct operation of UHD:

```
$ uhd_find_devices    # Returns IP address & serial no. of USRP
$ uhd_usrp_probe      # Returns information about USRP config.
```

5. The UHD and FPGA must be running the same version. If the UHD and FPGA firmware are different versions, `uhd_usrp_probe` returns an error similar to the following:

```
Error: RuntimeError:
Please update the firmware and FPGA images for your device.
See the application notes for USRP2/N-Series for instructions.
Expected FPGA compatibility number 7, but got 6...
```

Write correct firmware images to the USRP.

(a) Download binaries for FPGA image 003.002.003 from: `http://files.ettus.com/binaries/master_images/archive/older/` and use the Archive Manager to extract the files to the home directory.

(b) Write FPGA firmware binaries to USRP:

```
$ cd /usr/local/src/uhd323/host/utils
$ ./usrp_n2xx_net_burner_gui.py
```

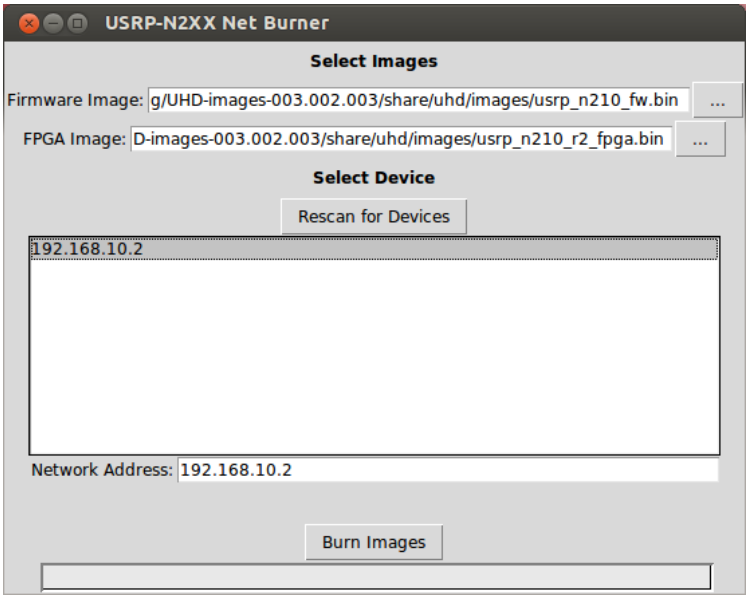

(c) Power-cycle the USRP and verify correct operation of UHD:

```
$ uhd_usrp_probe
```

6. To configure the USRP to communicate with the GPSDO module:

```
$ cd /usr/local/share/uhd/utils
$ ./usrp_burn_mb_eeprom --key=gpsdo --val=internal
$ cd /usr/local/src/uhd323/host/utils
$ ./usrp_n2xx_net_burner.py --addr=192.168.10.2 --reset
  # Wait for USRP to reset
$ uhd_usrp_probe    # Verify GPSDO is recognized by USRP
```

7. UHD utilities are stored in the following directory:

   `/usr/local/src/uhd323/host/utils`

B.5 Build GnuRadio with UHD Blockset

GnuRadio is a GUI signal-processing application which, when installed with the UHD blockset, allows a user to build a variety of networks to communicate to/from the USRP, as well as store data and perform runtime data manipulation. GnuRadio uses the existing UHD installation to communicate with the USRP.

There are a variety of procedures that will build GnuRadio with numerous different configurations. The most up to date instructions can be found on the GNU Radio website at `http://www.gnuradio.org`

1. Download and install GnuRadio dependencies.

   (a) GnuRadio dependencies (from Ubuntu 11.04)[2], execute:

```
$ sudo apt-get -y install libfontconfig1-dev \
libxrender-dev libpulse-dev swig g++ automake autoconf \
libtool python-dev libfftw3-dev libcppunit-dev \
libboost-all-dev libusb-dev fort77 sdcc sdcc-libraries \
libsdl1.2-dev python-wxgtk2.8 git-core guile-1.8-dev \
libqt4-dev python-numpy ccache python-opengl libgsl0-dev \
```

[2]From `http://gnuradio.org/redmine/projects/gnuradio/wiki/UbuntuInstall`

```
python-cheetah python-lxml doxygen qt4-dev-tools \
libqwt5-qt4-dev libqwtplot3d-qt4-dev pyqt4-dev-tools \
python-qwt5-qt4
```

(b) Additional dependencies (for Ubuntu 12.04), execute:

```
$ sudo apt-get -y install wget libxi-dev python-docutils \
gtk2-engines-pixbuf r-base-dev
```

2. Download newest GnuRadio from git:

```
$ cd $HOME
$ git clone http://gnuradio.org/git/gnuradio.git
```

3. Move GnuRadio to location and install:

```
$ cp -r $HOME/gnuradio /usr/local/src && rm -rf $HOME/gnuradio
$ cd /usr/local/src
$ chmod -R a+rx gnuradio
$ cd gnuradio
$ mkdir build
$ cd build
$ cmake ../
$ make
$ make test
$ sudo make install
$ export PYTHONPATH=$PYTHONPATH:/usr/lib/python2.7/dist-packages
$ export LD_LIBRARY_PATH=$LD_LIBRARY_PATH:/usr/bin
$ sudo ldconfig
```

4. The `make test` command may produce the error "`ImportError:: No module named digital_swig`", which requires correction of the script `run_tests`.

(a) Open the script file `run_tests`:

```
$ cd /usr/local/src/gnuradio/gr-trellis/src/python/
$ gedit run_tests
```

(b) After the line setting PYTHONPATH (which begins "PYTHONPATH=...") add the line `export PYTHONPATH`.

(c) Save the file and exit.

(d) Re-check the make file:

```
$ make test
```

5. Install the icon set for GnuRadio-Companion:

```
$ cd /usr/local/libexec/gnuradio
$ ./grc_setup_freedesktop install
```

6. Restart the computer for settings to take effect.

7. To launch GnuRadio Companion, find "GRC" in the Unity Launcher, or, in terminal mode:

```
$ gnuradio-companion
```

A window with a new flow graph should be displayed. Available flow graph blocks are displayed on the right. Verify that GnuRadio has the UHD blockset.

8. To verify GnuRadio and the UHD blockset function, some useful example flowgraphs are available for execution straight from the command line, such as an FFT. These require the USRP to be powered on and accessible to host computer.

```
$ cd /usr/local/src/gnuradio/gr-uhd/apps/
$ ./uhd_fft
```

A window displaying the FFT of a received signal on the USRP should be displayed, along with various USRP settings, as shown below, examining the DGPS spectrum.

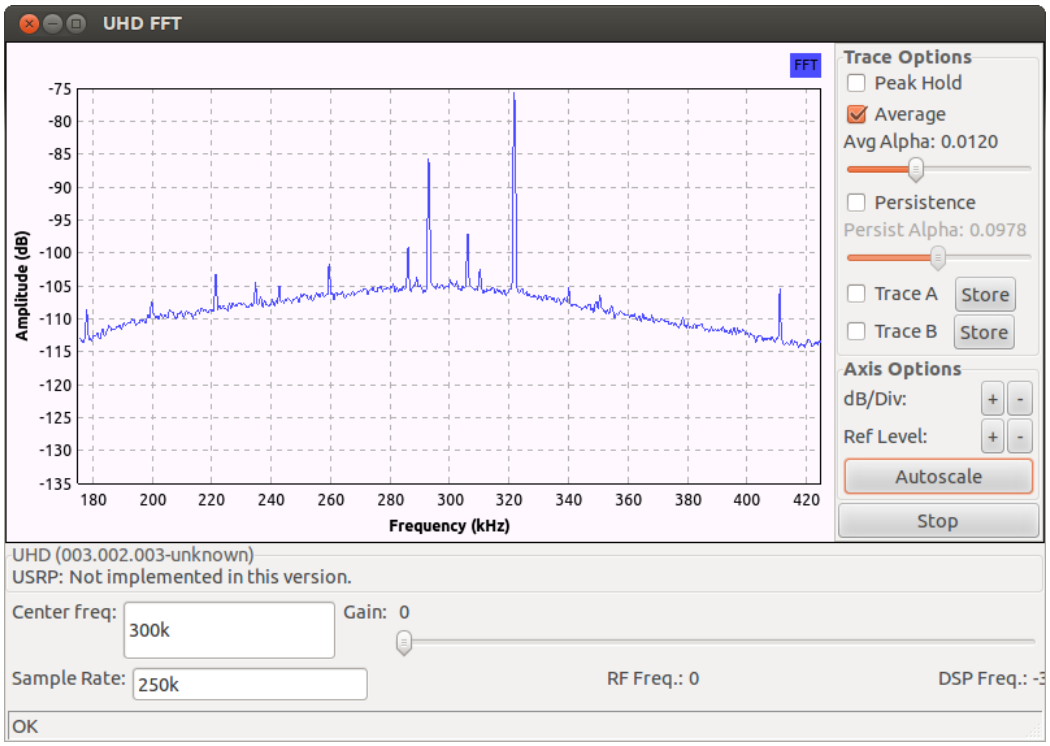
UHD FFT
FFT
Amplitude (dB)
-75
-80
-85
-90
-95
-100
-105
-110
-115
-120
-125
-130
-135
180
200
220
240
260
280
300
320
340
360
380
400
420
Frequency (kHz)
Trace Options
Peak Hold
Average
Avg Alpha: 0.0120
Persistence
Persist Alpha: 0.0978
Trace A
Store
Trace B
Store
Axis Options
dB/Div:
Ref Level:
Autoscale
Stop
UHD (003.002.003-unknown)
USRP: Not implemented in this version.
Center freq:
300k
Gain: 0
Sample Rate:
250k
RF Freq.: 0
DSP Freq.: -3
OK

APPENDIX C

USRP N210 Setup on MATLAB R2012a

C.1 Purpose

This Appendix describes the procedure used in this thesis to install the Simulink Support Package version 3.0.1 (which includes a joint Ettus-MathWorks USRP Universal Hardware Driver (UHD) version 003.002.003) for MathWorks MATLAB R2012a on the Windows 7 x64 operating system. This procedure may also be used to install the support package on MATLAB R2012a in Mac OS X 10.6.8 and Ubuntu 12.04. MATLAB R2012b has a self-installer, see the MathWorks web site below for details.

NOTE: This software installation guide assumes the USRP is already loaded with firmware images 003.002.003 (a procedure outlined in Appendix B). There are numerous methods for installing the UHD in the Windows environment and the USRP firmware images from Windows, but these methods are not discussed here.

MathWorks provides this software support package. The most up to date instructions can be found on the MathWorks website at:
`http://www.mathworks.com/discovery/sdr/usrp.html`.

C.2 Establish USRP IP-Layer Communication

This is essentially the same process as Ubuntu 12.04: (a) Creating a physical connection between the USRP and NIC and (b) editing the NIC IP settings. As mentioned previously, the USRP requires a Gigabit Ethernet connection to the host NIC or network switch/router.

1. Connect the USRP to the computer: plug in the Ethernet cable between the USRP and the computer, then power on the USRP.

2. Select "Start Menu > Control Panel". From the Control Panel, select "Network and Internet > Network and Sharing Center > Change adapter settings" on the left sidebar. As shown below, select the intended NIC for use (usually, "Local Area

Connection"), then select "Change settings of this connection" from the title bar (or right-click and select "Properties").

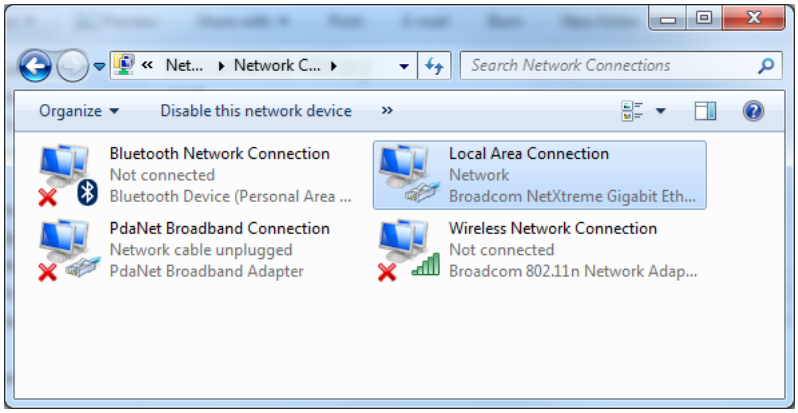

3. On the "Networking" tab of the dialog box, select "Internet Protocol Version 4 (TCP/IPv4)", then select "Properties".

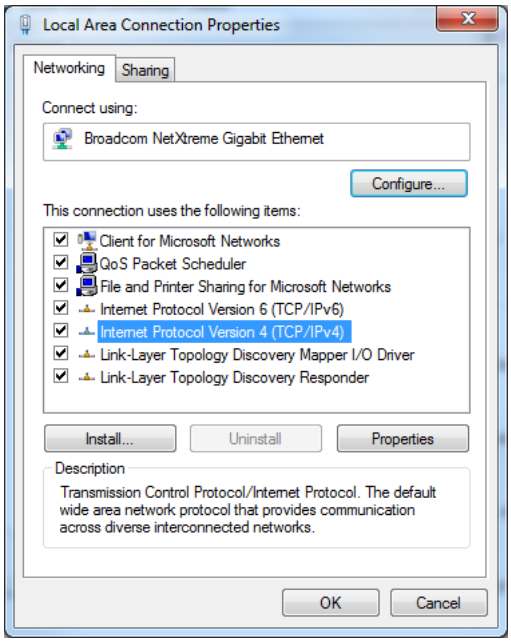

4. Select "Use the following IP address". Set the IP address to `192.168.10.1`, and the subnet mask to `255.255.255.0`. Like Ubuntu, the gateway may be left blank or set to `192.168.10.1`. Select "OK" and close all settings windows.

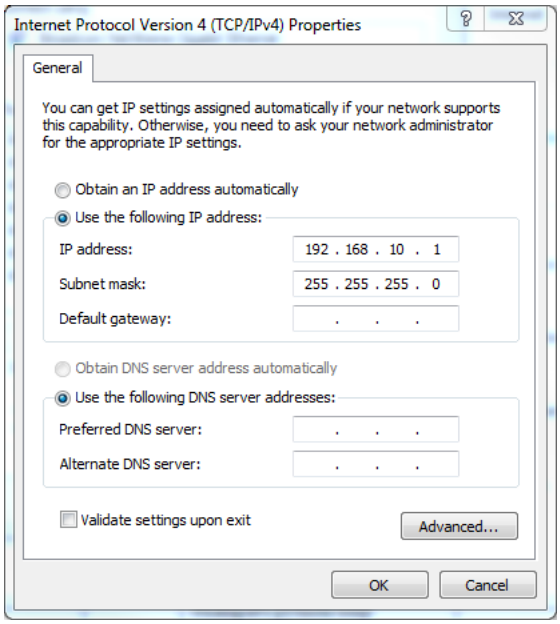

5. The USRP should now be recognized by the operating system. To test the connection between the host computer and USRP, open a Command Prompt from "Start > All Programs > Accessories > Command Prompt" and execute:

   `> ping 192.168.10.2`

   A successful ping will return four replies with no timeouts.

C.3 Install the USRP Support Package in MATLAB

1. Start with a Windows 7 computer loaded with MATLAB R2012a. This software package does not currently work with previous versions of MATLAB (and has not been tested on subsequent versions). NOTE: The process to install the USRP Support Package in MATLAB works in both Windows 7 x64 and Ubuntu 12.04 x64 environments.

2. The USRP Support Package is dependent on the Python environment. Download and install the Python environment from:

   `www.python.org/download/`

3. Download and install the USRP Support Package.

(a) Download and install the USRP Support Package version 3.0.1 from MathWorks:

`http://www.mathworks.com/discovery/sdr/usrp.html`

(b) Extract the .zip file to a folder that is not within the MATLAB installation folder and does not have any spaces, e.g.:

`C:\USRP\MATLAB_SDRU`

(c) Open the "README.txt" file and follow the installation instructions. You must install to a folder that does not have any spaces, e.g.: the path mentioned above.

(d) If using Ubuntu 12.04, the following line should be appended to the "Add SDRu" shortcut button command list, which will remove restrictions use of the system's memory and networking capabilities:

```
system('sudo sysctl -w net.core.wmem_max=1048576 &&
sudo sysctl -w net.core.rmem_max=50000000');
```

4. Launch Simulink. A window should be opened with available blocksets and blocks displayed. Check to see that MATLAB is using the UHD by checking for the "Communications with USRP" blockset.

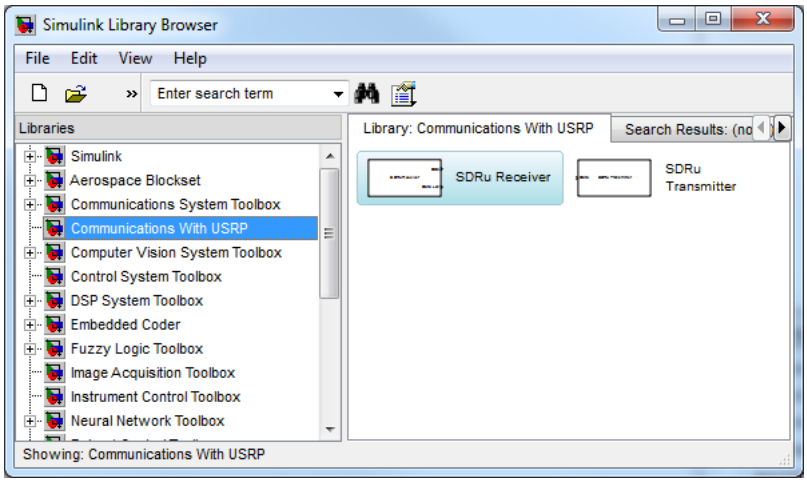

APPENDIX D

List of Abbreviations

2DRMS	2 × distance root-mean-squared
C/A	Coarse acquisition
CORS	Continuously-Operating Reference Station
DBSRX2	USRP receiver daughterboard, 800 MHz to 2300 MHz
DGPS	Differential GPS
DGNSS	Differential GNSS
DOP	Dilution of precision
ECEF	Earth-centered, Earth-fixed x, y, z position coordinates
EGNOS	European Geostationary Navigation Overlay Service
FPGA	Field-programmable gate array
GBAS	Ground-based augmentation system
GLONASS	*Globalnaya Navigatsionnaya Sputnikovaya Sistema*
GNSS	Global navigation satellite system
GPS	Global Positioning System
GPSDO	GPS-disciplined oscillator
GRC	GnuRadio Companion
GUI	Graphical user interface
IGS	International GNSS Service
IRNSS	Indian Regional Navigational Satellite System
L1	U.S. Air Force GPS radio-frequency band (centered at 1575.42 MHz)
LFRX	USRP Low Frequency Receiver daughterboard, 0 Hz to 30 MHz
LIS	Long Island Sound
LORAN-C	Long-Range Aids to Navigation system C
MATLAB	Matrix Laboratory
MIMO	Multiple-input, multiple-output

MSK	Minimum-shift keying modulation technique
NATO	North Atlantic Treaty Organization
NAVSTAR	Navigation Signal Timing and Ranging
NDGPS	Nationwide DGPS
PPS	Precise-positioning service (with respect to GPS service levels)
PPS	Pulse-per-second (with respect to timing)
PRC	Pseudorange correction
PRN	Pseudorandom noise
QZSS	Quasi-Zenith Satellite System
R95	Radius from true position containing 95% of the user's positions
RAAS	Regional Area Augmentation System
RTCM	Radio Technical Commission for Maritime Services
SBAS	Space-based augmentation system
SC-104	Standards Committee 104
SDR	Software-defined radio
SED	Storm-enhanced plasma density
SLI	Spatial linear interpolation
SPS	Standard positioning service
SNR	Signal-to-noise ratio
STANAG	Standardization Agreement
SV(N)	Satellite vehicle (number)
UHD	Universal Hardware Driver
URI	University of Rhode Island
USCG(A)	United States Coast Guard (Academy)
USRP	Universal Software Radio Peripheral
UTC	Coordinated Universal Time
WAAS	Wide-Area Augmentation System
WADGPS	Wide-area DGPS
WGS84	World Geodetic System 1984 reference ellipsoid

APPENDIX E

List of Symbols

$\odot$	Binary operator: element-wise multiplication of two vectors
$\boldsymbol{A}$	Non-singular x, y beacon position matrix for SLI algorithm
a_b	PRC weighting coefficient for beacon b
$\boldsymbol{a}$	PRC weighting coefficient vector for a single satellite, vector form of a_b
a, b, c	Plane weighting coefficients for SLI algorithm, see (2.11)–(2.13)
B	Number of DGPS beacons
b	Beacon in use
c	Speed of light, $2.997\,924\,58\,\mathrm{m{\cdot}s^{-1}}$
$c_{(\phi,\omega)}$	Cross-correlation value at a specified codephase and frequency shift
$\boldsymbol{c}$	Coefficients of the plane equation for SLI algorithm
$D_{\mathrm{N/E}}$	Distance north/east of the rover position
d	Constant scale factor for noise mean and covariance
$\boldsymbol{d}, \boldsymbol{d'}$	Data vector, Doppler-offset data vector
dt_{R}, dt_s	Receiver and satellite s clock bias
δ_{tr}	Difference in transmitted time of GPS signal
δ_{rcv}	Difference in received time of GPS signal
$\delta\boldsymbol{\rho}$	Difference between true and calculated pseudoranges at time t, see (4.4)
$\delta\boldsymbol{x}$	Difference between true and estimated position at time t, see (4.4)
Δ	Divisor for calculating the SLI plane equation coefficients, see (2.10)
e_s	Additional observational error for satellite s
f_{c}	Center frequency of sampled signal
f_{s}	Sampling frequency
$\boldsymbol{G}$	Manipulated visibility matrix, see (4.21)
$\boldsymbol{H}$	Visibility matrix, see (4.5)
$I(n)$	In-phase component of sampled complex data signal

$I_\phi(n)$	Codephase-shifted in-phase component of a data signal
I_s	Ionospheric path time delay for satellite s
$\mathbf{I}$	Identity matrix
m_s	Multipath time delay for satellite s
$\boldsymbol{n}$	For SLI: position-PRC vector normal to the SLI hyperplane
$\boldsymbol{n}$	For noise: random variable of total noise in networked DGPS
$\boldsymbol{n}_\mathrm{R}, \boldsymbol{n}_\mathrm{B}$	Noise vector at the rover and beacon
N	Total number of data samples
p_0	Pseudorange correction at the point $(0, 0)$ on the SLI hyperplane
$p(n)$	Expanded PRN sequence, used for GPS cross-correlation
$\boldsymbol{p}_b, \boldsymbol{p}_\mathrm{R}$	Position-PRC vector of the beacon or rover, of form (2.9)
$Q_{\mathrm{Avg,...,SLI}}$	Quality factor of the four networking algorithms
$Q(n)$	Quadrature component of sampled complex data signal
$Q_\phi(n)$	Codephase-shifted quadrature-phase component of a data signal
r_b	Range to beacon b
ρ_s	True range to a satellite s
$\hat{\rho}_s$	Calculated range to satellite s
$\mathring{\rho}_s$	Pseudorange correction for satellite s
$\boldsymbol{\rho}_0$	True ranges to satellites
$\hat{\boldsymbol{\rho}}$	Estimated (calculated) pseudoranges to satellites
$\mathring{\boldsymbol{\rho}}_\mathrm{R,B}$	Pseudorange (atmospheric) correction vector at the rover and beacon
S	Total satellite number
S_B	Signal down-converted to baseband
S_IF	Signal down-converted to intermediate frequency
$S(n)$	Complex data signal, sampled
σ_x, σ_y	Standard deviation of position error with respect to x, y directions
σ_C	Standard deviation of total correction noise
$\boldsymbol{\sigma}$	Standard deviations vector of all satellites' pseudoranges at a beacon
T_s	Tropospheric path time delay for satellite s

ϕ	GPS codephase
$\boldsymbol{x}$	User's position-PRC vector at the origin for SLI algorithm
$\boldsymbol{x}_0$	User's true position
$\hat{\boldsymbol{x}}$	User's estimated position
$\boldsymbol{z}$	Pseudorange correction values for SLI algorithm
$\boldsymbol{\omega}$	GPS Doppler-shift time vector

BIBLIOGRAPHY

16-Bit, 160 MSPS 2x/4x/8x Interpolating Dual TxDAC+ D/A Converter, C ed., Analog Devices, Norwood, MA, Jan. 2006, pp. 5–8.

Barr, S. P., Swaszek, P. F., Hartnett, R. J., and Johnson, G. W., "Performance of multi-beacon DGPS," in *Proc. 2013 Int. Tech. Meeting Inst. Navigation (ION ITM 2013)*, San Diego, CA, Jan. 2013.

7806R Coax-RG-58 Type, 3rd ed., Belden Inc., St. Louis, MO, pp. 1–3.

Blossom, E., Corgan, J., Ettus, M., *et al.* GnuRadio. "GnuRadio wiki." [Accessed: 1 Jul. 2011]. [Online]. Available: http://gnuradio.org/redmine/projects/gnuradio/wiki

Borre, K., Akos, D. M., Bertelsen, N., Rinder, P., and Jensen, S. H., *A Software-Defined GPS and Galileo Receiver: a Single-Frequency Approach.* Boston, MA: Birkhäuser, 2007.

Charkhandeh, S., "X86-based real time L1 GPS software receiver," M.S. thesis, Dept. Geomatics Eng., Univ. Calgary, Calgary, Canada, 2007.

Coelho, F., "Software defined GPS/Galileo receiver," M.S. thesis, Inst. Superior Técnico, Univ. Técnica Lisboa, Lisbon, Portugal, Apr. 2011.

Collins, J. P., "Assessment and development of a tropospheric delay model for aircraft users of the Global Positioning System," M.S. thesis (Tech. Report No. 203), Dept. Geodesy, Geomatics Eng., Univ. New Brunswick, Fredericton, New Brunswick, Canada, Sept. 1999.

Dabčević, K., "Evaluation of software defined radio platform with respect to implementation of 802.15.4 ZigBee," M.S. thesis, Sch. Innovation, Design, Eng., Univ. Mälardalen, Västerås, Sweden, 2011.

Ettus Research. "UHD—internal GPSDO application notes." [Accessed: 5 Apr. 2012]. [Online]. Available: http://files.ettus.com/uhd_docs/manual/html/gpsdo.html

Ettus Research. "USRP users mailing list." [Accessed: 1 Jul. 2011]. [Online]. Available: http://lists.ettus.com/pipermail/usrp-users_lists.ettus.com/

Installing the Ettus Research GPSDO Kit for USRP N200 Series & E100 Series, 1st ed., Ettus Research, Mountain View, CA, Jan. 2012, pp. 1–2.

USRP N200/N210 Networked Series, Ettus Research, Mountain View, CA, Jan. 2012, pp. 1–2.

FAA-E-2892b, Change 1, Specification for the Wide Area Augmentation System (WAAS), Federal Aviation Administration Solicitation DTFA01-96-C-00 025 Mod. 0111, Aug. 2001.

"Forum: GNU radio." [Accessed: 18 Jul. 2011]. Aug. 2011. [Online]. Available: http://www.ruby-forum.com/forum/gnuradio

Global Positioning System Standard Positioning Service Performance Standard, Global Positioning Systems Directorate Specification GPS SPS PS, Sept. 2008.

Navstar GPS Space Segment/Navigation User Segment Interfaces, Global Positioning Systems Directorate Specification IS-GPS-200, Rev. F, Sept. 2011.

GnuRadio. "GnuRadio mailing list." [Accessed: 25 Nov. 2011]. [Online]. Available: http://lists.gnu.org/archive/html/discuss-gnuradio/

Grant, A. J., "Availability, continuity, and selection of maritime DGNSS radiobeacons," Ph.D. dissertation, Sch. Informatics, Univ. Wales, Bangor, United Kingdom, 2002.

Hackman, C. and Matsakis, D., "Accuracy and precision of USNO GPS carrier-phase time transfer," in *Proc. 42nd Annu. Precise Time and Time Interval (PTTI) Meeting*, Reston, VA, Nov. 2010, pp. 197–214.

Harkleroad, G., Tang, W., and Johnson, N., "Estimation of error correlation distance for differential GPS operation," in *IEEE Position Location Navigation Symp. (IEEE PLANS 1990)*, San Diego, CA, Mar. 1990, pp. 378–382, doi:10.1109/PLANS.1990.66203.

Huba, J. D., Joyce, G., and Krall, J., "Three-dimensional equatorial spread F modeling," *Geophys. Res. Lett.*, vol. 35, pp. 325–331, May 2008, doi:10.1029/2008GL033509.

Iskander, M. F., Ed., *Electromagnetic Fields and Waves.* Long Grove, IL: Waveland Press, 2000.

Johnson, G. W., "LORAN: Creating a viable backup for GPS," Ph.D. dissertation, Dept. Elect., Comput., Biomed. Eng., Univ. Rhode Island, Kingston, RI, 2005.

Johnson, G. W., Oates, C., Wiggins, M., Swaszek, P. F., Page, A. T., Hartnett, R. J., and Cleveland, A. B., "USCG NDGPS accuracy and spatial decorrelation assessment," in *Proc. 2012 Global Navigation Satellite Syst. Inst. Navigation (ION GNSS 2012)*, San Diego, CA, Sept. 2012, pp. 3665–3674.

Johnson, G. W., Swaszek, P. F., and Hartnett, R. J., "Performance assessment of the recent NDGPS recap—initial simulation results," in *Proc. 2012 Int. Tech. Meeting Inst. Navigation (ION ITM 2012)*, Newport Beach, CA, Jan. 2012, pp. 1369–1376.

Kaplan, E. D. and Hegarty, C. J., Eds., *Understanding GPS: Principles and Applications*, 2nd ed. Norwood, MA: Artech House, 2006.

Klobuchar, J. A., "Ionospheric time-delay algorithm for single-frequency GPS users," *IEEE Trans. Aerosp. Electron. Syst.*, vol. 23, pp. 325–331, May 1987.

Model 3905C IEEE-488 Programmable Filter Mainframe, Krohn-Hite Corp., Brockton, MA, pp. 1-1–2-6.

Model 3905C/3916C, Krohn-Hite Corp., Brockton, MA, pp. 1–2.

Langley, R. B., "Dilution of precision," *GPS World*, pp. 52–59, May 1999.

Last, D., Grant, A., Williams, A., and Ward, N., "Enhanced accuracy by regional operation of Europe's new radiobeacon differential system," in *Proc. 15th Int. Tech. Meeting Satellite Division Inst. Navigation (ION GPS 2002)*, Portland, OR, Sept. 2002, pp. 2723–2732.

7.5A, 5A, 3A Low Dropout Positive Adjustable Regulators, G ed., Linear Technology, Milpitas, CA, pp. 1–5.

"Loading firmware on the USRP N210." [Accessed: 18 Jul. 2011]. Apr. 2011. [Online]. Available: http://greencrest.blogspot.com/2011/04/loading-firmware-on-usrp-n210.html

Lupash, L. O., "A new algorithm for the computation of the geodetic coordinates as a function of Earth-centered Earth-fixed coordinates," *J. Guidance, Control, Dynamics*, vol. 8, no. 6, pp. 787–789, Nov. 1985, doi:10.2514/3.20057.

Z-12R DGPS Reference Station With Fischer Connectors & RS-422 Operation and Technical Manual, Magellan Corp., Ashtech Precision Products, Santa Clara, CA, Jan. 1999, pp. 1–7.

Z-12R DGPS Reference Station Operation and Technical Manual Supplement, Magellan Corp., Ashtech Precision Products, Santa Clara, CA, Aug. 2001, pp. 1–7.

Manicka, N., "GNU radio testbed," M.S. thesis, Dept. Comp. Info. Sci., Univ. Delaware, Newark, DE, 2007.

McKay, J. B., "Optimization of a GPS-based navigation reference system," M.S. thesis, Sch. Eng., Air Force Inst. Technology, Wright–Patterson AFB, OH, 1996.

Millington, G., "Ground-wave propagation over an inhomogeneous smooth earth," in *Proc. IEE—Part III: Radio and Commun. Eng.*, vol. 96, Jan. 1949, pp. 53–64, doi:10.1049/pi-3.1949.0013.

Misra, P. and Enge, P., *Global Positioning System: Signals, Measurements, and Performance*. Lincoln, MA: Ganga–Jamuna Press, 2006.

Mueller, T., "Minimum variance network DGPS algorithm," in *IEEE Position Location Navigation Symp. (IEEE PLANS 1994)*, Las Vegas, NV, Apr. 1994, pp. 418–425, doi:10.1109/PLANS.1994.303344.

Mueller, T., Loomis, P., and Sheynblat, L., "Wide area DGPS design issues study," U.S. Coast Guard, Los Gatos, CA, Tech. Rep. CG-D-01-95, Jan. 1995.

National Oceanic and Atmospheric Agency. "Continuously operating reference station (CORS)." [Accessed: 14 Mar. 2013]. Mar. 2013. [Online]. Available: http://geodesy.noaa.gov/CORS/

Navstar Global Positioning System (GPS)–System Characteristics, Part 1, North Atlantic Treaty Organization Standardization Agreement (STANAG) 4294, Aug. 1990.

NY2O. "Real time satellite tracking." [Accessed: 5 Apr. 2012]. Apr. 2012. [Online]. Available: http://www.n2yo.com/whats-up/?c=20

RTCM Recommended Standards for Differential Navstar GPS Service, Radio Technical Commission for Maritime Services (RTCM) Special Committee No. 104 Standard 2.1, Jan. 1994.

GPS Inline Amplifiers L1 & L1L2, Raven Industries, Sioux Falls, SD, pp. 1–2.

"Record of Decision (ROD) on the U.S. Coast Guard Long Range Aids to Navigation (Loran-C) Program," *Federal Register*, vol. 75, no. 4, pp. 997–998, Jan. 2010.

Sjöberg, L., Hedling, G., and Tiwari, A., "A wide area solution that takes advantage of the existing radio broadcast and national geodetic network infrastructure," in *IEEE Position Location Navigation Symp. (IEEE PLANS 1996)*, Atlanta, GA, Apr. 1996, pp. 596–603, doi:10.1109/PLANS.1996.509133.

Skone, S. and Coster, A., "Performance evaluation of DGPS versus SBAS/WADGPS for marine users," in *Proc. 20th Int. Tech. Meeting Satellite Division Inst. Navigation (ION GNSS 2007)*, Fort Worth, TX, Sept. 2007, pp. 1904–1913.

Skone, S., Yousuf, R., and Coster, A., "Combating the perfect storm: improving marine Differential GPS accuracy with a wide-area network," *GPS World*, pp. 31–38, Oct. 2004.

Skone, S., Yousuf, R., and Coster, A., "Performance evaluation of the Wide Area Augmentation System for ionospheric storm events," *J. Global Positioning Syst.*, vol. 3, no. 1–2, pp. 251–258, 2004.

5071A Primary Frequency Standard, Symmetricom Inc., San Jose, CA, Aug. 2009, pp. 17–31.

TLK2701 1.6 to 2.7 Gbps Transceiver, Texas Instruments, Dallas, TX, Mar. 2008, p. 1.

Dual Channel, 14-bits, 125/105/80/65 MSPS ADC with DDR LVDS/CMOS Outputs, C ed., Texas Instruments, Dallas, TX, Feb. 2012, pp. 1–4.

LMR-400 Flexible Low Loss Communications Coax, Times Microwave Systems, Wallingford, CT, pp. 22–23.

Differential Global Positioning System Broadcast Standard, United States Coast Guard Manual COMDTINST M16 577.1, Apr. 1993.

United States Coast Guard Navigation Center. "NDGPS general information." [Accessed: 10 Jan. 2013]. Jan. 2013. [Online]. Available: http://www.navcen.uscg.gov/?pageName=dgpsMain

United States Naval Observatory. "Current GPS constellation." [Accessed: 5 Apr. 2012]. Apr. 2012. [Online]. Available: http://tycho.usno.navy.mil/gpscurr.html

United States Naval Observatory. "Naval oceanography portal—leap seconds." [Accessed: 5 Aug. 2012]. Sept. 2012. [Online]. Available: http://www.usno.navy.mil/USNO/time/master-clock/leap-seconds

Wyman, G. C., "A software radio testbed for Coast Guard communication and navigation applications," M.S. thesis, Dept. Elect., Comput., Biomed. Eng., Univ. Rhode Island, Kingston, RI, 2010.

Spartan-3A DSP FPGA Family Data Sheet, 3rd ed., Xilinx, San Jose, CA, Oct. 2010, pp. 2–3.

Yousuf, R., "Evaluation and enhancement of the Wide Area Augmentation System (WAAS)," M.S. thesis, Dept. Geomatics Eng., Univ. Calgary, Calgary, Canada, 2005.